RECENT STUDIES IN MATHEMATICS AND ITS APPLICATIONS

EDITED BY
Rıdvan EZENTAŞ

AUTHORS
Esen İYİGÜN
Liudmyla HART
Mustafa MIZRAK
Mohammad FERDOWS
Nur UYLAŞ SATI
Rıdvan EZENTAŞ
Sultana JAHAN

İKSAD
Publishing House

RECENT STUDIES IN MATHEMATICS AND ITS APPLICATIONS

EDITED BY

Rıdvan EZENTAŞ

AUTHORS

Esen İYİGÜN

Liudmyla HART

Mustafa MIZRAK

Mohammad FERDOWS

Nur UYLAŞ SATI

Rıdvan EZENTAŞ

Sultana JAHAN

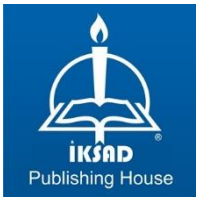

(The Licence Number of Publicator: 2014/31220)
TURKEY TR: +90 342 606 06 75
USA: +1 631 685 0 853
E mail: iksadyayinevi@gmail.com
www.iksadyayinevi.com

ISBN: 978-625-7562-89-8
Cover Design: İbrahim KAYA
September / 2021
Ankara / Turkey
Size = 16x24 cm

CONTENTS

CHAPTER 5

HEAT AND MASS TRANSFER FLOW FILLED WITH HYBRID NANOFLUID BY NON-ISOTHERMAL MOVING SURFACE: A TRANSPIRATION AND THERMAL RADIATION APPROACH

PREFACE

The purpose of the book titled “Recent Studies in Mathematics and Its Applications” is to create an academic forum for academics and researchers working in these fields. Mathematics and its applications cover many fields due to research topics. This book consists of five chapters that bring together different topics.

In the first chapter, a novel binary semi-supervised classification method based on polyhedral conic functions (PCFs) is defined.

Second chapter is concerned with the semiclassically scaled modified nonlinear Schrödinger equation.

In the third chapter, 4 different Null curves with 1 and 2 indexes are introduced, and Spinors structure, which is the physics application of 1-index null curve, is given.

The fourth chapter is devoted to the further development of the theoretical apparatus of projection-iteration methods for solving nonlinear operator equations of the first kind in Banach spaces based on a Newton-like method.

In the fifth chapter, the effect of some motor oils has been investigated in order to prevent energy wastage due to high temperature during the operation of the engines of the machineries.

While doing this, dimensionless ordinary differential equations are transformed by utilizing the similarity transformed technique from the partial differential equations. To solve the similarity transformation, the MAPLE computational software scheme has been used. I would like to thank the staff of ISPEC publishing house for their devoted work, who brought together valuable scientists and scientists for the creation of this book.

Rıdvan EZENTAŞ, Prof. Dr.

CHAPTER 1

A BINARY SEMI-SUPERVISED DATA CLASSIFICATION TECHNIQUE WITH POLYHEDRAL CONIC FUNCTIONS

Nur UYLAŞ SATI[1]

[1] Asst. Prof. Dr., Muğla Sıtkı Koçman University, Bodrum Maritime Vocational School, Motor Vehicles and Transportation Technologies, Ship Construction Programme . nursati@mu.edu.tr. ORCID: 0000-0003-1553-9466

INTRODUCTION

Recently, by the development of technology, it has become easier to obtain, store and use of data. In the light of this development, data classification, one of the data mining methods, is included in many researches. The purpose of data classification is to define a model that can predict the target class of future data by use of the relevant data available. Data classification is discussed in three types in terms of the labels of the training data; the process is named unsupervised, supervised and semi supervised, respectively for unlabeled, labeled and both labeled and unlabeled data.

The number of researches about semi-supervised learning has increased recently, because many datasets is formed with many unlabeled and a few labeled data. Semi-supervised learning can be dealt as supervised learning with additional unlabeled data that help elucidating the distribution of the examples. On the other hand it can be dealt as unsupervised learning by adding constraints. Semi supervised learning can be used in various applications as spam filtering, speech recognition, text classification, video regulation, image categorization, protein 3D structure prediction, webpage classification etc. Extensive review can be found in A Survey on Semi-supervised Learning (Van Engelen & Hoos, 2020).

In semi-supervised learning commonly used methods are support vector machines (SVMs), graph-based methods, self-training and co-training. These methods are briefly expressed below.

Self-training is a commonly used semi-supervised algorithm that uses a wrapper method around a supervised classifier, for instance, it can be used to enhance various classifiers. To implement self-training, the classifier must be able to output a certainty score, i.e., a prediction of how likely the estimated class label is correct (Zhu, 2008). In 2016 by Kanga et al., a semi-supervised support vector regression method via self-training is proposed and an application to virtual metrology in semiconductor manufacturing is made (Kanga, Kimb, & Choc, 2016). In 2015 by Hajmohammadi et al., integration of active learning and self-training for cross-lingual sentiment classification with density analysis of unlabeled data are studied (Hajmohammadi, Ibrahim, Selamat & Fujita, 2015). A self-training semi-supervised SVM algorithm and its implementation in an EEG-based brain computer interface speller system is proposed in 2007 by Chinaei (Chinaei, 2007).

Co-training paradigm was determined by Blum and Mitchell in 1998 (Blum & Mitchel, 1998). It trains two classifiers separately on two adequate and unnecessary views, i.e. two feature sets each of which is adequate for learning and conditionally uncommitted to the other given class label, and uses the estimations of every classifier on unlabeled samples to enhance the training set of the other (Zhou & Li, 2007).

Transductive support vector machines (TSVMs) utilize determined iterative algorithms which step by step search a confidential separating hyper plane with a transductive process that includes both labeled and unlabeled data in the training phase (Bruzzone, Chi & Marconcini, 2006; Ordin, 2010). In this study, we use a similar approach from the point of using whole dataset in training phase, for Algorithm 3 proposed in Section 3.

Graph based methods model the dataset as a graph. The nodes of the graph account for each data, and the edges represent the similarities between them. Almost whole the graph-based methods fundamentally predict a function on the graph. This function has two properties: It should be near to the given labels on the labeled samples, and also it should be smooth on the entire graph (Zha, Mei, Wang, Wang & Hua, 2009).

Besides, Semi-Supervised Learning and Collective Classification methods in Waikato Environment for Knowledge Analysis (WEKA) are frequently encouraged in the literature (Garner, 1995) Collective classification is an approach that uses the relational structure of the combined labeled and unlabeled data-set to enhance classification accuracy (Neville & lensen, 2003). *Learning with local and global consistency (LLGC), Yet another two stage idea (YATSI) and Collective Tree* approaches in collective classification are explained respectively as follows: *LLGC* is one of the collective classification approaches which was presented in 2003 by Zhou and his friends (Zhou, Bousquet, Lal, Weston & Schoelkopf, 2003). It forms a

smooth classifier function for labeled and unlabeled data. In the defined form, similar examples should have similar class labels locally, and globally, the predicted labels should agree well with the given training labels. An efficient and effective LLGC variant was proposed by Pfahringer and his friends in 2007 (Pfahringer Leschi & Reutemann, 2007). They aimed to sparse the similarity matrix and they reported the results on large text classification problems. *YATSI*, a collective classifier was presented in 2006 by Driessens and his friends. It uses the defined classifier to train on the training set. The obtained model is used to pre-label the unlabeled data. Then all labeled data consisting of original training and pre-labeled data is used in a weighted nearest neighbor algorithm (Driessens, Reutemann, Pfahringer & Leschi, 2006). *Collective Tree* algorithm constructs a tree by using *k* randomly chosen attributes at each node (Lichman, 2013). It divides the attribute such that it splits the current subset of all instances into two halves. The process ends if one of the conditions is met: Only training instances would be wrapped. Only test instances in the leaf would be wrapped. Only training instances of one class would be wrapped (Laorden, Sanz, Santos, Galan-Garcia, & Bringas, 2013). These collective classification algorithms are frequently used in the testing phases of the researches as they are easy to access and implement by using commonly used machine learning tool Waikato Environment for Knowledge Analysis (WEKA) (Santas, Laorden & Bringas, 2011; Sigdel, Dinç, Dinç, Sigdel, Pusey & Aygün, 2014; Levatic, Dzeroski, Supek & Smuc, 2013; Almogahed & Kakadiaris, 2014).

In 2018, a collective learning model was suggested for semi-supervised classification (Uylaş Sati, 2018). Firstly three different approaches (k-means, mean, all distances) are used in the initialization for defining the classes (labels) of the unlabeled instances then the state of art supervised classification algorithms were applied. It is seen that the structure of the given dataset and the used software programs have an important effect on the obtained results.

In 2020, polyhedral conic functions are used in multiclass semi-supervised classification with membership functions (Uylaş Sati, 2020). Firstly the membership function is defined then the unlabeled points are labeled according to the obtained membership values. Also these values are used in the objective function of the linear programming problem.

In this study, a novel binary semi-supervised classification method based on polyhedral conic functions (PCFs) is defined. In the first defined separation algorithm, unlabeled instances are directly used in the predefined PCFs algorithm by adding constraints to the problem. In the second defined algorithm, firstly clustering method is used for specifying the unlabeled points' classes as suggested in (Uylaş Sati, 2018) then predefined PCFs algorithm is used. In Section 1, separation via polyhedral conic functions in supervised classification is expressed. Novel defined algorithms are explained and proposed in detail in Section 2. Numerical experiments on the defined algorithms are proposed in Section 3.

THE MATHEMATICAL MODEL OF SEPARATION WITH POLYHEDRAL CONIC FUNCTIONS

Polyhedral conic functions (PCFs) have been defined by Gasimov and Öztürk in 2006 for a binary supervised classification.

Polyhedral conic functions was defined as follows:

$$g_{(w,\xi,\gamma,a)} : R^n \to R = w'(x-a) + \xi \left\| x-a \right\|_1 - \gamma \qquad (1)$$

where $w, a \in R^n, \xi, \gamma \in R$, $w'x = w_1x_1 + ... + w_nx_n$, $\left\| x \right\|_1 = \left| x_1 \right| + ... + \left| x_n \right|$.

The first classification algorithm by use of polyhedral conic functions was defined and prediction results were obtained with 100% accuracy (Gasimov & Öztürk, 2006).

The defined algorithm was developed to decrease running-time and also to overcome over-fitting the problem (Uylaş, 2013; Uylaş Sati, 2015, 2016). To decrease the running time, a clustering algorithm is used in Step 0. Thus the number of iterations to find the center point is reduced in the interest of saving time. Also to overcome the difference between training accuracy and testing accuracy, that's called over-fitting, misclassification is allowed for both classes, not just for one. The developed algorithm was defined as follows (Uylaş Sati, 2015):

Algorithm 1 (Separation with PCFs and Clustering Method)

Define A and B sets, respectively:

$A=\left\{a^i \in R^n, i \in I\right\}$, $B=\left\{b^j \in R^n, j \in J\right\}$ where $I=\{1,...,m\}, J=\{1,...,p\}$.

Step 0. Imply *k*-means clustering algorithm on set of *A*. Let "*k"* be the number of clusters and *s*=1. I_s=*I*.

Step 1. Let a_s be the center of *s*th cluster. Solve the below sub problem

$$(P_s) \quad \min\left[\frac{1}{m}\sum_{i=1}^{m} y_i + C\frac{1}{p}\sum_{i=1}^{p} z_j\right] \tag{2}$$

$$w(a^i - a_s) + \xi\left\|a^i - a_s\right\|_1 - \gamma + 1 \le y_i, \quad i \in I_s \tag{3}$$

$$-w(b^j - a_s) - \xi\left\|b^j - a_s\right\|_1 + \gamma + 1 \le z_j, \quad j \in J \tag{4}$$

$$y_i, z_j \ge 0, C \ge 1, w \in R^n, \xi \in R, \gamma \ge 1$$

Let $w_s, \xi_s, \gamma_s, a_s$ be a solution of (P_s). Let

$$g_s(x) = g_{(w_s, \xi_s, \gamma_s, a_s)}(x)$$

Step 2. If $s<k$, let s=s+*1*, $I_s=\left\{i \in I_{s-1} : g_{s-1}\left(a^i\right) > 0\right\}$ and go to *Step 1*.

Step 3. Identify the function *g(x)* (dividing the sets *A* and *B*) as

$$g(x) = \min_s g_s(x)$$

and STOP.

Besides, also in 2015, Öztürk et al. developed *k*-means based PCF algorithm for multi-class supervised data classification. The "s" (number of clusters) pieces of PCFs were constituted for every class to separate each from the rest (Öztürk & Çiftçi, 2015).

SEMI-SUPERVISED CLASSIFICATION WITH PCFS

Supervised classification is different from semi-supervised classification when considered from their training phases. Semi-supervised classification uses both labeled and unlabeled data in training but supervised classification uses just labeled ones. In real world, many datasets consist of too many unlabeled data and a few labeled ones since gathering labeled instances is so costly and hard to find while unlabeled instances are abundant. In this study, we use polyhedral conic functions for semi- supervised classification.

In the following algorithm, defined for semi-supervised data classification problems, we use an approach that allows constraints for unlabeled instances in addition to previous defined Algorithm 1 approach. Suggested algorithm is given as follows:

Algorithm 2 (Semi-Supervised Classification with PCFs)

Define A and B labeled sets and C unlabeled set respectively:

$A=\left\{a^i \in R^n, i \in I\right\}$, $B=\left\{b^j \in R^n, j \in J\right\}$, C=$\left\{c^t \in R^n, t \in T\right\}$ where

$I=\{1,...,m\}, J=\{1,...,p\}, T=\{1,...,n\}$

Step 0. Implement *k*-means clustering algorithm on set of *A*. Define *k* as the number of clusters. Let *s*=1. I_s=*I*.

Step 1. Define a_s as the center of *s* indexed cluster. Solve the below sub problem

$$(P_s) \quad \min \frac{1}{m}\sum_{i=1}^{m} y_i + \frac{M}{t}\sum_{t=1}^{n} z_t \tag{5}$$

$$w(a^i - a_s) + \xi \left\| a^i - a_s \right\|_1 - \gamma + 1 \le y_i, \quad i \in I_s \tag{6}$$

$$-w(b^j - a_s) - \xi \left\| b^j - a_s \right\|_1 + \gamma + 1 \le 0, \quad j \in J \tag{7}$$

$$\left| (w(c^t - a_s) + \xi \left\| c^t - a_s \right\|_1 - \gamma) \right| \le z_t, \quad t \in T \tag{8}$$

$$y_i, z_t \ge 0, w \in R^n, \xi \in R, \gamma \ge 1, \ 1>M>0$$

Let $w_s, \xi_s, \gamma_s, y_s$ be a solution of (P_s). Let

$$g_s(x) = g_{(w_s, \xi_s, \gamma_s, a_s)}(x)$$

Step 2. If $s<k$, let *s*=*s*+*1*, $I_s = \left\{ i \in I_{s-1} : g_{s-1}\left(a^i\right) > 0 \right\}$ and go to *Step 1*.

Step 3. Identify the function *g(x)* (dividing the sets *A* and *B*) as

$$g(x) = \min_s g_s(x)$$

and STOP.

In Algorithm 2, Clustering method is used in the initialization part as in Algorithm 1 but we do not use misclassification for points of B set as in constraint (4) since misclassifications are already used for unlabeled ones, just because we do not know their labels. If we allow misclassification for both labeled training instances (points of A and B sets) the problem can deviate from the aim and we can allow under fitting the problem, in other words we can decrease the generalization accuracy majorly. Also we benefit from transductive semi-supervised Support Vector Machine (SVM) approach for the unlabeled instances and use both labeled and unlabeled examples in the training operation (Bennett, & Demiriz, 1998; Astorino & Fuduli, 2015). By constraint (8) the unlabeled points are tried to be positioned near to the separation function, that is if $x \in C$, $|g(x)|$ value should be close to "0". The *M* value used in objective function (5) is determined as a penalty parameter for the distance between separation function and unlabeled point. It is defined as a rational number between 0 and 1 since we want the effect of the labeled points' misclassification defined in (6) should be bigger than unlabeled points' effect in defining the separation function. If we enlarge the *M* value, implicitly we increase the effect of unlabeled points on the separating function that will be defined. A globally optimal solution to the sub problem (5) can be obtained by use of linear programming techniques.

In the second defined algorithm for semi-supervised classification problem we integrate clustering algorithm and Algorithm 1. For specifying the unlabeled points' classes, the center points of labeled datasets are used. K-means, an unsupervised clustering method, is used for defining the center points (Bagirov, & Mardaneh, 2006). Such that in the initialization, clustering method is applied on both A and B sets. The obtained center points are used to specify the unlabeled points' classes. In fact, the Euclidian distance between center points (*cp*) and C points(*c*), defined in R^n, are calculated as follows (Uylaş Sati, 2018):

$$d(cp_s^k, c^t) = \sqrt{((cp_1)_s{}^k - (c_1)^t)^2 + \ldots\ldots\ldots + ((cp_n)_s{}^k - (c_n)^t)^2}$$
$$= \sqrt{\sum_{i=1}^{n} ((cp_i)_s^k - (c_i)^t)^2}$$
$$k = 1,2; \quad s = A,B; \quad t = 1,\ldots,t; \quad i = 1,\ldots,n.$$

The closest center point's class is labeled to the points of C set. Then the previous defined Algorithm 1 is applied for supervised classification on the redetermined A and B datasets.

The suggested Algorithm 3 is given as follows:

Algorithm 3 (Semi-Supervised Classification via Clustering and PCFs)

Define A and B labeled sets and C unlabeled set respectively:

$A=\left\{a^i \in R^n, i \in I\right\}$, $B=\left\{b^j \in R^n, j \in J\right\}$, C=$\left\{c^t \in R^n, t \in T\right\}$ where

$I=\{1,...,m\}$, $J=\{1,...,p\}$, $T=\{1,...,t\}$.

Step 0. (Initialization step) Implement *k*-means clustering algorithm on set of A and B. Define *k=2.*

Label the points of C set with the nearest center points' label. And redetermine the A and B datasets according to the new labels.

Step 1. Implement *k*-means clustering algorithm on set of *A.* Define *k* as the number of clusters. Let *s*=1. $I_s=I$.

Step 2. Define a_s as the center of *sth* cluster. Solve the below sub problem.

$$(P_s) \quad \min\left[\frac{1}{m}\sum_{i=1}^{m} y_i + C\frac{1}{p}\sum_{i=1}^{p} z_j\right]$$

$$w(a^i - a_s) + \xi\left\|a^i - a_s\right\|_1 - \gamma + 1 \le y_i, \quad i \in I_s$$

$$-w(b^j - a_s) - \xi\left\|b^j - a_s\right\|_1 + \gamma - 1 \le z_j, \quad j \in J$$

$$y_i, z_j \ge 0, C \ge 1, w \in R^n, \xi \in R, \gamma \ge 1$$

Let $w_s, \xi_s, \gamma_s, a_s$ be a solution of (P_s). Let

$$g_s(x) = g_{(w_s, \xi_s, \gamma_s, a_s)}(x).$$

Step 3. If $s < k$, let s=*s+1*, $I_s = \left\{ i \in I_{s-1} : g_{s-1}\left(a^i\right) > 0 \right\}$ and go to *Step 2*.

Step 4. Identify the function *g(x)* (dividing the sets *A* and *B*) as

$$g(x) = \min_s g_s(x)$$

and STOP.

NUMERICAL EXPERIMENTS

In order to consider the efficiency of the suggested algorithms, primarily, we generate datasets to imply on Algorithm 3 and 4. Synthetic datasets' details are given in Table 1.

Table 1: Synthetic Datasets' Details

	number of attributes	number of labeled instances	number of unlabeled instances
Dataset1	2	62	38
Dataset2	4	64	36
Dataset3	10	32	28
Dataset4	3	18	32

For performance assessment ten- fold cross validation is used (Kohavi, 1995). The testing datasets are constituted by using labeled points, the rest of the cross validation process leave unchanged; in other words, both labeled and unlabeled instances are used for

obtaining the separating function but just labeled instances are used for the testing process. Testing accuracy result is defined by the maximum of 10 training accuracies. Training accuracy is defined by a formulation as follows:

- cc: number of correct classifications
- te: number of labeled points

$$\text{Accuracy (Acc.)} = \frac{100 \times cc}{te}$$

Obtained 10-fold cross validation results (training, testing and running time) on each synthetic datasets with the presented parameters are given in Table 2. The best results are written in bold numbers. In Table 3, the values of M parameter in Algorithm 2 and the experimented number of clusters in each implementation is given.

Table 2: 10-fold Cross Validation Results of Algorithm 3 and 4 on Synthetic Datasets

		Algorithm 2	**Algorithm 3**
Dataset1	**Training acc. %**	54.83	**62.90**
	Testing acc. %	**50.0**	40.0
	Time (sec.)	0.7	**0.1**
Dataset2	**Training acc. %**	59.37	**75**
	Testing acc. %	34.03	**45.5**
Dataset2	**Time (sec.)**	61.24	**0.2**
Dataset3	**Training acc. %**	71.87	**100**
	Testing acc. %	60.0	75.0

	Time (sec.)	0.34	**0.05**
Dataset4	**Training acc. %**	**94.11**	64.70
	Testing acc. %	**40.0**	**40.0**
	Time (sec.)	1.05	**0.49**

Table 3: Values of Parameters

	***M* value** **In Algorithm2**	**Number of clusters** **In Algoirthm2**	**Number of clusters** **In Algoirthm3**
Dataset1	0,2	3	10
Dataset2	0,3	3	10
Dataset3	0,5	2	5
Dataset4	0,5	2	2

We can make the following inferences about defined algorithms by interpreting the results:

- Since number of the attributes or instances increase, running time of the algorithms increase too, due to the sub problem's dimension increment in both algorithms.
- Algorithm 2 gets better accuracy results if the used clustering algorithm gets the real structure of the dataset. Algorithm 3 is more effective than Algorithm 2 for running time in implementations with big datasets since it uses clustering method for labeling the unlabeled points. Algorithm 3 cannot be implemented on the datasets that have just one labeled point in

set of A or one labeled point in set of B since number of clusters cannot be smaller than 2.

- Defining the number of the clusters in clustering methods is so important and it depends on the distribution of the datasets for both algorithms. Various numbers (1-10) are tried and the one that gives the best result is used. It effects well if the determined clustering algorithm reflects the actual structure of the data. For future studies this subject can be dealt.
- For Algorithm 2 if the number of unlabeled instances are very few, it doesn't have an impact on the separating function that will be defined. In the same manner the smaller the M is chosen, the less effect of the unlabeled points on the objective function and implicitly on the separating function.
- Besides, experiments are made by using real-world datasets to see the performance of the algorithms on large datasets. UCI machine learning repository is used to obtain the datasets. Details of real-world datasets are given in Table 4. Randomly 5%, 15% and 20% of the dataset is used as labeled data and the rest as unlabeled. The implementations of Algorithm 2 and 3 are done on a productive software environment MATLAB. During the implementations the "M" and "k" parameter values are fixed to be respectively 0,5 and 2.

Table 4: Details of Real World Datasets

	Number of attributes	Number of instances
Liver	6	345
WBCD	9	683
Ionosphere	34	351
Heart	13	297
Blood Transfusion	5	748

For presenting comparative results, we also make implementations on the accessible state of art Collective Classification methods; LLGC, YATSI and Collective Tree, that we explained in Introduction section. The implementations are done on open source machine learning software WEKA-Semi-supervised learning and Collective Classification Package. "random split" is chosen for evaluation options. The WEKA default setting of parameters were used for every algorithm. In Table 5, the accuracy values and the running times of the implementations are presented.

Table 5: Running Times and Accuracy Values on Real-World Datasets

Dataset Algorithms	**5%** **Acc.**	**Running Time (sec.)**	**15%** **Acc.**	**Running Time (sec.)**	**20%** **Acc.**	**Running Time (sec.)**
Liver						
LLGC	**58.53**	0.02	58.70	0.02	59.05	0.02
YATSI	57.62	0.01	56.65	0.01	57.60	0.01

CollectiveTree	56.09	0.01	56.65	0.01	55.79	0.01
Algorithm 2	57.97	17.09	60.0	21.1	**67.82**	14.81
Algorithm 3	57.10	2.22	**62.02**	1.96	57.68	2.35
WBCD						
LLGC	64.76	0.11	65.23	0.11	65.63	0.11
YATSI	93.53	0.01	**97.24**	0.01	**97.70**	0.01
CollectiveTree	89.07	0.01	92.94	0.01	93.96	0.01
Algorithm 2	95.08	495.5	92.25	430.7	95.90	468.2
Algorithm 3	**96.72**	8.45	97.22	7.9	96.78	7.73
Ionosphere						
LLGC	34.53	0.02	66.44	0.02	66.90	0.02
YATSI	**71.77**	0.01	70.46	0.01	**82.20**	0.01
CollectiveTree	63.66	0.01	**72.81**	0.01	72.95	0.01
Algorithm 2	39.03	461.3	35.89	758.0	52.13	775.0
Algorithm 3	47.29	2.43	67.52	2.33	69.80	2.31
Heart						
LLGC	55.85	0.02	43.23	0.02	56.48	0.02
YATSI	**71.09**	0.01	**76.85**	0.01	76.85	0.01

CollectiveTree	59.37	0.01	65.50	0.01	68.98	0.01
Algorithm 2	52.08	17.17	75.41	27.56	**83.33**	23.62
Algorithm 3	51.25	1.17	67.5	1.08	70.41	1.13
BloodTransfusion						
LLGC	74.23	0.15	75.31	0.15	75.25	0.15
YATSI	**76.40**	0.01	**75.41**	0.01	**76.88**	0.01
CollectiveTree	64.97	0.01	65.88	0.01	67.72	0.01
Algorithm 2	68.71	498.6	23.79	399.6	23.79	767.7
Algorithm 3	68.44	8.56	59.22	7.62	65.77	8.95

We can see from Table 5 that the best accuracy results are taken when we get the 20% of the dataset as labeled data. Thus, we can say that since the number of labeled data increases the effectiveness of the Algorithms 2 and 3 can increase too.

The best accuracy results of Liver and Heart datasets are obtained by Algorithm 2 however on the other datasets best results are obtained by YATSI. Overall, the accuracy results seem to be good on Liver, Heart and possibly on WBCD. For the other two datasets, we can say that used *k*-means clustering algorithm in Algorithm 2 and 3 don't get the real structure of the datasets with the determined *k* number of clusters. Therefore we can say that convincing results according to accuracy

values can be obtained by using polyhedral conic functions and proper clustering methods in semi-supervised classification.

WEKA algorithms are more effective when running times are considered. Since they are implemented on an effective specific machine learning software with ready to use codes while Algorithms 2 and 3 are implemented on MATLAB. However when we compare the Algorithms 2 and 3 in terms of running time values, we can say that Algorithm 3 is more speedy then Algorithm 2. The reason for this, the dimension of the linear programming sub problem in Algorithm 2 is larger than the one in Algorithm 3.

CONCLUSION

In this study, new semi-supervised classification algorithms were developed by using polyhedral conic functions that was predefined for supervised classification applications. We suggested two algorithms, in the first one we used both labeled and unlabeled data in the training phase and in the second one by use of clustering method we firstly defined the classes of unlabeled points then applied a supervised PCF classification algorithm. In both algorithms, we utilized polyhedral conic functions.

We generated datasets to use in the numerical experiments for testing the performances of two defined algorithms with different parameter values. Also we make experiments for presenting comparative results on real-world datasets by using WEKA collective algorithms. The results show that our proposed approaches are as effective as WEKA

clustering algorithms according to the accuracy values. Besides, our approach provides a novel angle to study the polyhedral conic functions (PCFs) in semi-supervised classification on the future researches.

REFERENCES

Almogahed, B. A., & Kakadiaris, I. A. (2014). Empowering Imbalanced Data in Supervised Learning: A Semi-Supervised Learning Approach. 24th International Conference on Artificial Neural Networks ICANN2014, 149, v1.

Astorino, A., & Fuduli, A. (2015). Support Vector Machine Polyhedral Separability in Semisupervised Learning. Journal of Optimization Theory and Applications, vol.164, pp.1039-1050.

Bagirov, A. M., & Mardaneh, K. (2006). Modified global k-means algorithm for clustering in gene expression data sets. WISB '06 Proceedings of the 2006 workshop on Intelligent systems for bioinformatics (73) 23.

Bennett, K. P., & Demiriz, A. (1998). Semi-supervised support vector machines., In D. A. Cohn M. S. Kearns, S. A. Solla, editor, Advances in Neural Information Processing Systems -10-, pp. 368-374, Cambridge, MA, MIT Press.

Blum, A., & Mitchel, T. (1998). Combining labeled and unlabeled data with co-training. COLT' 98 Proceedings of the eleventh annual conference on Computational learning theory, Pages 92-100, Madison, Wisconsin, USA.

Bruzzone, L., Chi, M., & Marconcini, M. (2006). A Novel Transductive SVM for Semisupervised Classification of Remote-Sensing Images. IEEE Transactions on Geoscience and remote sensing, vol. 44, no. 11, November.

Chinaei, L. (2007). Active Learning with Semi-Supervised Support Vector Machines. (Master dissertation). Computer Science Waterloo, Ontario, Canada.

Driessens, K., Reutemann, P., Pfahringer, B., Leschi, L. (2006). Using weighted nearest neighbor to benefit from unlabeled data. In: Advances in Knowledge Discovery and Data Mining, 10th Pacific-Asia Conference, 2006, 60-69.

Garner, S. (1995). Weka: The Waikato environment for knowledge analysis. In Proceedings of the New Zealand Computer Science Research Students Conference, pages 57-64.

Gasimov, R.N., & Öztürk, G. (2006). Separation via Polyhedral Conic Functions. Optimization Methods and Software 21(4)527.

Hajmohammadi, M. S., Ibrahim, R., Selamat, A., & Fujita, H. (2015). Combination of active learning and self-training for cross-lingual sentiment classification with density analysis of unlabeled samples. Information Sciences 317, 67–77.

Kanga, P., Kimb, D., & Choc, S. (2016). Semi-supervised support vector regression based on self –training with label uncertainty: An application to virtual metrology in semi-conductor manufacturing. Expert Systems With Applications 5185–106.

Kohavi, R. (1995). A study of cross-validation and bootstrap for accuracy estimation and model selection. International Joint Conference on Artificial Intelligence, San Francisco, 1137.

Laorden, C., Sanz, B., Santos, I., Galan-Garcia, P. & Bringas, P. G. (2013). Collective classification for spam filtering. Logic Journal of the IGPL 21 (4), 540-548.

Levatic, J., Dzeroski, S., Supek, F. & Smuc, T. (2013). Semi-Supervised Learning for Quantitative Structure-Activity Modeling. Informatica 37 (2013) 173–179.

Lichman, M. (2013). UCI Machine Learning Repository Irvine, CA: University of California, School of Information and Computer Science. [http://archive.ics.uci.edu/ml].

Neville, T., & Lensen, D. (2003). Collective classification with relational dependency networks. In Proceedings of the Workshop on Multi-Relational Data Mining (MRDM).

Ordin, B. (2010). Nonsmooth Optimization algorithm for semi-supervised data classification. Dynamics of Continuous, Discrete and Impulsive Systems Series B: Applications & Algorithms 17, 741-749.

Öztürk, G., & Çitfçi, M. (2015). Clustering Based Polyhedral Conic Functions Algorithm in Classification. Journal of Industrial and Management Optimization, Doi:10.3934/jimo.2015.11.921, Volume 11, Number 3, July.

Pfahringer B., Leschi C. & Reutemann P. (2007). Scaling Up Semi-supervised Learning: An Efficient and Effective LLGC Variant. In: Zhou ZH., Li H., Yang Q. (eds) Advances in Knowledge Discovery and Data Mining. PAKDD 2007. Lecture Notes in Computer Science, vol 4426. Springer, Berlin, Heidelberg.

Santas, I., Laorden, C. & Bringas, P. (2011). Collective classification for unknown malware detection, Proceedings of the International Conference on Security and Cryptography (SECRYPT), ISBN: 978-989-8425-71-3, Seville, Spain.

Sigdel, M., Dinç, İ., Dinç, S., Sigdel, M. S., Pusey, M. L. & Aygün, R. S. (2014) Evaluation of Semi-supervised Learning for Classification of Protein Crystallization Imagery, Proc IEEE Southeastcon, doi: 10.1109/SECON.2014.6950649

Uylaş N. (2013). Methods based on mathematical optimization for data classification, (Doctoral dissertation), Ege University Institute of Natural and Applied Sciences.

Uylas Sati N. (2015). A Binary Classification Algorithm Based on Polyhedral Conic Functions. Düzce University Journal of Science and Technology, 3, pp. 152-161.

Uylas Sati N. (2016). A Binary Classification Approach Based On Support Vector Machines Via Polyhedral Conic Functions. Celal Bayar University Journal of Science, Volume 12, Issue 2, pp. 135-149.

Uylaş Satı, N. (2018). A Collective Learning Approach for Semi-Supervised Data Classification, Pamukkale University Journal of Engineering Sciences, Vol.24, No.5, pp. 864-869

Uylaş Satı, N. (2020). A novel semisupervised classification method via membership and polyhedral conic functions, Turkish Journal of Electrical Engineering and Computer Sciences, Vol.28, No.1, pp. 80-92

Van Engelen, J.E. & Hoos, H.H. (2020). A Survey on Semi-Supervised Learning, Machine Learning, vol. 109, pp.373–440

Zha, Z. J., Mei, T., Wang, J., Wang, Z., & Hua X. S. (2009). Graph-based semi-supervised learning with multiple labels. J. Vis. Commun. Image R. 20, 97–103.

Zhou, D., Bousquet, O., Lal. T.N., Weston, J., & Schoelkopf, B. (2003). Learning with Local and Global Consistency. In: Advances in Neural Information Processing Systems 16.

Zhou, Z., & Li M. (2007). Semi supervised Regression with Co-training-Style Algorithms. Journal IEEE Transactions on Knowledge and Data Engineering archive. Volume 19 Issue 11, November, Pages 1479-1493.

Zhu, X. (2008). Semi-Supervised Learning Literature Survey. Computer Sciences TR 1530 University of Wisconsin – Madison, Last modified on July 19.

DECLARATIONS

This study is presented in "Ispec 10th International Conference on Engineering & Natural Sciences 16-18 may / 2021"[2]

[2] Nur Uylaş Satı,'A Binary Semi-Supervised Data Classification Technique With Polyhedral Conic Functions', Ispec 10th International Conference on Engineering & Natural Sciences 16-18 may / 2021 Siirt University (The Proceedings Book),ed. Dr. Ethem İlhan ŞAHİN, ISPEC Publications – 2021, 42.

CHAPTER 2

CHIRPED SOLITARY-PULSE SOLUTIONS OF THE SEMICLASSICALY SCALED MODIFIED NONLINEAR SCHRÖDİNGER EQUATION[1]

Mustafa MIZRAK[2]

[1] This study was presented as oral presentation at ISPEC 10th International Engineering and Science Congress held in Siirt on 16-18 May 2021.

[2]Asst. Prof. Dr. , Şırnak University, Faculty of Engineering, Department of Computer Engineering, Şırnak, Turkey, mmizrak@sirnak.edu.tr
ORCID: 0000-0003-0783-0675

INTRODUCTION

Recently, many scientists have been keen to studying the nonlinear Schrödinger (NSL) equation, which has many applications in optical fibres, plasma and other science and engineering fields. Basically, the NSL equation defines the propogation of an optical ulse in a Kerr law or non-Kerr law environment [1]. The NSL equation is familiar nonlinear partial differential equation that describes the evolution of optical solitons in fiber [2].

Optical solitons in a fiber are pulses emitted without any change in pulse shape or intensity. Because of their outsanding stability properties, optical solitons are now at the center of an active research area of nonlinear wave propogation in optical fibers. The first studies in this area were done by Hasegawa and Tappert [3].

Recently, chirping solitons is one of the interesting wave phenomena. Chirp means chirping sound of birds. For instance, in optical transmission systems, ultra short pulses can show chirp that can interact with the dispersion properties of the substances in which they spread to spectrum communication and some devices such as sonar and radar [4].

Nonlinear terms of the modified nonlinear Schrödinger equation consist of a cubic term and a derivative cubic term which demonstrate the short pulse in long single mode optical fibers, considering the natural characteristic of the asymmetric output pulse spectrum.

This paper is concerned with the semiclassically scaled modified nonlinear Schrödinger equation:1

$$i\alpha q_t + \frac{1}{2}\alpha^2 q_{xx} + |q|^2 q + i\alpha\beta\left(|q|^2 q\right)_x = 0, \qquad \alpha, \beta > 0, \qquad (1)$$

which can be thought as a perturbation (with perturbation parameter β)of the NSL equation [5-9].

MATHEMATICAL ANALYSIS

It is of aim to find exact chirped soliton solutions of the semicalssically scaled modified nonlinear Schrödinger equation. Firstly, we want to find traveling-wave solutions of Eq.(1) in the form [10-14]

$$q(x,t) = \rho(\xi) e^{i(\chi(\xi) - \omega t)}, \qquad (2)$$

where $\xi = kx - vt$, the amplitude and the phase functions denoted by $\rho = \rho(\xi)$ and $\chi = \chi(\xi)$, respectively. In addition, v and ω indicate the wave velocity and the frequency of the wave oscillation, respectively. The chirp is defined by

$$\delta\omega(x,t) = -\frac{\partial}{\partial t}[\chi(\xi) - \omega t] = -\chi'(\xi). \qquad (3)$$

By Eq.(2) placed in Eq.(1), the real and imaginary parts provide a pair of relations in two dependent varibles ρ and χ . Real part is equal to

$$\rho^3+\rho\alpha\omega+\alpha v\rho\chi'-\frac{1}{2}\alpha^2k^2\rho(\chi')^2+\frac{1}{2}\alpha^2k^2\rho''=0, \qquad (4)$$

while imaginary part deducible as

$$\alpha^2k^2\rho'\chi'+\frac{1}{2}\alpha^2k^2\rho\chi''-\alpha v\rho'+3k\alpha\beta\rho^2\rho'=0, \qquad (5)$$

where primes express the differentiations with respect to ξ. Mutiplying Eq.(5) by ρ and integrating once, the following equation is obtained:

$$\chi'=\frac{v}{\alpha k^2}+\frac{2A}{\alpha^2k^2\rho^2}-\frac{3\beta\rho^2}{2\alpha k}, \qquad (6)$$

where A is integration constant. Therefore, the resulting chirp is obtained as:

$$\delta\omega=-\frac{v}{2k^2}-\frac{A}{k^2\rho^2}+\frac{3\delta\rho^2}{2k}, \qquad (7)$$

which indicates the chirping has two intensity dependent chirping terms. When Eq.(6) substituing in Eq.(4) gets

$$-\frac{2A^2}{k^2\alpha^2\rho^3}+\left(\frac{v^2}{2k^2}+\frac{3A\beta}{\alpha k}+\alpha\omega\right)\rho+\rho^3-\frac{9k^2\alpha^2\beta^2}{8\alpha k^2}\rho^5+\frac{1}{2}k^2\alpha^2\rho''=0. \qquad (8)$$

Multiplying Eq.(8) by ρ' and integrating with respect to ξ, we have

$$(\rho')^2=\frac{4B}{k^2\alpha^2}-\frac{4A^2}{k^4\alpha^4\rho^2}-\left(\frac{v^2}{k^4\alpha^2}+\frac{6A\beta}{k^3\alpha^3}+\frac{2\omega}{k^2\alpha}\right)\rho^2-\frac{\rho^4}{k^2\alpha^2}+\frac{3\beta^2}{4\alpha k^2}\rho^6. \qquad (9)$$

where B is second integration constant.

Eq.(9) describes the evolution of wave amplitude in nonlinear environment that governed by Eq.(1).

2. CHIRPED SOLITON SOLUTIONS

We offer distinct chirping soliton solutions for the Eq.(1) under different parametric conditions. Before finding exact solutions to Eq.(9), by changing variables of amplitude function of the form

$$\rho^2(\xi) = U(\xi)\ , \tag{10}$$

Thus, Eq.(9) converts the following auxiliary elliptic equation [15-20]:

$$(U')^2 = a_0 + a_1 U + a_2 U^2 + a_3 U^3 + a_4 U^4, \tag{11}$$

where

$$a_0 = -\frac{16A^2}{k^4\alpha^4}, a_1 = \frac{16B}{k^2\alpha^2}, a_2 = -\frac{4v^2}{k^4\alpha^2} - \frac{24A\beta}{k^3\alpha^3} - \frac{8\omega}{k^2\alpha}, a_3 = -\frac{4}{k^2\alpha^2}, a_4 = \frac{3\beta^2}{\alpha k^2}. \tag{12}$$

2.1. Bright soliton solutions

We obtained three types of bright soliton solutions for Eq.(11) under the following parametric conditions:

1st case: For $a_0 = a_1 = a_3 = 0,\ a_2 > 0,\ a_4 < 0,\ \ \varepsilon = \pm 1$ **;** so, Eq.(11) has a bright soliton solution:

$$U(\xi) = \varepsilon \sqrt{-\frac{a_2}{a_4}}\ \mathrm{sech}\left(\sqrt{a_2}\xi\right). \tag{13}$$

Based on above finding, we get the first chirped bright soliton solution for Eq.(1) of the form

$$q(x,t)=\left[\varepsilon\sqrt{-\frac{a_2}{a_4}}\,\mathrm{sech}\left(\sqrt{a_2}\xi\right)\right]^{\frac{1}{2}}e^{i\left[\chi(\xi)-\omega t\right]}. \qquad (14)$$

The corresponding chirping is given by

$$\delta\omega=-\frac{v}{2k^2}-\sqrt{-\frac{a_4}{a_2}}\,\frac{\varepsilon A}{k^2\,\mathrm{sech}\left(\sqrt{a_2}\xi\right)}+\frac{3\varepsilon\delta}{2k}\sqrt{-\frac{a_2}{a_4}}\,\mathrm{sech}\left(\sqrt{a_2}\xi\right). \qquad (15)$$

2nd case: For $a_0=a_1=a_4=0,\ a_2>0,\ a_3<0$;after that, Eq.(11) has a bright soliton solution:

$$U(\xi)=-\frac{a_2}{a_3}\mathrm{sech}^2\left(\frac{\sqrt{a_2}}{2}\xi\right). \qquad (16)$$

By using above findings , we can show the second family of chirped bright soliton solution of Eq.(1) as

$$q(x,t)=\left[-\frac{a_2}{a_3}\mathrm{sech}^2\left(\frac{\sqrt{a_2}}{2}\xi\right)\right]^{\frac{1}{2}}e^{i\left[\chi(\xi)-\omega t\right]}\ , \qquad (17)$$

and corresponding chirping is of the form

$$\delta\omega=-\frac{v}{2k^2}+\frac{a_3A}{k^2a_2\,\mathrm{sech}^2\left(\frac{\sqrt{a_2}}{2}\xi\right)}-\frac{3\delta a_2}{2ka_3}\mathrm{sech}^2\left(\frac{\sqrt{a_2}}{2}\xi\right). \qquad (18)$$

3rd case: For $a_0=a_1=0,\ a_2>0,$ in that case Eq.(11) has a bright soliton solution

$$U(\xi)=\frac{2a_2}{\varepsilon\sqrt{\Delta}\cosh\left(\sqrt{a_2}\xi\right)-a_3},\qquad \Delta=a_3^2-4a_2a_4>0,\quad \varepsilon=\pm1. \tag{19}$$

In the light of these results, we get the following chirped bright soliton solution for Eq.(1):

$$q(x,t)=\left[\frac{2a_2}{\varepsilon\sqrt{\Delta}\cosh\left(\sqrt{a_2}\xi\right)-a_3}\right]^{\frac{1}{2}}e^{i\left[\chi(\xi)-\omega t\right]}. \tag{20}$$

The corresponding chirp is found as

$$\delta\omega=-\frac{v}{2k^2}-\frac{A\left(\varepsilon\sqrt{\Delta}\cosh\left(\sqrt{a_2}\xi\right)-a_3\right)}{2a_2k^2}+\frac{3\delta a_2}{k\left(\varepsilon\sqrt{\Delta}\cosh\left(\sqrt{a_2}\xi\right)-a_3\right)}. \tag{21}$$

2.2. Dark soliton solutions

We get three types of dark soliton solutions for Eq.(11) under the following parametric conditions:

1st case: For $a_1=a_3=0,\ a_0=\frac{a_2^2}{4a_4},\ a_2<0,\ a_4>0,\ \varepsilon=\pm1$, so, Eq.(11) has a dark soliton solution:

$$U(\xi)=\varepsilon\sqrt{-\frac{a_2}{2a_4}}\tanh\left(\sqrt{-\frac{a_2}{2}}\xi\right). \tag{22}$$

Thus, the first chirped dark soliton solution to the Eq.(1) is given as

$$q(x,t)=\sqrt{\varepsilon\sqrt{-\frac{a_2}{2a_4}}\tanh\left(\sqrt{-\frac{a_2}{2}}\xi\right)}e^{i[\chi(\xi)-\omega t]}\ . \qquad (23)$$

The corresponding chirping is given by

$$\delta\omega=-\frac{v}{2k^2}-\sqrt{-\frac{2a_4}{a_2}}\frac{A}{\varepsilon k^2\tanh\left(\sqrt{-\frac{a_2}{2}}\xi\right)}+\frac{3\varepsilon\delta}{2k}\sqrt{-\frac{a_2}{2a_4}}\tanh\left(\sqrt{-\frac{a_2}{2}}\xi\right). \quad (24)$$

2nd case: For $a_0=a_1=0,\ a_2>0,\ a_4>0,\ a_3=-2\sqrt{a_2a_4},\ \varepsilon=\pm1,$ after that, Eq.(11) has a dark soliton solution:

$$U(\xi)=\frac{1}{2}\sqrt{\frac{a_2}{a_4}}\left[1+\varepsilon\tanh\left(\frac{1}{2}\sqrt{a_2}\xi\right)\right]. \qquad (25)$$

The second family of chirped dark soliton solution of Eq.(1) as

$$q(x,t)=\sqrt{\frac{1}{2}\sqrt{\frac{a_2}{a_4}}\left[1+\varepsilon\tanh\left(\frac{1}{2}\sqrt{a_2}\xi\right)\right]}e^{i[\chi(\xi)-\omega t]}, \quad (26)$$

and corresponding chirping is of the form

$$\delta\omega=-\frac{v}{2k^2}-\sqrt{\frac{a_4}{a_2}}\frac{2A}{k^2\left(1+\varepsilon\tanh\left(\frac{1}{2}\sqrt{a_2}\xi\right)\right)}+\frac{3\delta}{4k}\sqrt{\frac{a_2}{a_4}}\left(1+\varepsilon\tanh\left(\frac{1}{2}\sqrt{a_2}\xi\right)\right). \quad (27)$$

3rd case: For $a_0=a_1=0,\ a_2>0,$ in that case Eq.(11) has a dark soliton solution:

$$U(\xi)=\frac{2a_2}{\varepsilon\sqrt{\Delta}\cosh\left(\sqrt{a_2}\xi\right)-a_3},\qquad \Delta=a_3^2-4a_2a_4>0,\quad \varepsilon=\pm1. \quad (28)$$

Hence, we get the following chirped dark soliton solution for Eq.(1):

$$q(x,t)=\left[\frac{2a_2}{\varepsilon\sqrt{\Delta}\cosh\left(\sqrt{a_2}\xi\right)-a_3}\right]^{1/2} e^{i\left[\chi(\xi)-\omega t\right]}. \quad (29)$$

For this case, corresponding chirping is obtained as

$$\delta\omega=-\frac{v}{2k^2}-\frac{A\left(\varepsilon\sqrt{\Delta}\cosh\left(\sqrt{a_2}\xi\right)-a_3\right)}{2a_2k^2}+\frac{3\delta a_2}{2k\left(\varepsilon\sqrt{\Delta}\cosh\left(\sqrt{a_2}\xi\right)-a_3\right)}. \quad (30)$$

2.3. Periodic soliton solutions

We found three types of periodic soliton solutions for Eq.(11) by the following parametric conditions:

1st case: For $a_0=a_1=a_3=0,\ a_2<0,\ a_4>0,\ \varepsilon=\pm1,$ so,Eq.(11) has a periodic soliton solution

$$U(\xi)=\varepsilon\sqrt{-\frac{a_2}{a_4}}\sec\left(\sqrt{-a_2}\xi\right). \quad (31)$$

We get the following chirped periodic soliton solution for Eq.(1):

$$q(x,t)=\left[\varepsilon\sqrt{-\frac{a_2}{a_4}}\sec\left(\sqrt{-a_2}\xi\right)\right]^{1/2} e^{i\left[\chi(\xi)-\omega t\right]}. \quad (32)$$

The chirping is given as

$$\delta\omega = -\frac{v}{2k^2} - \sqrt{-\frac{a_4}{a_2}}\,\frac{\varepsilon A}{k^2 \sec\left(\sqrt{-a_2}\,\xi\right)} + \frac{3\varepsilon\delta}{2k}\sqrt{-\frac{a_2}{a_4}}\sec\left(\sqrt{-a_2}\,\xi\right). \quad (33)$$

2nd case: For $a_1 = a_3 = 0,\ a_0 = \frac{a_2^2}{4a_4},\ a_2 > 0,\ a_4 > 0,\ \ \varepsilon = \pm 1$, after that, Eq.(11) has a periodicsoliton solution:

$$U(\xi) = \varepsilon\sqrt{-\frac{a_2}{2a_4}}\tan\left(\sqrt{\frac{a_2}{2}}\xi\right). \quad (34)$$

Then we get the following chirped periodic soliton solution for Eq.(1):

$$q(x,t) = \left[\varepsilon\sqrt{-\frac{a_2}{2a_4}}\tan\left(\sqrt{\frac{a_2}{2}}\xi\right)\right]^{1/2} e^{i\left[\chi(\xi)-\omega t\right]}. \quad (35)$$

The chirping is given as

$$\delta\omega = -\frac{v}{2k^2} - \sqrt{-\frac{2a}{a_2}}\,\frac{\varepsilon A}{k^2\tan\left(\sqrt{\frac{a_2}{2}}\xi\right)} + \frac{3\varepsilon\delta}{2k}\sqrt{-\frac{a_2}{2a_4}}\tan\left(\sqrt{\frac{a_2}{2}}\xi\right). \quad (36)$$

3rd case: For $a_0 = a_1 = a_4 = 0,\ a_2 < 0,\ a_4 > 0$, in that case Eq.(11) has a periodic soliton solution:

$$U(\xi) = -\frac{a_2}{a_3}\sec^2\left(\frac{\sqrt{-a_2}}{2}\xi\right). \quad (37)$$

We have the following chirped periodic soliton solution for Eq.(1):

$$q(x,t)=\left[-\frac{a_2}{a_3}\sec^2\left(\frac{\sqrt{-a_2}}{2}\xi\right)\right]^{1/2} e^{i\left[\chi(\xi)-\omega t\right]}. \qquad (38)$$

And corresponding chirping is found as

$$\delta\omega=-\frac{v}{2k^2}+\frac{a_3A}{a_2k^2\sec^2\left(\frac{\sqrt{-a_2}}{2}\xi\right)}-\frac{3\delta a_2}{2ka_3}\sec^2\left(\frac{\sqrt{-a_2}}{2}\xi\right). \qquad (39)$$

3. CONCLUSIONS

In this study, we have obtained chirped bright, dark and periodic soliton solutions for the semiclassically scaled modified nonlinear Schrödinger equation. Next introducing a new antsatz which including a new form of chirping, the solutions searched for a general fourth order elliptic equation containing many parameters.

It has been shown that the wave amplitude satisfies a nonlinear differential equation containing two integration constants such that ca be easily obtained by initial parameters of the wave. We solved the resulting amplitude equation analytically and obtained findings for bright, dark and periodic soliton solutions. We have identified the nonlinear chirpassociated with each of these soliton solutions.

REFERENCES

[1] Zayed, E.M.E., Alngar, M.E.M. (2020). Application of newly proposed sub-ODE method to locate chirped optical solitons to Triki–Biswas equation, Optik - International Journal for Light and Electron Optics , 207, 1643

[2] Zulfiqar, A. and Jamshad Ahmad, J. (2020). Soliton Solutions of Fractional Modified Unstable Schrödinger Equation Using Exp-Function Method, Results in Physics , 19, 103476.

[3] Mihalache, D et al. (1993). Analytic method for solving the modified nonlinear Schrodinger equation describing soliton propagation along optical fibers, Physical Review A ,Volume 47, Number 4 April 1993.

[4] Mibaile, J. et al. (2018). Chirped solitons in derivative nonlinear Schrödinger equation, Chaos, Solitons and Fractals, 107, pp. 49-54.

[5] DiFranco, J.C. , Miller, P. D. and Muite, B. K. (2011). On The Modified Nonlinear Schrödinger Equation in the Semiclassical Limit: Supersonic, Subsonic, and Transsonic Behavior, Acta Mathematica Scientia 2011, 31B(6):2343-2377.

[6] Chen, Z.Y. and Huang, N.N. (1989). Method of Meromorphic Matrix of Transformation For Giving Soliton Solutions of The Modified Nonlinear Schrodinger Equation, Physics Letters A, Volume 142, Number 1, 27 November 1989.

[7] Doktorov, E. V. and Shchesnovich, V. S. (1995). Modified nonlinear Schrödinger equation: Spectral transform and N-soliton solution, Journal of Mathematical Physics , 36, 7009.

[8] Ding, Q. and Zhu, Z. (2002). On the gauge equivalent structure of the modified nonlinear Schrödinger equation, Physics Letters A , 295, pp.192-197.

[9] Wang, H.T. et al. (2019). Modulational instability, interactions of localized wave structures and dynamics in the modified self-steepening nonlinear Schrödinger equation, Wave Motion, 91, 10239.

[10] Serge, D. Y. et al. (2017). Optical chirped soliton in metamaterials, Nonlinear Dyn, 90, pp.13-18.

[11] Triki, H. et al. (2017). New envelope solitons for Gerdjikov-Ivanov model in nonlinear fiber optics, Superlattices and Microstructures ,111, pp.326-334.

[12] Biswas, A. et al. (2018). Sub-pico-second chirped optical solitons in mono-mode fibers with Kaup-Newell equation by extended trial function method, Optik ,168, pp. 208-216.

[13] Daoui , A.K. et al. (2019). Propagation of chirped gray optical dips in nonlinear metamaterials, Optics Communications, 430, pp. 461-466.

[14] Triki, H. et al. (2019). Chirped envelope optical solitons for Kaup–Newell equation, Optik - International Journal for Light and Electron Optics,177, pp. 1-7.

[15] Zayed, E.M.E., and Alngar, M.E.M. (2020). Application of newly proposed sub-ODE method to Locate chirped optical solitons to Triki-Biswas equation, Optik - International Journal for Light and Electron Optics, 207, 1643

[16] Zayed, E.M.E. et al. (2020). Chirped and chirp-free optical solitons in fiber Bragg grating having dispersive reflectivity with polynomial form of nonlinearity using sub-ODE approach, Optik, 204 , 164096.

[17] Xu, G. (2014). Extended auxiliary equation method and its applications to three generalized NLS equations, Abst. Appl. Anal. , Article ID 541370, 7 pp.

[18] Ali, A.T. (2011). New generalized Jacobi elliptic function rational expansion method, J. Comput. Appl. Math., 235, pp. 4117-4127.

[19] Li-Hua, Z. and Jin-Yu, H. (2009). Sub-ODE's new solutions and their applications to two nonlinear partial differential equations with higher-order nonlinear terms, Commun.Theor. Phys., 52, pp.773-778.

[20] Zeng, X. and Yong, X. (2008). A new mapping method and its applications to nonlinear partial differential equations, Phys. Lett. A , 372, pp. 6602-6607.

CHAPTER 3

INVESTIGATION OF NULL CURVES ACCORDING TO DIFFERENTIAL GEOMETRY AND PHYSICAL FIELDS

Rıdvan EZENTAŞ [1] & Esen İYİGÜN[2]

[1] Prof.Dr., Bursa Uludag University, Faculty of Education, Department of Mathematics and Science Education, Bursa, Turkey. rezentas@uludag.edu.tr
ORCID: 0000-0001-8619-8334
[2] Prof.Dr., Bursa Uludag University, Faculty of Art & Science, Department of Mathematics, Bursa, Turkey. esen@uludag.edu.tr
ORCID: 0000-0001-6821-0248

INTRODUCTION

A vector is expressed in terms of direction, direction, and magnitude. A zero vector that does not have a magnitude but can have a direction is called a null vector. If the length of the velocity vector of a curve is zero then this curve is called a null curve [30]. For more than a century, mathematicians have studied the fundamental characters of null vectors and null curves. They then played an important role in the development of the basic branches of Physics, based on Mathematics, Geometry and, in particular, Classical Physics and Quantum field theories [7].

The symmetric, two-linear, non-positively defined inner product on an n-dimensional manifold g(,) Lorentz metric, the size of the maximal dimensional subspace in which this inner product is negatively defined is called the index of the manifold. Riemannian manifold (R^n Euclidean n-space) in 0-indexed manifold, the 1-indexed manifold with n≥2 is called the Lorentz manifold (R_1^n Semi-Euclidean space with index 1). In the k-indexed manifold, it is called R_1^n Semi-Euclidean n-space with index k.

When the literature in the fields of mathematics and physics is examined, there are some studies that usually involve spinors and spinning particles for null curves in R_1^4 [28, 34]. In 1913, E. Cartan discovered spinors in search of new representations of spin groups. In 1938, E. Cartan named null vectors and equivalence structures in completely null planes "simple spinors". E. Cartan also defined Cartan

transformations between the directions of spinors and completely null planes. It has been observed that these Cartan transforms play an important role in studies in Mathematics and Physics where null vectors and spinors are used. Spinors are mathematical expressions that remain constant under rotation, similar to tensors. Here, each k-rank tensor corresponds to a 2k-rank spinors. For example, for each vector in R_1^4, a spinors of 2x2 type, denoted by a Hermitian matrix of rank 2, corresponds [34].

One of the topics that has been studied for a long time is the study of spinning particles under quantization. The most popular approach is to symmetrical the relative particle model that corresponds to the optimal time of the spinning particle path. The double of the spinning particle that can be made symmetrical is called the massive spinning particle. It is known that there is a geometric particle model based on the geometry of null curves in R_1^4. There are also wave equations corresponding to massive spinning particles in complete or incomplete turns [28]. Barros, Ferrandez, Javaloyes and Lucas created the geometry of relative particles due to torsion in R_v^d [4]. Ferrandez, Gimenez, Lucas gave the relationship of the geometry of null curves and relative particles in R_1^4 [14]. Samuel and Nityananda established a law of transport along non-geodesic null curves between pole vectors [33].

The most general definitions of null curves were first given by Enneper and Weitrass in R^3 and by Eisenhart in R^4 [12, 38, 13]. There are many studies on null curves and Cartan null curves in the field of

mathematics. Duggal and Jin gave the most general definitions of null curves and Cartan null curves in the Semi-Euclidean space [11]. Çöken and Çiftçi reconstructed the Cartan roofs of null curves and Bertrand null curves in R_1^4 [10]. Aslaner and Boran created the geometry of null curves in R_1^4 [3]. In the following studies, Sanlı and Yaylı found the relationships between Cartan null curves and their indicators in R_1^4 [35]. Akgün and Sivridağ created state vectors of Cartan null curves in R_1^4 and R_2^4 [1]. İyigün investigated the relationships between the Frenet equations and harmonic curves of a null curve in R_1^4 [16]

İyigün obtained generalized null helices by finding the harmonic curvatures of the null curve with osculator order 5 in R_1^5 using a Frenet framework consisting of 3 null and 2 spacelike vectors [17]. İyigün describes CCR-curves and harmonic curves in R_1^4 [18]. İyigün obtained the Darboux vectors and Darboux vertices of a non-null Frenet curve in R_1^4 [19]. Iyigün gave the characterization of generalized null helices in R_1^6 using a Frenet framework consisting of 2 null and 4 timelike vectors [20].

İyigün worked on a unit-speed pseudo-null curve in the R_2^4 and obtained its image in pseudo hyperbolic space [21]. Uçum, Keçioğlu and İlarslan worked on generalized semi-null Bertrand curves in R_2^4 and then Uçum, İlarslan and Sasaki in R_2^4 (1 -3) Cartan null have obtained some special results on Bertrand curves [36, 37]. İyigün investigated Partially null curves and their harmonic curves in R_2^4.

İyigün investigated whether Pseudo null curves and Cartan null curves lie in some subspaces of this space in the R_2^4 [24]. İyigün gave some applications of null curves and generalized null helices in R_2^4 using a Frenet framework consisting of 2 null and 2 timelike vectors [25]. İyigün gave a characterization of hyperbolic Partially null curves in R_2^4 [26].

In this study, the definitions of Null, Pseudo, Partially and Cartan Null Curves in R_1^4 and R_2^4 are given and the differences between Null curves and Pseudo, Partially and Cartan Null Curves are shown. In addition, Spinors structure using null curves in R_1^4, which is a Physics application, is given.

NULL, PSEUDO, PARTİALLY AND CARTAN NULL CURVES IN R_1^4

Let the flat Lorentz metric $g = -dx_1^2 + dx_2^2 + dx_3^2 + dx_4^2$ be defined on the coordinate system $\{x_1, x_2, x_3, x_4\}$ in R_1^4. A vector $u = (u_1, u_2, u_3, u_4)$ is called spacelike if $g(u,u) > 0$, timelike if $g(u,u) < 0$, null if $g(u,u) = 0$ and $u \neq 0$. The norm of the vector u is defined as $\|u\| = \sqrt{|g(u,u)|}$. If $g(u,u) = 1$ then u is called a unit vector. The angle between two spacelike vectors u and w in R_1^4 is calculated by $g(u,w) = \|u\|\|w\|cos\theta$, $(0 \leq \theta \leq \pi)$ and if $g(u,w) = 0$, these two vectors are called orthogonal to each other.

For the $s \in I$ parameter of the $\alpha: I \subset R \to R_1^4$ curve, where the velocity vector is $\alpha'(s)$, the α curve is called the spacelike curve if

$g(\alpha'(s),\alpha'(s)) > 0$, timelike curve if $g(\alpha'(s),\alpha'(s)) < 0$, null curve if $g(\alpha'(s),\alpha'(s)) = 0$ and $\alpha'(s) \neq 0$, unit speed curve if $g(\alpha'(s),\alpha'(s)) = 1$ [21].

Let $\alpha: I \to R_1^4$ spacelike or timelike curve in R_1^4, and $g(\alpha'(s),\alpha'(s)) = \mp 1$ and $g(\alpha''(s),\alpha''(s)) = 1$ for $s \in I$ parameter. Consider the Frenet frame $\{T, N, B_1, B_2\}$ defined as T tangent vector, N normal vector, B_1 first binormal vector and B_2 second binormal vector [30].

Let the null curve α be the first, second and third Frenet curves k_1, k_2, k_3, respectively. Frenet equations for $k_1 = 1$,

$$\begin{bmatrix} T' \\ N' \\ B_1{}' \\ B_2{}' \end{bmatrix} = \begin{bmatrix} 0 & k_1 & 0 & 0 \\ k_2 & 0 & -k_1 & 0 \\ 0 & -k_2 & 0 & k_3 \\ -k_3 & 0 & 0 & 0 \end{bmatrix} \begin{bmatrix} T \\ N \\ B_1 \\ B_2 \end{bmatrix}$$

and the following conditions are satisfied [5].

$$g(N,N) = g(B_2,B_2) = g(T,B_1) = 1,$$

$$g(T,T) = g(T,N) = g(T,B_2) = g(N,B_1) = 0,$$

$$g(N,B_2) = g(B_1,B_1) = g(B_1,B_2) = 0.$$

If the Frenet equations are

$$\begin{bmatrix} T' \\ N' \\ B_1{}' \\ B_2{}' \end{bmatrix} = \begin{bmatrix} 0 & k_1 & 0 & 0 \\ 0 & 0 & k_2 & 0 \\ 0 & k_3 & 0 & -k_2 \\ -k_1 & 0 & -k_3 & 0 \end{bmatrix} \begin{bmatrix} T \\ N \\ B_1 \\ B_2 \end{bmatrix}$$

and

$$g(T,T) = g(B_1,B_1) = g(N,B_2) = 1,$$

$$g(T,N) = g(T,B_1) = g(T,B_2) = g(N,N) = 0,$$

$$g(N,B_1) = g(B_1,B_2) = g(B_2,B_2) = 0,$$

then the α curve is called a Pseudo null curve [6] .

If the Frenet equations are

$$\begin{bmatrix} T' \\ N' \\ B_1{}' \\ B_2{}' \end{bmatrix} = \begin{bmatrix} 0 & k_1 & 0 & 0 \\ -k_1 & 0 & k_2 & 0 \\ 0 & 0 & k_3 & 0 \\ 0 & -k_2 & 0 & -k_3 \end{bmatrix} \begin{bmatrix} T \\ N \\ B_1 \\ B_2 \end{bmatrix}$$

and

$$g(T,T) = g\big(g(N,N)\big) = g(B_1,B_2) = 1,$$

$$g(T,N) = g(T,B_1) = g(T,B_2) = g(N,B_1) = 0,$$

$$g(N,B_2) = g(B_1,B_1) = g(B_2,B_2) = 0,$$

then the α curve is called a Partially null curve [6].

If the Frenet equations are

$$\begin{bmatrix} T' \\ N' \\ B_1{}' \\ B_2{}' \end{bmatrix} = \begin{bmatrix} 0 & 0 & 1 & 0 \\ 0 & 0 & k_1 & k_2 \\ -k_1 & -1 & 0 & 0 \\ -k_2 & 0 & 0 & 0 \end{bmatrix} \begin{bmatrix} T \\ N \\ B_1 \\ B_2 \end{bmatrix}$$

ve

$$g(T,N) = \ g(B_1,B_1) = g(B_2,B_2) = 1,$$

$$g(T,T) = g(T,B_1) = g(T,B_2) = g(N,N) = 0,$$

$$g(N,B_1) = \ g(N,B_2) = g(B_1,B_2) = 0$$

then the α curve is called a Cartan null curve [1].

PSEUDO, PARTİALLY AND CARTAN NULL CURVES IN R_2^4

Let the indefinite metric $g = -dx_1^2 - dx_2^2 + dx_3^2 + dx_4^2$ be defined on the coordinate system $\{x_1, x_2, x_3, x_4\}$ in R_2^4. For the $s \in I$ parameter of the $\alpha: I \subset R \to R_2^4$ curve is called the spacelike curve or timelike curve if $g\big(\alpha'(s), \alpha'(s)\big) = \mp 1$, null curve if $g\big(\alpha'(s), \alpha'(s)\big) = 0$ [5].

Let us construct the Frenet framework $\{T, N, B_1, B_2\}$ where $\alpha: I \to R_2^4$ is the spacelike or timelike curve, $T = \alpha'$ tangent vector, $N = \alpha''$ normal vector, $B_1 = \frac{\alpha'''}{\|\alpha'''\|}$ is the first binormal vector and B_2 is the second binormal vector that satisfies

$$g(B_2, B_2) = 1,\ g(T, B_2) = g(N, B_2) = g(B_1, B_2) = 0.$$

Let α curve be the first, second and third Frenet curves k_1, k_2, k_3, respectively. If the Frenet equations are

$$\begin{bmatrix} T' \\ N' \\ B_1{}' \\ B_2{}' \end{bmatrix} = \begin{bmatrix} 0 & k_1 & 0 & 0 \\ 0 & 0 & k_2 & 0 \\ 0 & k_3 & 0 & -\varepsilon_2 k_2 \\ -\varepsilon_1 k_1 & 0 & -\varepsilon_2 k_3 & 0 \end{bmatrix} \begin{bmatrix} T \\ N \\ B_1 \\ B_2 \end{bmatrix}$$

and for $\varepsilon_1 \varepsilon_2 = -1$,

$$g(T, T) = \varepsilon_1 = \mp 1\ , g(B_1, B_1) = \varepsilon_2 = \mp 1,\ \ g(N, B_2) = 1,$$

$$g(T, N) = g(T, B_1) = g(T, B_2) = g(N, N) = 0$$

$$g(N, B_1) = g(B_1, B_2) = g(B_2, B_2) = 0$$

then the α curve is called a Pseudo null curve [32].

If the Frenet equations are

$$\begin{bmatrix} T' \\ N' \\ B_1{}' \\ B_2{}' \end{bmatrix} = \begin{bmatrix} 0 & k_1 & 0 & 0 \\ k_1 & 0 & k_2 & 0 \\ 0 & 0 & k_3 & 0 \\ 0 & -\varepsilon_2 k_2 & 0 & -k_3 \end{bmatrix} \begin{bmatrix} T \\ N \\ B_1 \\ B_2 \end{bmatrix}$$

and for $\varepsilon_1 \varepsilon_2 = -1$,

$$g(T, T) = \varepsilon_1 = \mp 1\ , g(N, N) = \varepsilon_2 = \mp 1,\ \ g(B_1, B_2) = 1,$$

$$g(T,N) = g(T,B_1) = g(T,B_2) = g(N,B_1) = 0,$$

$$g(N,B_2) = g(B_1,B_1) = g(B_2,B_2) = 0$$

then the α curve is called a Partially null curve [32].

If the Frenet equations are

$$\begin{bmatrix} T' \\ N' \\ B_1' \\ B_2' \end{bmatrix} = \begin{bmatrix} 0 & k_1 & 0 & 0 \\ -\varepsilon_1 k_2 & 0 & -\varepsilon_1 k_1 & 0 \\ 0 & k_2 & 0 & k_3 \\ -\varepsilon_2 k_3 & 0 & 0 & 0 \end{bmatrix} \begin{bmatrix} T \\ N \\ B_1 \\ B_2 \end{bmatrix}$$

and for $\varepsilon_1\varepsilon_2 = -1$,

$$g(N,N) = \varepsilon_1\,,\ g(B_2,B_2) = \varepsilon_2,\ \ g(T,B_1) = 1,$$

$$g(T,T) = g(T,N) = g(T,B_2) = g(N,B_1) = 0,$$

$$g(N,B_2) = g(B_1,B_1) = g(B_1,B_2) = 0$$

then the α curve is called a Cartan null curve [11].

The diagrams showing the differences between the conditions for a curve to be a null curve and the conditions for R_1^4 to be pseudo null, partially null and Cartan null are given below.

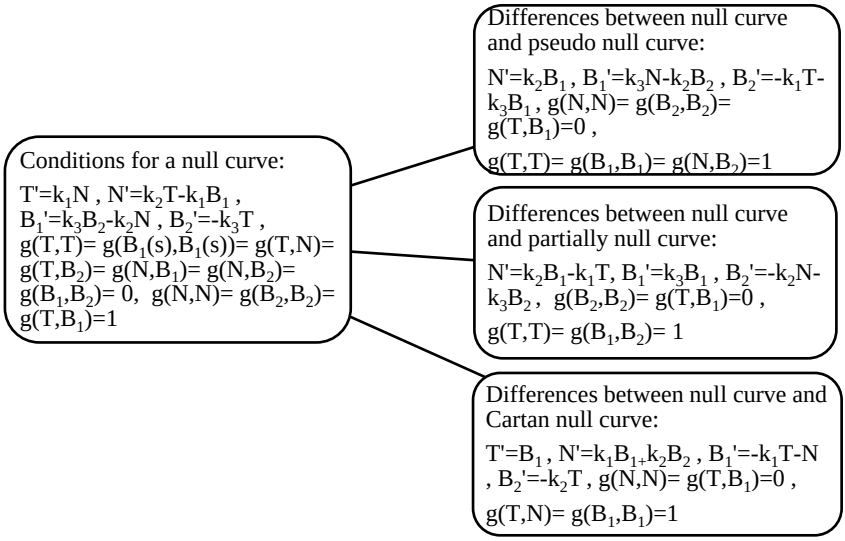

The diagrams showing the differences between the conditions for a curve to be a null curve and the conditions for R_2^4 to be pseudo null, partially null and Cartan null are given below.

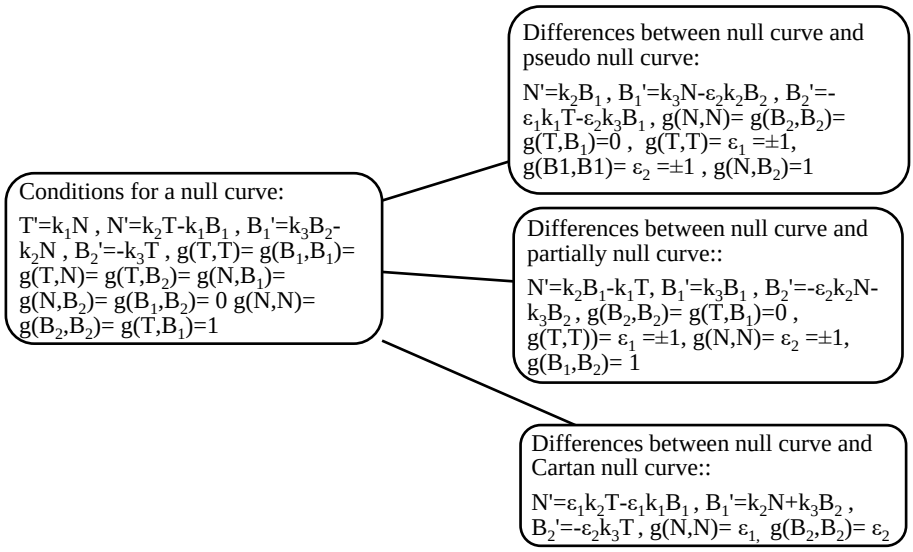

In R_1^4, the conditions required for a curve to be a pseudo null curve show some differences according to the null curve. These differences are

$$N' = k_2B_1, B_1{}' = k_3N - k_2B_2, B_2{}' = -k_1T - k_3B_1,$$

and

$$g(T,T) = g(B_1,B_1) = g(N,B_2) = 1,$$

$$g(N,N) = g(B_2,B_2) = g(T,B_1) = 0.$$

However, in R_1^4, the conditions for a curve to be a partially null curve contain some differences according to the null curve. Here,

$$N' = k_2B_1 - k_1T,\ {B_1}' = k_3B_1\ ,\ {B_2}' = -k_2N - k_3B_2\ ,$$

and

$$g(T,T) = g(B_1,B_2) = 1,$$

$$g(N,B_2) = \ g(B_2,B_2) = g(T,B_1) = 0.$$

In addition, the conditions required for a curve to be a Cartan null curve in R_1^4 contain serious differences according to the null curve. These are

$$T' = B_1,\ N' = k_1B_1 + k_2B_2\ ,\ {B_1}' = -k_1T - N,\ {B_2}' = -k_2T\ ,$$

and

$$g(T,N) = g(B_1,B_1) = 1,$$

$$g(T,B_1) = g(N,N) = 0.$$

There are also differences between a curve being a pseudo null curve and partially null in R_1^4. Frenet's equations are

$$N' = k_2B_1,\quad {B_1}' = k_3N - k_2B_2,\quad {B_2}' = -k_1T - k_3B_1$$

for a pseudo null curve and

$$N' = k_2B_1 - k_1T, \quad B_1{}' = k_3B_1 , \quad B_2{}' = -k_2N - k_3B_2$$

for a partially null curve. Also under metric conditions, pseudo null curve is

$$g(B_1, B_1) = g(N, B_2) = 1 , g(N, N) = g(B_1, B_2) = 0$$

while partially null curve is

$$g(N, N) = g(B_1, B_2) = 1 , \ g(B_1, B_1) = g(N, B_2) = 0.$$

The differences between the pseudo null curve and the Cartan null curve are, while the Frenet equations for the pseudo null curve are

$$N' = k_2B_1, B_1{}' = k_3N - k_2B_2, B_2{}' = -k_1T - k_3B_1,$$

for the Cartan null curve,

$$T' = B_1, \ N' = k_1B_1 + k_2B_2 , B_1{}' = -k_1T - N, B_2{}' = -k_2T.$$

Also under metric conditions, pseudo null curve is

$$g(B_1, B_1) = g(N, B_2) = 1 , g(N, N) = g(B_1, B_2) = 0$$

while partially null curve is

$$g(T, T) = 0 , \ g(B_2, B_2) = g(T, N) = 1.$$

However, the differences between Partially null curve and Cartan null curve are, Frenet equations for pseudo null curve are

$$N' = k_2B_1 - k_1T, B_1{}' = k_3B_1 \ , B_2{}' = -k_2N - k_3B_2$$

while for Cartan null curve

$$T' = B_1, \ N' = k_1B_1 + k_2B_2 \ , B_1{}' = -k_1T - N, B_2{}' = -k_2T.$$

And under metric conditions, partially null curve is

$$g(T,T) = g(N,N) = g(B_1,B_2) \ = 1,$$

$$g(B_1,B_1) = g(T,N) = \ g(B_2,B_2) = \ 0$$

while partially null curve is

$$g(T,T) = g(N,N) = g(B_1,B_2) \ = 0,$$

$$g(B_1,B_1) = g(T,N) = \ g(B_2,B_2) = \ 1.$$

The differences between the null curve in R_1^4 and the pseudo null, partially null and Cartan null curves in R_2^4 are as follows: In R_2^4, the conditions required for a curve to be a pseudo null curve show some differences according to the null curve in R_1^4. These differences are

$$N' = k_2B_1, B_1{}' = k_3N - -\varepsilon_2k_2B_2, B_2{}' = -\varepsilon_1k_1T - \varepsilon_2k_3B_1,$$

and

$$g(T,T) = \varepsilon_1 = \mp 1, \quad g(B_1,B_1) = \varepsilon_2 = \mp 1, \ \ g(N,B_2) = 1$$

$$g(N,N) = \ g(B_2,B_2) = \ g(T,B_1) = 0.$$

However, in R_2^4, the conditions for a curve to be a partially null curve contain some differences according to the null curve in R_1^4. Here,

$$N' = k_2B_1 + k_1T,\ {B_1}' = k_3B_1\ ,\ {B_2}' = -\varepsilon_2 k_2 N - k_3B_2\ ,$$

and

$$g(T,T) = \varepsilon_1 = \mp 1,\ g(N,N) = \varepsilon_2 = \mp 1,\ g(B_1,B_2) = 1$$

$$g(B_2,B_2) = g(T,B_1) = 0.$$

In addition, the conditions required for a curve to be a Cartan null curve in R_2^4 contain serious differences according to the null curve in R_1^4. These are

$$N' = -\varepsilon_1 k_2 T\ - \varepsilon_1 k_1 B_1\ ,\ {B_1}' = k_2N + k_3B_2\ ,\ {B_2}' = -\varepsilon_2 k_3 T,$$

and

$$g(N,N) = \varepsilon_1,\ g(B_2,B_2) = \varepsilon_2.$$

SPINORS

Spinors are mathematical expressions that remain constant under rotation, similar to tensors, and each k-rank tensor corresponds to a 2k-rank spinors. Spinors of rank 1 are represented by a two-component complex vector or by the angle and sign of a null 4-vector. The 4-vector here consists of a complex vector with 2 components, where *u* is a right-handed spinor,

$$V^{\mu} =< u/\sigma^{\mu} : u >$$

or $\tilde{u}$ is a left-handed spinor,

$$V^{\mu} =< \tilde{u}/\sigma^{\mu} : \tilde{u} > .$$

Any 2x2 type Λ matrix with unit determinant Lorenz-transformed a spinors. Such matrices can be written

$$\Lambda = e^{(i\sigma \cdot \frac{\theta}{2} - \sigma \cdot \frac{\rho}{2})}$$

where ρ is rapidity If Λ is a unitary transformation is a rotation in space; if Λ is Hermitian it is boost. If $s' = \Lambda(v)s$ then the Lorentz-transform is a spinors on the right, while the $\tilde{s}' = \Lambda(-v)\tilde{s}$, Lorentz-transform indicates a spinors on the left [34].

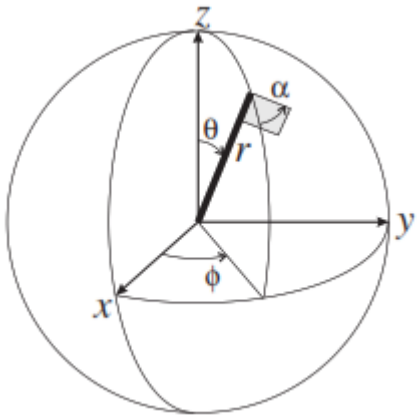

In the set given with $(r, \theta, \phi, \alpha)$ parameter in the figure, r in standard spherical coordinates indicates the length of the flagpole, θ and ϕ indicates the rotation angles, while α indicates only the direction of the flag. Here spinors

(flagpole) can rotate like a vector. The angles θ, ϕ, α change due to the rotational motion, while the length r of the spinor remains constant.

Let two complex numbers depending on the parameter $(r, \theta, \phi, \alpha)$ be defined as

$$a \equiv \sqrt{r} \cos\left(\frac{\theta}{2}\right) e^{\frac{i(-\alpha-\phi)}{2}},$$

$$b \equiv \sqrt{r} \sin\left(\frac{\theta}{2}\right) e^{\frac{i(-\alpha+\phi)}{2}}.$$

Accordingly, a two-component complex vector

$$\boldsymbol{s} = s e^{\frac{-i\alpha}{2}} \begin{pmatrix} \cos\left(\frac{\theta}{2}\right) e^{\frac{-i\phi}{2}} \\ \sin\left(\frac{\theta}{2}\right) e^{\frac{i\phi}{2}} \end{pmatrix}$$

shows a spinors.

Here the length of s spinors is equal to the length of the flagpole. A spinor of size s has a falagpole of lenght

$$r = |a|^2 + |b|^2 = s^2 \text{ [34].}$$

Examples of spinor with complex number representation are given in the Figure. Here, the north and south poles (1,0) and (0,1) standard base vectors are placed. A turn along angle θ_r in complex space corresponds to a rotation along an angle $2\theta_r$ in the 3 dimensional real

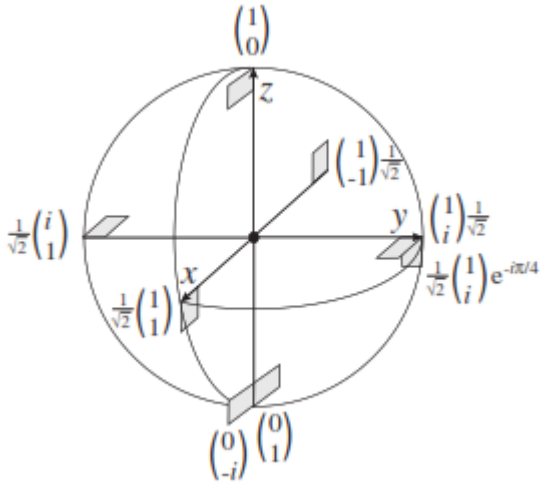

space. One revolution around the z-axis corresponds to a diagonal matrix. Take the spinor (1, 1) positively directed along the x-axis. The angle φ will increase by the angle θ_r for one turn around z. Accordingly, the rotation matrix of the spinor along the angle θ_r around the z-axis is denoted by

$$\begin{pmatrix} e^{\frac{-i\theta_r}{2}} & 0 \\ 0 & e^{\frac{i\theta_r}{2}} \end{pmatrix}.$$

SPINORS IN $\mathbf{R_1^4}$

Let $\alpha: I \to R_1^4$ be a spacelike curve and for $s \in I$ $\{T, N, B_1, B_2\}$ be the Frenet frame. Let the Lorentz metric $g = dx_1^2 - dx_2^2 - dx_3^2 - dx_4^2$ be defined on the coordinate system $\{x_1, x_2, x_3, x_4\}$ in R_1^4. If $g(T,T) = 0$ then the α curve is called a null curve, where $\alpha' = T$) is the tangent vector. Also, the α null curve must satisfy the following conditions.

$$g(B_1', T) = g(T, F) = 1, \quad g(B_1, B_1) = g(G, G) = -1,$$

$$g(T, B_1) = g(B_1', B_1) = g(F, F) = g(G, B_1) = 0,$$

$$g(G,T) = g(G,F) = g(B_1,F\,) = 0,$$

where F, G are two new vectors and

$$B_1{}' = \lambda\, T + F + \mu$$

for $\lambda, \mu \in R$. From here,

$$N = F + \mu B_2 + \frac{1}{2}\mu^2 T$$

and

$$B_2 = G + \mu T$$

is obtained. On the other hand, considering the orthogonality of these vectors,

$$B_1{}' = k_1\, T + N$$

for $k_1 = \lambda - \frac{1}{2}\mu^2$ [28].

Frenet equations are defined by

$$\begin{bmatrix} T' \\ N' \\ B_1{}' \\ B_2{}' \end{bmatrix} = \begin{bmatrix} 0 & 0 & 1 & 0 \\ 0 & 0 & k_1 & k_2 \\ k_1 & 1 & 0 & 0 \\ k_2 & 0 & 0 & 0 \end{bmatrix} \begin{bmatrix} T \\ N \\ B_1 \\ B_2 \end{bmatrix}$$

with Frenet curvatures k_1, k_2 of a null curve α in R_1^4. Let the arc length of the null curve defined in R_1^4 be defined by

$$L = \int \begin{pmatrix} 2\varphi\sqrt{-g(T',T')} \\ +g\left(P,\left(T - T\sqrt{-g(T',T')}\right)\right) \\ -\delta g(T,T) \end{pmatrix} ds.$$

Where P and δ are Lagrange multipliers, $\varphi \in R$ and

$$\sqrt{-g(T',T')} = (g(-\alpha'',\alpha''))^{1/4}.$$

Accordingly, the equations of motion used in the parameterization of the arc length are

$$\alpha' = T\ ,$$

$$T' = -\frac{1}{\varphi}P_+,$$

$$P_+{}' = \frac{1}{\varphi}g(P,P)T - P,$$

$$P' = 0.$$

If Frenet's equations are used in these equations of motion, it is obtained as

$$P_+ = -\varphi B_1\ ,$$

$$P = \varphi N + \frac{1}{2\varphi}g(P,P)T$$

$$k_1 = -\frac{1}{2\varphi^2} g(P,P).$$

It is possible to arrive at a manageable expression for the symplectic form on some surface. In this model, if it is defined by

$$E_+ = T - \frac{\varphi}{g(P,P)} P$$

as the new free coordinate consisting of canonical variables, it is written as

$$Z = P_+ + i\left(\sqrt{g(P,P)}\right)E_+$$

according to the complex coordinate system. Thus,

$$g(Z,Z) = 0\ ,$$

$$g(Z,\bar{Z}) + 2\varphi^2 = 0,$$

$$g(P,Z) = 0$$

is obtained. For the Pauli-Luban-sky vector

$$S_\mu(s) = \epsilon_{\mu\nu\rho\sigma} g(P^\upsilon, P_+{}^\rho) T^\sigma$$

satisfying these conditions,

$$g\left(S_\mu, S_\mu\right) = -\varphi^4.$$

In order to obtain irreducible representations of the Poincaré group under its quantization-physical states, η is a parameter independent of mass and $g(P,P)=\eta^2$ can be decomposed into irreducible representations of the Poincaré group. Wherein η^2 can be taken positive, negative or zero. If η^2 is taken positive, the irreducible representation of the Poincare group is physically a spinor. If η^2 is taken negative, the irreducible representation of the Poincare group becomes a non-physical tachyonic. If η^2 is taken as zero, the irreducible representation of the Poincare group will be a non-physical continuous spin.

In addition, according to the complex spinors coordinate system, the complex 4-vector of y is defined as

$$[y^{kl}]=\frac{1}{\sqrt{2}}\begin{bmatrix} y^0+y^3 & y^1+iy^2 \\ y^1-iy^2 & y^0-y^3 \end{bmatrix}$$

and

$$|y^{kl}|=\frac{1}{2}\delta_{\mu\nu}y^{\mu}y^{\nu}.$$

Since the Lorentz group is the identity component between SL(2, $\mathbb{C}$) and a local isomorphism, there is such a Lorentz transformation on y, which is equivalent to a SL(2, $\mathbb{C}$) matrix representation. $[\epsilon^{kl}]=[\epsilon_{kl}]$ and $\epsilon^{01}=+1$ for antisymmetric tensors in spinors. Since Z is null, ξ and η are the basic spinors forms $Z^{kl}=\sqrt{2}\,\varphi\xi^k\bar{\eta}^l$ and $\xi^k\eta_l=1$ [28].

Although not yet available in the literature, similar to the example of spinors defined in R_1^4 given above, it comes to mind that there may be other Physics applications in R_2^4. While in R_1^4 the metric used for spinors is defined as $g = dx_1^2 - dx_2^2 - dx_3^2 - dx_4^2$, in R_2^4 it is defined as $g = -dx_1^2 - dx_2^2 + dx_3^2 + dx_4^2$. The definitions of null curves given in both spaces are also similar. These similarities strengthen the possibility of other Physics applications in R_1^4 and R_2^4.

REFERENCES

[1] Akgün, M. A., Sivridağ, A. I. (2015). "On the null Cartan curves of $R_1 4$ ", Global Journal of Mathematics, 1(1), 41-50.

[2] Akgün, M. A., Sivridağ, A. I. (2015). "On the characterizations of null Cartan curves in $R_2 4$ ", International Journal of Mathematics, 1(1), 1-13.

[3] Aslaner, R., Boran, A. İ. (2009). "On the geometry of null curves in the Minkowski 4-space", Turk. J. Math. 33, 265-272.

[4] Barros, M., Ferrandez, A., Javaloyes, M. A., Lucas, P. (2004). "Geometry of relativistic particles with torsion", International Journal of Modern Physics A, 19(11), 1737-1745.

[5] Bonnor W.B. (1969), Null curves in a Minkowski space–time. Tensor, 20, 229–242.

[6] Bonnor W.B. (1985). Curves with null normals in Minkowski space–time. A random walk in relativity and cosmology. Wiley Easten Limited, Canada.

[7] Budinich, P. (1986). "Null vectors, Spinors, and Strings", Commun. Math. Phys., 107, 455-465.

[8] Cartan, E. (1913). “Les groupes projectifs qui ne laissent invariante aucune multiplicité planet”, Bull. Soc. Math. France 41, 53-96.

[9] Cartan, E. (1938). La theorie des spineures. Paris: Hermann.

[10] Çöken, A. C., Çiftçi, Ü. (2005). "On the Cartan curvatures of a null curve in Minkowski Spacetime", Geometriae Dedicata, 114, 71-78.

[11] Duggal, K. L., Jin, D. H. (2007). "Null curves and hypersurfaces of Semi-Riemannian manifolds". London: World Scientific.

[12] Enneper, A. (1864). "Analytisch-geometrische Untersuchungen", Z. Math. Phys., 9, 96-125.

[13] Eisenhart, L.P. (1912). “Minimal surfaces in Euclidean four-space”, Amer. J. Math. 34, 215.

[14] Ferrandez, A., Gimenez, A., Lucas, P. (2007). "Relativistic particles and the geometry of 4-D null curves", Journal of Geometry and Physics, 57, 2124-2135.

[15] Gürbüz, N. (2013). "The model particle with torsion for 4 dimensional null Cartan curves", Life Science Journal, 10(4), 188-190.

[16] İyigün, E. (2012). "On harmonic curvatures of null generalized helices in L4 ", Selçuk Journal of Applied Mathematics, 13(2), 63-67.

[17] İyigün, E. (2012). "The characterization of null generalized helices in 5-dimensional Lorentzian space", Journal of Pure and Applied Mathematics: Advances and Applications, 8(2), 93-103.

[18] İyigün, E. 2012. "CCR-curves in the Minkowski 4-space $R_1$4 ", Bull. Pure and Applied Math. 6(2), 328-332.

[19] İyigün, E. (2016). "The Darboux vector of non-null curve in $E_1$4", Journal of Pure and Applied Mathematics: Advances and Applications, 15(1), 81-92.

[20] İyigün, E. (2016). "Null generalized helices in Lorentzian space in L6 ", Pioneer Journal of Mathematics and Mathematical Sciences, 16(2), 97-107.

[21] İyigün, E. (2016). "Some characterization of Pseudo null curves in $R_2$4", Pioneer Journal of Advances in Applied Mathematics, 16(1-2), 29-38.

[22] İyigün, E. (2017). "A study on a partially null curve in $E_2$4", Communications Series A1: Math. And Statistics, Preprint.

[23] İyigün, E. (2017). " Some properties of Cartan null curves in Semi-Euclidean 4-space with Index 2", International Conference on Recent Advances in Pure and Applied Mathematics (ICRAPAM 2017), Istanbul Commerce University, Kuşadası/Aydın

[24] İyigün, E. (2017). "On The Pseudo Null Curves in 4-dimensional Semi-Euclidean Space with Index 2", 15th International Geometry Symposium, Amasya University, Amasya

[25] İyigün, E. (2018). "A characterization of null generalized helices in $R_1$4 ", Journal of Analysis and Computation, 14(1), 87-92

[26] İyigün, E. (2019). “A study on a partıally null curve ın E24 “,Commun. Fac. Sci. Univ. Ank. Ser. A1 Math. Stat. 68(1), 277-282.

[27] Krippendorff, K. (2004). “Content analysis: an introduction to its methodology” (2nd ed.). Thousand Oaks, CA: Sage Publications.

[28] Nersessian, A., Ramos, E. (1998). "Massive spinning particles and the geometry of null curves", Physics Letters B, 445, 123-128.

[29] Nersessian, A. (2000). "Large massive 4d particle with torsion and conformal mechanics", Physics Letters B, 473, 94-101.

[30] O'Neill B. (1983). “Semi-Riemannian geometry with applications to relativity”, Academic Press, New York,

[31] Petrovic-Torgasev, M., Sucurovic, E. (2000). "Some characterizations of the spacelike, the timelike and the null curves on the pseudohyperbolic space H_0^2 in $E_1 3$ ", Kragujevac J. Math., 22, 71-82.

[32] Petrovic-Torgasev, M., İlarslan K., Nesovic E. (2005). “On partially null and pseudo null curves in the Semi-Euclidean space $R_2 4$”, J. Geom. 84, 106-116.

[33] Samuel, J., Nityananda, R. (2000). "Transport along null curves", J. Phys. A: Math. Gen., 33, 2895-2905.

[34] Steane, A.M. (2013). “An introduction to spinors” https://www.researchgate.net/ deref/http%3A%2F%2Farxiv.org%2Fabs%2F1312.3824v1

[35] Şanlı, Z., Yaylı, Y. (2013). "On indicatrices of null Cartan curves in $R_1 4$ ", International Journal of Engineering Research & Technology (IJERT), 2 (10), 2567-2570.

[36] Uçum, A., Keçilioğlu, O., İlarslan, K. (2016). "Generalized pseudo null Bertrand curves in Semi-Euclidean 4-space with index 2 ", Rend. Circ. Mat. Palermo, 65, 459-472.

[37] Uçum, A., İlarslan, K., Sakaki, M. (2016). "On (1,3)-Cartan null Bertrand curves in Semi-Euclidean 4-space with index 2 ", J. Geom., 107, 579-591.

[38] Weierstrass, K. (1866). “Ntersuchungen ber die Flachen, deren mittlere Krummung berall gleich null ist.”, Monatsber. Dtsch. Akad. Wiss. Berlin, 612- 625.

CHAPTER 4

COMBINED APPROACH TO SOLVING NONLINEAR OPERATOR EQUATIONS BASED ON A NEWTON-LIKE METHOD

Liudmyla HART [1]

[1] Prof.Dr., Physical and Mathematical Sciences, Faculty of Applied Mathematics, Department of Computational Mathematics and Mathematical Cybernetics,Oles Honchar Dnipro National University, Ukrainell_hart@ukr.net
ORCID: 0000-0003-2617-7851

INTRODUCTION

Numerous theoretical and applied problems described by differential, integral or integro-differential equations and their systems, problems of the best control of such systems, problems of the best approximation of functions, and many others are often treated as operator equations in suitable functional spaces or infinite-dimensional constrained optimization problems. The successful development of apparatus for studying such problems is impossible without the use of effective mathematical methods and modern means of information processing, which are improved along with computing systems and simultaneously provide not only a tool, but also a language of a high degree of universality. Considering the complexity of mathematical formulations of the mentioned classes of problems, the approximate (especially numerical) methods and algorithms are most used in their solution, among which there are projection and iterative ones, as well as some combined approaches superposing the ideas of the latter and having certain advantages over them. There are a large number of approximate methods and algorithms for solving these classes of problems, but their presence does not exclude a possibility of creating new methods that are more efficient and improving existing ones.

Increasing the efficiency of algorithms is one of the urgent tasks of modern informatics. As is known, iterative methods, despite the exponential convergence rate and simple computational schemes, have a limited area of application. In turn, projection methods, having a

wide range of applications, are characterized by a power-law convergence rate (sometimes rather slow) and computational instability. Therefore, the effective synthesis of projection and iterative methods, due to the need to eliminate their inherent shortcomings, as well as the theoretical substantiation and analysis of the corresponding numerical algorithms form an important direction in the development of modern theory of algorithms and computations.

Various mixed approaches to solving different classes of operator equations are presented in works of G.Erman, G.M.Vainikko, V.V.Petryshyn, H.Gajewski, R.Kluge, V.V.Ivanov, V.P.Tanana, A.Yu.Luchka, T.Chen, M. Seddeek, in the group of multigrid methods of W.Hackbusch, R.P.Fedorenko, V.V.Shaydurov, as well as in works of A.B.Bakushinsky, M.Yu.Babich, Ya.D.Pyanylo, B.G.Gabdulkhaev, S.D.Balashova, Yu.D.Fedorenko, E.L.Hart and other authors. A brief overview of the relevant scientific literature is contained, for example, in [1]. In this paper, we study projection-iteration methods based on the principle of whatever approximation of the original equation by a sequence of approximate operator equations defined on subspaces of the basic space (or on spaces isomorphic to subspaces of the basic space) with the subsequent application of the iterative method for the approximate solution of approximating equations. The main idea of the studied projection-iteration methods for solving operator equations of the first kind is as follows [2]. An equation in the form

$$A\,u = f\,, \tag{1}$$

with a nonlinear operator A acting on a Banach space X ($f \in X$ is a known element), is approximated by a sequence of approximate equations

$$A_n u_n = f_n, \quad n = 1, 2, \ldots, \tag{2}$$

where A_n is a nonlinear operator acting on a subspace X_n of the basic space ($X_1 \subset X_2 \subset \ldots \subset X_n \subset \ldots \subset X$; $X_1 \neq \varnothing$). To solve approximate equations (2), some iterative method is used, at that for each of these equations only a few approximations $u_n^{(k)}$ $(k = 1, 2, \ldots, k_n)$ are found and the last of them $u_n^{(k_n)}$ is assumed to be equal to the initial approximation $u_{n+1}^{(0)}$ in the iterative process for the next, $(n+1)$-th approximate equation. The sequence $\{u_n^{(k_n)}\}_{n=1}^{\infty} \subset X$ is considered as a sequence of approximations to a solution u^* of equation (1). This approach to finding an approximate solution of the original equation naturally eliminates the difficulties that arise when solving the same equation using the conventional projection method and makes it easier to choose a suitable initial approximation compared to solving the original equation using the iterative method. In this paper, we study a projection-iteration method based on a Newton-like method, which generalizes the results for the projection-iteration implementation of the Newton-Kantorovich method to solve a nonlinear operator equation with a Fréchet differentiable operator in a Banach space [3].

As you know, Newton's method, originally intended to solve algebraic equations, is currently the fundamental tool in numerical analysis, operations research, optimization and control. The basic method ideas, the main theoretical results of convergence, the latest developments in this area, the most up-to-date versions of the method, as well as its various applications can be found, for example, in papers [4–13]. Newton's method was studied in more detail under the so-called Kantorovich conditions [4–6] (assuming that the derivative of operator A is invertible at the initial point and satisfies the Lipschitz condition in the considered domain). It was also studied under the Vertgeim conditions [8] (the derivative of operator A is invertible at the initial point but satisfies only Hölder condition) and under the Mysovskih conditions [7] (the derivative of operator A is invertible is invertible at all points in the considered domain and its inverse operator is bounded). In [14, 15], we studied Newton's method as well as a Newton-like method under generalized Cauchy's conditions, which, instead of the inverse operator of the derivative, imply the existence of some linear operator close to it on the considered domain. In this paper, we present a projection-iteration implementation of the Newton-like method under the Cauchy's conditions to solve nonlinear operator equation (1) with a Fréchet differentiable operator in a Banach space. Based on [16], where approximate operator equations (2) were considered on subspaces X_n $(n=1,2,...)$ of basic space X, here we study the case of projection onto spaces $\tilde{X}_n$ isomorphic to subspaces X_n $(n=1,2,...)$. We prove some convergence theorems,

obtain error estimates and discuss the advantages of the proposed approach and some of its modifications.

2. PRELIMINARIES

Let us consider equation (1) $A\,u = f$ with a nonlinear operator A, which is Fréchet differentiable on some set Ω of a Banach space X. Suppose that there is a solution u^* of equation (1) on Ω.

Let us recall the main idea of Newton's method for solving operator equation (1) under the above assumptions. Let $u^{(0)} \in \Omega$ be an arbitrary element. Assuming that the Frechet derivative $A'(u)$ is continuous by u on a closed ball

$$S(u^{(0)}, R) = \{u \in X : \ \| u - u^{(0)} \| \le R\} \subset \Omega,$$

we obtain from the finite-increments formula, that in a sufficiently small neighborhood of point $u^{(0)}$, an element $A\,u$ is close enough to an element $A\,u^{(0)} + A'(u^{(0)})(u - u^{(0)})$, and therefore a solution of the equation $A\,u^{(0)} + A'(u^{(0)})(u - u^{(0)}) = f$ is close enough to u^*. This equation is already linear, and if $[A'(u^{(0)})]^{-1}$ exists, then its solution $u^{(1)}$ can be found by the formula $u^{(1)} = u^{(0)} - [A'(u^{(0)})]^{-1}(A\,u^{(0)} - f)$. Continuing this process, we obtain a sequence of approximations

$$u^{(k+1)} = u^{(k)} - [A'(u^{(k)})]^{-1}(A\,u^{(k)} - f), \quad k = 0,1,... \qquad (3)$$

to a solution of equation (1), which defines Newton's iterative method.

The theoretical substantiation of Newton's method (3) under the Kantorovich-type conditions, when the existence of the bounded inverse operator $[A'(u^{(0)})]^{-1}$ is assumed only at the initial point $u^{(0)}$, is contained in [6]. In a number of cases, it turns out to be expedient to replace this condition with the Cauchy-type condition, according to which an estimate for the norm of operator $\Gamma(u)=[A'(u)]^{-1}$ is known not only at point $u^{(0)}$, but also on entire ball $S(u^{(0)},R)$ (that allows one to weaken constraints on a choice of $u^{(0)}$). The conditions of existence of a solution u^* of equation (1), the domain of its location, as well as the convergence of iterative sequence (3) under the Cauchy-type conditions are established in [7]. A generalization of results of [7], when instead of operator $\Gamma(u)=[A'(u)]^{-1}$, it is required the existence of a bounded operator $D(u)$ close to $\Gamma(u)$ on $S(u^{(0)},R)$, is contained in [14].

We call a process of successive approximations like (3), with the replacement of an operator $\Gamma(u^{(k)})=[A'(u^{(k)})]^{-1}$ by an operator $D(u^{(k)})$ close to it, a Newton-like method for equation (1):

$$u^{(k+1)}=u^{(k)}-D(u^{(k)})(A\,u^{(k)}-f),\quad k=0,1,... \tag{4}$$

The feasibility of process (4) and the convergence of the corresponding sequence of approximations $\{u^{(k)}\}_{k=0}^{\infty}$ to u^* on

$S(u^{(0)}, R)$ under the Cauchy-type conditions are established by the following theorem.

Theorem 1 [15] (on the convergence of a Newton-like method). *Let an operator* A *be Fréchet differentiable on some ball* $S(u^{(0)}, R)$ *of a Banach space* X *and let its derivative* $A'(u)$ *satisfy the Lipschitz condition on this ball:*

$$\| A'(u) - A'(v) \| \le L \| u - v \|, \quad \forall u, v \in S(u^{(0)}, R), \ L > 0. \qquad (5)$$

Assume that there exists a linear operator $D(u)$ *on* $S(u^{(0)}, R)$, *which has a continuous inverse, and for all* $u \in S(u^{(0)}, R)$

$$\| D(u) \| \le b, \quad \| E - D(u) A'(u) \| \le \delta < 1, \qquad (6)$$

where $b > 0$, $\delta > 0$; E *is an identity operator in* X. *If the initial approximation* $u^{(0)}$ *satisfies the conditions*

$$\| A u^{(0)} - f \| \le \eta^{(0)}, \quad h^{(0)} = b^2 L \eta^{(0)} + \frac{2bL\delta}{1-\delta} < 2, \quad r^{(0)} = \frac{b\eta^{(0)}}{1 - h^{(0)}/2} \le R,$$

where $\eta^{(0)} > 0$, *then equation (1) has a solution* u^* *on a ball* $S(u^{(0)}, r^{(0)}) \subset X$ *and the sequence of approximations* $\{u^{(k)}\}_{k=0}^{\infty}$ *defined by formulas (4) converges to* u^* *with the error estimate*

$$\| u^{(k)} - u^* \| \le \frac{b\eta^{(0)}}{1 - h^{(0)}/2} (h^{(0)}/2)^k . \qquad (7)$$

Note that Newton-like method (4) in the general case converges linearly, except for the situation $\delta = 0$, when this method has a quadratic rate of convergence, since it turns into the usual Newton's method (3). In this case, the error estimate (7) becomes significantly overestimated; a more appropriate result is contained in [14].

3. PROJECTION-ITERATION APPROACH BASED ON A NEWTON-LIKE METHOD

3.1. Projection onto subspaces of the basic space

Let a nonlinear operator A in equation (1) $A u = f$ act in a Banach space X and be Fréchet differentiable on a ball

$$S(u_N^{(0)}, R) = \{u \in X : \ \| u - u_N^{(0)} \| \le R\} \subset \Omega .$$

We approximate equation (1) by a sequence of approximate equations (2) $A_n u_n = f_n, \quad n = 1, 2, \ldots$ with nonlinear operators A_n, each of which acts on the corresponding subspace $X_n \subset X$ and is Fréchet differentiable on a set $\Omega_n = X_n \bigcap S(u_N^{(0)}, R)$, starting with some index $n = N \ge 1$; $f_n = P_n f$, P_n is a linear projector that maps X onto X_n ($P_n : X \to X_n$, $P_n u_n = u_n$ for $u_n \in X_n$).

Suppose that for each $n \geq N$ the following proximity conditions hold:

$$\| A_n u_n - P_n A u_n \| \leq \alpha_n, \quad \| A_n'(u_n) - P_n A'(u_n) \| \leq \alpha_n', \quad \forall u_n \in \Omega_n ; \quad (8)$$

$$\| P_n A u - A u \| \leq \beta_n, \quad \| P_n A'(u) - A'(u) \| \leq \beta_n', \quad \forall u \in S(u_N^{(0)}, R) ; \quad (9)$$

$$\| P_n f - f \| \leq \gamma_n, \quad \forall f \in X , \quad (10)$$

where α_n, α_n', β_n, β_n', γ_n are positive numbers such that α_n, α_n', β_n, β_n', $\gamma_n \to 0$ when $n \to \infty$. Suppose also that the derivative $A_n'(u_n)$ satisfies the Lipschitz condition on set Ω_n:

$$\| A_n'(u_n) - A_n'(v_n) \| \leq L' \| u_n - v_n \|, \quad \forall u_n, v_n \in \Omega_n, \quad L' > 0 . \quad (11)$$

If there exist continuous linear operators $\Gamma_n(u_n) = [A_n'(u_n)]^{-1}$, $\forall u_n \in \Omega_n$ for all $n \geq N$, then one can apply Newton's method (3) to each of equations (2), starting with index $n = N$, and construct a sequence of approximations $\{u_n^{(k_n)}\}_{n=N}^{\infty}$ to a solution u^* of equation (1) by the formulas

$$u_n^{(k+1)} = u_n^{(k)} - [A_n'(u_n^{(k)})]^{-1}(A_n u_n^{(k)} - f_n), \quad k = 0,1,...,k_n - 1; \quad (12)$$

$$u_{n+1}^{(0)} = u_n^{(k_n)}, \quad n \geq N, \quad u_N^{(0)} \in \Omega_N \subset X .$$

We call the process of successive approximations (12) the projection-iteration method for equation (1), based on Newton's method.

A theorem about the existence of a solution u^* to equation (1), about the domain of its location and the projection-iteration process (12) convergence under the Cauchy-type conditions is given in [3]. Paper [3] also contains a generalization of this theorem, when instead of operators $\Gamma(u)=[A'(u)]^{-1}$ and $\Gamma_n(u_n)=[A'_n(u_n)]^{-1}$ it is required the existence of operators $D(u)$ and $D_n(u_n)$, which are close to $\Gamma(u)$ on $S(u_N^{(0)},R)$ and to $\Gamma_n(u_n)$ on Ω_n ($n\geq N$) respectively.

To solve equation (1), in [16], we proposed a projection-iteration process like (12), with the replacement of an operator $\Gamma_n(u_n^{(k)})=[A'_n(u_n^{(k)})]^{-1}$ by an operator $D_n(u_n^{(k)})$ close to it:

$$u_n^{(k+1)}=u_n^{(k)}-D_n(u_n^{(k)})(A_nu_n^{(k)}-f_n),\quad k=0,1,...,k_n-1; \qquad (13)$$

$$u_{n+1}^{(0)}=u_n^{(k_n)},\quad n\geq N,\quad u_N^{(0)}\in\Omega_N\subset X\,.$$

We call the process of successive approximations (13) the projection-iteration method for equation (1), based on a Newton-like method.

The following theorem gives sufficient conditions for the feasibility and convergence of the sequence of approximations $\{u_n^{(k_n)}\}_{n=N}^{\infty}$ defined by formulas (13) to u^* on ball $S(u_N^{(0)},R)$.

Theorem 2 [16] (on the convergence of the projection-iteration method based on a Newton-like method). *Let an operator A be*

Fréchet differentiable on some ball $S(u_N^{(0)}, R)$ *of a Banach space* X *and let its derivative* $A'(u)$ *satisfy the Lipschitz condition (5) on this ball. Let an operator* A_n $(n \geq N)$ *be Fréchet differentiable on a set* $\Omega_n = X_n \bigcap S(u_N^{(0)}, R)$ *and let its derivative* $A_n'(u_n)$ *satisfy the Lipschitz condition (11). Assume that the proximity conditions (8)–(10) hold true and there exist a linear operator* $D(u)$ *on* $S(u_N^{(0)}, R)$ *and linear operators* $D_n(u_n)$ *on* Ω_n $(n \geq N)$, *such that*

$$\| D(u) \| \leq b, \quad \| E - D(u)A'(u) \| \leq \delta < 1, \quad \forall u \in S(u_N^{(0)}, R); \qquad (14)$$

$$\| E - D_n(u_n)A_n'(u_n) \| \leq \delta_n < 1, \quad \forall u_n \in \Omega_n, \qquad (15)$$

where E *is an identity operator in* X; $b > 0$, $\delta > 0$, $\delta_n > 0$, *at that* $bL\delta/(1-\delta) < 1$ *and* $\delta_n \to 0$ when $n \to \infty$. *If the initial approximation* $u_N^{(0)} \in \Omega_N$ *satisfies the conditions*

$$\| A_N u_N^{(0)} - f_N \| \leq \eta_N^{(0)}, \qquad (16)$$

$$h_N^{(0)} = b_N^2 L' \eta_N^{(0)} + \frac{2b_N L' \delta_N}{1-\delta_N} < 2, \quad r_N = b_N \eta_N^{(0)} G_N \leq R, \qquad (17)$$

where $\eta_N^{(0)} > 0$, $b_N = \dfrac{b}{1 - b\rho_N}$, $\rho_N = \alpha'_N + \beta'_N + \dfrac{L'\delta_N}{1-\delta_N} + \dfrac{L\delta}{1-\delta}$,

$$G_N = H_N + \sum_{m=N}^{\infty} (h_N^{(0)}/2)^{S_m} < 2H_N, \quad H_N = \frac{1}{1 - h_N^{(0)}/2}, \quad s_m = \sum_{i=N}^{m} (k_i - 1),$$

then equation (1) has a solution u^* *on a ball* $S(u_N^{(0)}, r_N) \subset X$ *and a sequence of approximations* $\{u_n^{(k_n)}\}_{n=N}^{\infty}$ *defined by formulas (13) converges to* u^* *with the error estimate*

$$\| u_n^{(k_n)} - u^* \| \le \chi_n, \quad n \ge N, \tag{18}$$

where $\chi_n = b_N \eta_N^{(0)} V_n (h_N^{(0)}/2)^{S_n}$, $V_n = H_N + \sum_{m=n+1}^{\infty} (h_N^{(0)}/2)^{S_m - S_n} < 2H_N$.

Note that the projection-iteration process (13) based on a Newton-like method, generally converges more slowly than the projection-iteration process (12) based on Newton's method. An exception is the case when $\delta = 0$, $\delta_n = 0$ $(n \ge N)$ in formulas (14), (15), because then method (13) is transformed into (12); in this case, the error estimate (18) becomes significantly overestimated, and a more appropriate estimate is contained in [3].

3.2. Projection onto spaces isomorphic to subspaces of the basic space

When solving practical problems, which are reduced to operator equations of the form (1) in a Banach space X, the most common case is when the approximate equations are given not in subspaces $X_n \subset X$ of the basic space, but in some spaces $\tilde{X}_n$ isomorphic to them. Let us present a way to transfer the above results to this case.

Let, as in Section 3.1, a nonlinear operator A acting in a Banach space X be Fréchet differentiable on some ball $S(u_N^{(0)}, R)$ of this space. We approximate equation (1) by a sequence of approximate equations

$$\tilde{A}_n \tilde{u}_n = \tilde{f}_n, \quad n = 1, 2, \ldots, \tag{19}$$

where $\tilde{A}_n$ is a nonlinear operator acting in a Banach space $\tilde{X}_n$ that is isomorphic to subspace $X_n \subset X$.

For each $n = 1, 2, \ldots$, we denote by Φ_n a linear operator performing a one-to-one mapping of X_n onto $\tilde{X}_n$, and by $\bar{\Phi}_n = \Phi_n P_n$ a linear operator that is an extension of Φ_n to the whole space X, where P_n is a linear operator of projecting X onto X_n ($P_n^2 = P_n, \ \| P_n \| = 1$). For simplicity, we will assume that spaces X_n and $\tilde{X}_n$ are isometric, which implies that $\| \Phi_n \| = \| \Phi_n^{-1} \| = 1$.

It is easy to show [17] that, if $\tilde{f}_n = \bar{\Phi}_n f$ ($n \geq N$), then from equation (19) one can pass to the corresponding equation (2) given in subspace X_n, and vice versa. In this case, $A_n = \Phi_n^{-1} \tilde{A}_n \Phi_n$ that is, equations (19) and (2) are equivalent in the sense that the solvability of one of them implies the solvability of the other one, and vice versa, and their exact solutions (in the case of existence) are interconnected by the relations: $\tilde{u}_n^* = \Phi_n u_n^*, \ u_n^* = \Phi_n^{-1} \tilde{u}_n^*$.

We denote by $\tilde{\Omega}_n$ an image of set $\Omega_n = X_n \bigcap S(u_N^{(0)}, R)$ under the mapping Φ_n, that is $\tilde{\Omega}_n = \{\tilde{u}_n \in \tilde{X}_n : \ \tilde{u}_n = \Phi_n u_n, \ u_n \in \Omega_n\}$, and assume that each of operators $\tilde{A}_n$, starting with $n = N \geq 1$, is Fréchet differentiable on set $\tilde{\Omega}_n$ and its derivative $\tilde{A}_n'(\tilde{u}_n)$ satisfies the Lipschitz condition on this set:

$$\| \tilde{A}_n'(\tilde{u}_n) - \tilde{A}'(\tilde{v}_n) \| \leq \tilde{L} \| \tilde{u}_n - \tilde{v}_n \|_{\tilde{X}_n}, \quad \forall \tilde{u}_n, \tilde{v}_n \in \tilde{\Omega}_n, \ \tilde{L} > 0. \quad (20)$$

Suppose that for each $n \geq N$ the following proximity conditions hold:

$$\| \tilde{A}_n \tilde{u}_n - \bar{\Phi}_n A \Phi_n^{-1} \tilde{u}_n \|_{\tilde{X}_n} \leq \tilde{\alpha}_n, \ \ \| \tilde{A}_n'(\tilde{u}_n) - \bar{\Phi}_n A'(\Phi_n^{-1} \tilde{u}_n) \Phi_n^{-1} \| \leq \tilde{\alpha}_n' \quad (21)$$

for all $\tilde{u}_n \in \tilde{\Omega}_n$;

$$\| \Phi_n^{-1} \bar{\Phi}_n A\, u - A\, u \|_X \leq \tilde{\beta}_n, \ \ \| \Phi_n^{-1} \bar{\Phi}_n A'(u) - A'(u) \| \leq \tilde{\beta}_n' \quad (22)$$

for all $u \in S(u_N^{(0)}, R)$;

$$\| \Phi_n^{-1} \bar{\Phi}_n f - f \|_X \leq \tilde{\gamma}_n, \ \ \forall f \in X, \quad (23)$$

where $\tilde{\alpha}_n$, $\tilde{\alpha}_n'$, $\tilde{\beta}_n$, $\tilde{\beta}_n'$, $\tilde{\gamma}_n$ are positive numbers such that $\tilde{\alpha}_n$, $\tilde{\alpha}_n'$, $\tilde{\beta}_n$, $\tilde{\beta}_n'$, $\tilde{\gamma}_n \to 0$ when $n \to \infty$.

If for each $n \geq N$ there exists a continuous linear operator $\tilde{\Gamma}_n(\tilde{u}_n) = [\tilde{A}_n'(\tilde{u}_n)]^{-1}, \ \forall \tilde{u}_n \in \tilde{\Omega}_n$, then one can apply Newton's method

(3) to solve equations (19), starting with index $n = N$, and construct a sequence of approximations $\{\Phi_n^{-1}\tilde{u}_n^{(k_n)}\}_{n=N}^{\infty}$ to a solution u^* of equation (1) by the formulas

$$\tilde{u}_n^{(k+1)} = \tilde{u}_n^{(k)} - [\tilde{A}_n'(\tilde{u}_n^{(k)})]^{-1}(\tilde{A}_n\tilde{u}_n^{(k)} - \tilde{f}_n), \quad k = 0,1,...,k_n - 1; \quad (24)$$

$$\tilde{u}_{n+1}^{(0)} = \Phi_{n+1}\Phi_n^{-1}\tilde{u}_n^{(k_n)}, \quad n \geq N, \quad \tilde{u}_N^{(0)} = \Phi_N u_N^{(0)} \in \tilde{\Omega}_N .$$

A theorem on the feasibility and convergence of process (24) under the Cauchy-type conditions for equation (1) is contained in [17].

Consider a projection-iteration process of approximations like (24) to solve equation (1), with the replacement of an operator $\tilde{\Gamma}_n(\tilde{u}_n^{(k)}) = [\tilde{A}_n'(\tilde{u}_n^{(k)})]^{-1}$ by an operator $\tilde{D}_n(\tilde{u}_n^{(k)})$ close to it on $\tilde{\Omega}_n$:

$$\tilde{u}_n^{(k+1)} = \tilde{u}_n^{(k)} - \tilde{D}_n(\tilde{u}_n^{(k)})(\tilde{A}_n\tilde{u}_n^{(k)} - \tilde{f}_n), \quad k = 0,1,...,k_n - 1; \quad (25)$$

$$\tilde{u}_{n+1}^{(0)} = \Phi_{n+1}\Phi_n^{-1}\tilde{u}_n^{(k_n)}, \quad n \geq N, \quad \tilde{u}_N^{(0)} = \Phi_N u_N^{(0)} \in \tilde{\Omega}_N .$$

The feasibility of the projection-iteration process (25) and the convergence of the corresponding sequence of approximations $\{\Phi_n^{-1}\tilde{u}_n^{(k_n)}\}_{n=N}^{\infty}$ to u^* on $S(u_N^{(0)}, R)$ are established by the following theorem.

Theorem 3 (on the convergence of the projection-iteration method based on a Newton-like method). *Let an operator A be Fréchet*

differentiable on some ball $S(u_N^{(0)}, R)$ *of a Banach space* X *and let its derivative* $A'(u)$ *satisfy the Lipschitz condition (5) on this ball. Let an operator* $\tilde{A}_n$ ($n \geq N$) *be Fréchet differentiable on a set* $\tilde{\Omega}_n \subset \tilde{X}_n$ *and let its derivative* $\tilde{A}_n'(\tilde{u}_n)$ *satisfy the Lipschitz condition (20). Let the proximity conditions (21)–(23) hold true. Assume that there exists a linear operator* $D(u)$ *on* $S(u_N^{(0)}, R)$ *with properties (14), where* $bL\delta/(1-\delta) < 1$, *and there exist linear operators* $\tilde{D}_n(\tilde{u}_n)$ *on* $\tilde{\Omega}_n$ ($n \geq N$) *such that*

$$\| \tilde{E}_n - \tilde{D}_n(\tilde{u}_n)\tilde{A}_n'(\tilde{u}_n) \| \leq \tilde{\delta}_n < 1, \quad \forall \tilde{u}_n \in \tilde{\Omega}_n, \tag{26}$$

where $\tilde{E}_n$ *is an identity operator in* $\tilde{X}_n$ ($n \geq N$); $\tilde{\delta}_n \to 0$, $n \to \infty$. *If the initial approximation* $\tilde{u}_N^{(0)} \in \tilde{\Omega}_N$ ($\tilde{u}_N^{(0)} = \Phi_N u_N^{(0)}$) *satisfies the conditions*

$$\| \tilde{A}_N \tilde{u}_N^{(0)} - \tilde{f}_N \|_{\tilde{X}_N} \leq \tilde{\eta}_N^{(0)}, \tag{27}$$

$$\tilde{h}_N^{(0)} = \tilde{b}_N^2 \tilde{L} \tilde{\eta}_N^{(0)} + \frac{2\tilde{b}_N \tilde{L} \tilde{\delta}_N}{1-\tilde{\delta}_N} < 2, \quad \tilde{r}_N = \tilde{b}_N \tilde{\eta}_N^{(0)} \tilde{G}_N \leq R, \tag{28}$$

where $\tilde{\eta}_N^{(0)} > 0$, $\tilde{b}_N = \dfrac{b}{1-b\tilde{\rho}_N}$, $\tilde{\rho}_N = \tilde{\alpha}'_N + \tilde{\beta}'_N + \dfrac{\tilde{L}\tilde{\delta}_N}{1-\tilde{\delta}_N} + \dfrac{L\delta}{1-\delta}$,

$$\tilde{G}_N = \tilde{H}_N + \sum_{m=N}^{\infty} (\tilde{h}_N^{(0)}/2)^{S_m} < 2\tilde{H}_N, \quad \tilde{H}_N = \frac{1}{1-\tilde{h}_N^{(0)}/2}, \quad s_m = \sum_{i=N}^{m} (k_i - 1),$$

then equation (1) has a solution u^* *on a ball* $S(u_N^{(0)}, \tilde{r}_N) \subset X$ *and a sequence of approximations* $\{\Phi_n^{-1}\tilde{u}_n^{(k_n)}\}_{n=N}^{\infty}$ *defined by formulas (25) converges to* u^* *with the error estimate*

$$\| \Phi_n^{-1}\tilde{u}_n^{(k_n)} - u^* \|_X \le \tilde{\chi}_n, \quad n \ge N, \tag{29}$$

where $\tilde{\chi}_n = \tilde{b}_N \tilde{\eta}_N^{(0)} \tilde{V}_n (\tilde{h}_N^{(0)}/2)^{S_n}$, $\tilde{V}_n = \tilde{H}_N + \sum_{m=n+1}^{\infty} (\tilde{h}_N^{(0)}/2)^{S_m - S_n} < 2\tilde{H}_N$.

Moreover, the elements $\tilde{u}_n^{(k_n)}$ *themselves are close to elements* $\bar{\Phi}_n u^*$ *in* $\tilde{X}_n$ ($n \ge N$) *in the sense that*

$$\| \tilde{u}_n^{(k_n)} - \bar{\Phi}_n u^* \|_{\tilde{X}_n} = O(\tilde{\chi}_n + \tilde{\gamma}_n) \to 0, \quad n \to \infty .$$

The proof of Theorem 3 is standard for theorems on the convergence of projection-iteration processes in isomorphic spaces. Let us establish a correspondence between the conditions of this theorem and the conditions of Theorem 2 on the convergence of the similar projection-iteration method (13) considered in subspaces $X_n \subset X$.

By the derivatives properties [6], the differentiation of an operator $\tilde{A}_n$ at point $\tilde{u}_n \in \tilde{\Omega}_n$ ($\tilde{u}_n = \Phi_n u_n$, $u_n \in \Omega_n$) for each $n \ge N$ implies the differentiation of an operator $A_n = \Phi_n^{-1} \circ \tilde{A}_n \circ \Phi_n$ at point $u_n \in \Omega_n$; moreover, due to the linearity of operators Φ_n and Φ_n^{-1}, it turns out that $A_n'(u_n) = (\Phi_n^{-1})'(\tilde{A}_n \tilde{u}_n) \circ \tilde{A}_n'(\tilde{u}_n) \circ \Phi_n'(u_n) = \Phi_n^{-1} \circ \tilde{A}_n'(\tilde{u}_n) \circ \Phi_n$.

Then, due to the isometricity of spaces X_n and $\tilde{X}_n$, the satisfaction of the Lipschitz condition (20) for operator $\tilde{A}'_n(\tilde{u}_n)$ on $\tilde{\Omega}_n$ implies the satisfaction of the Lipschitz condition (11) for operator $A'_n(u_n)$ on Ω_n ($n \geq N$). Indeed,

$$\| A'_n(u_n) - A'(v_n) \| = \| \Phi_n^{-1} \tilde{A}'_n(\tilde{u}_n) \Phi_n - \Phi_n^{-1} \tilde{A}'_n(\tilde{v}_n) \Phi_n \| \leq$$

$$\leq \| \tilde{A}'_n(\tilde{u}_n) - \tilde{A}'(\tilde{v}_n) \| \leq \tilde{L} \| \tilde{u}_n - \tilde{v}_n \|_{\tilde{X}_n} = \tilde{L} \| u_n - v_n \|_X, \quad \forall u_n, v_n \in \Omega_n,$$

that is, condition (11) is satisfied with a Lipschitz constant $L' = \tilde{L}$.

It is easy to see further that the fulfillment of the proximity conditions (21)–(23) leads to the fulfillment of the corresponding conditions (8)–(10). Indeed, for all $u_n \in \Omega_n$

$$\| A_n u_n - P_n A u_n \|_X = \| \Phi_n^{-1} \tilde{A}_n \Phi_n u_n - \Phi_n^{-1} \bar{\Phi}_n A u_n \|_X =$$

$$= \| \tilde{A}_n \tilde{u}_n - \bar{\Phi}_n A \Phi_n^{-1} \tilde{u}_n \|_{\tilde{X}_n} \leq \tilde{\alpha}_n;$$

$$\| A'_n(u_n) - P_n A'(u_n) \| \leq \| \Phi_n^{-1} \tilde{A}'_n(\tilde{u}_n) \Phi_n - \Phi_n^{-1} \bar{\Phi}_n A'(u_n) \| \leq$$

$$\leq \| \tilde{A}'_n(\tilde{u}_n) - \bar{\Phi}_n A'(\Phi_n^{-1} \tilde{u}_n) \Phi_n^{-1} \| \leq \tilde{\alpha}'_n,$$

that is, both conditions (8) hold true with constants $\alpha_n = \tilde{\alpha}_n$, $\alpha'_n = \tilde{\alpha}'_n$ ($n \geq N$). By virtue of the definition of operator $\bar{\Phi}_n = \Phi_n P_n$, conditions

(22), (23) coincide with the corresponding conditions (9), (10) for all $u \in S(u_N^{(0)}, R)$, moreover $\beta_n = \tilde{\beta}_n,\ \beta_n' = \tilde{\beta}_n',\ \gamma_n = \tilde{\gamma}_n$ ($n \geq N$).

Let us show that the existence of linear operators $\tilde{D}_n(\tilde{u}_n),\ \tilde{u}_n \in \tilde{\Omega}_n$ with properties (26) implies the existence of linear operators $D_n(u_n) = \Phi_n^{-1}\tilde{D}_n(\tilde{u}_n)\Phi_n,\ u_n \in \Omega_n$ ($n \geq N$) with properties (15), where $\delta_n \to 0,\ n \to \infty$. Indeed, for all $u_n \in \Omega_n$

$$\| E - D_n(u_n)A_n'(u_n) \| = \| E - \Phi_n^{-1}\tilde{D}_n(\tilde{u}_n)\Phi_n\Phi_n^{-1}\tilde{A}_n'(\tilde{u}_n)\Phi_n \| \leq$$

$$\leq \| \tilde{E}_n - \tilde{D}_n(\tilde{u}_n)\tilde{A}_n'(\tilde{u}_n) \| \leq \tilde{\delta}_n < 1,$$

that is, condition (15) holds with a constant $\delta_n = \tilde{\delta}_n$, and, obviously, $\delta_n \to 0,\ n \to \infty$.

Due to the established correspondences, it is easy to pass from formulas (25) to formulas (13), which are applied to approximate equations (19) in subspaces $X_n \subset X$. Really, if we act on both parts of the first of formulas (25) by operator Φ_n^{-1}:

$$\Phi_n^{-1}\tilde{u}_n^{(k+1)} = \Phi_n^{-1}\tilde{u}_n^{(k)} - \Phi_n^{-1}\tilde{D}_n(\tilde{u}_n^{(k)})(\tilde{A}_n\tilde{u}_n^{(k)} - \tilde{f}_n), \quad k = 0,1,...,k_n - 1,$$

then, taking into account that $\tilde{D}_n(\tilde{u}_n) = \Phi_n D_n(u_n)\Phi_n^{-1}$ for all $\tilde{u}_n \in \tilde{\Omega}_n$ ($\tilde{u}_n = \Phi_n u_n,\ u_n \in \Omega_n$), $\tilde{A}_n = \Phi_n A_n \Phi_n^{-1},\ \Phi_n^{-1}\tilde{f}_n = \Phi_n^{-1}\bar{\Phi}_n f = P_n f = f_n$ ($n \geq N$), we immediately obtain the corresponding formulas (13):

$$u_n^{(k+1)} = u_n^{(k)} - D_n(u_n^{(k)})(A_n u_n^{(k)} - f_n), \quad k = 0,1,...,k_n - 1.$$

If we act on both parts of the second of formulas (25) by operator Φ_{n+1}^{-1}, then we obviously obtain:

$$\Phi_{n+1}^{-1}\tilde{u}_{n+1}^{(0)} = \Phi_n^{-1}\tilde{u}_n^{(k_n)}, \quad n \geq N \quad \Leftrightarrow \quad u_{n+1}^{(0)} = u_n^{(k_n)}, \quad n \geq N.$$

Similarly, one can pass from (13) to (25), that is, formulas (13) and (25) are equivalent in the sense that the approximations they define are related as follows:

$$u_n^{(k_n)} = \Phi_n^{-1}\tilde{u}_n^{(k_n)}, \;\; \tilde{u}_n^{(k_n)} = \Phi_n u_n^{(k_n)} \;\; (n \geq N).$$

Finally, the fulfillment of condition (27) leads to the fulfillment of condition (16) with a constant $\eta_N^{(0)} = \tilde{\eta}_N^{(0)}$:

$$\| A_N u_N^{(0)} - f_N \|_X = \| \Phi_N^{-1}\tilde{A}_N \Phi_N u_N^{(0)} - \Phi_N^{-1}\bar{\Phi}_N f \|_X = \\ = \| \tilde{A}_N \tilde{u}_N^{(0)} - \tilde{f}_N \|_{\tilde{X}_N} \leq \tilde{\eta}_N^{(0)},$$

and both conditions in (28) coincide with the corresponding conditions in (17), wherein $h_N^{(0)} = \tilde{h}_N^{(0)}$, $r_N = \tilde{r}_N$, since $b_N = \tilde{b}_N$, $\rho_N = \tilde{\rho}_N$, $G_N = \tilde{G}_N$ $(n \geq N)$.

By virtue of the established relations, the existence and convergence of a sequence of approximations $\{\Phi_n^{-1}\tilde{u}_n^{(k_n)}\}_{n=N}^{\infty}$ defined by formulas (25) to a solution u^* of equation (1) immediately follow from

Theorem 2. To obtain the error estimate (29), it remains to replace in formula (18) an element $u_n^{(k_n)}$ by an element $\Phi_n^{-1}\tilde{u}_n^{(k_n)}$ ($n \geq N$) and constants b_N, $\eta_N^{(0)}$, $h_N^{(0)}$ by constants $\tilde{b}_N$, $\tilde{\eta}_N^{(0)}$, $\tilde{h}_N^{(0)}$, respectively. As for the statement of Theorem 3 about the proximity of elements $u_n^{(k_n)}$ and $\bar{\Phi}_n u^*$ in $\tilde{X}_n$ ($n \geq N$), then its validity is established using the error estimate (18) and the proximity condition (23):

$$\| \tilde{u}_n^{(k_n)} - \bar{\Phi}_n u^* \|_{\tilde{X}_n} = \| \Phi_n^{-1}\tilde{u}_n^{(k_n)} - \Phi_n^{-1}\bar{\Phi}_n u^* \|_X \leq \tilde{\chi}_n + \tilde{\gamma}_n, \quad n \geq N,$$

whence it follows that $\| \tilde{u}_n^{(k_n)} - \bar{\Phi}_n u^* \|_{\tilde{X}_n} \to 0, \ n \to \infty$. The theorem is proved. ■

Note that for a nonlinear operator equation (1) in a Banach space X, along with the projection-iteration method (24) based on Newton's method, one can also apply a projection-iteration process based on the modified Newton's method

$$\tilde{u}_n^{(k+1)} = \tilde{u}_n^{(k)} - [\tilde{A}_n'(\tilde{u}_n^{(0)})]^{-1}(\tilde{A}_n\tilde{u}_n^{(k)} - \tilde{f}_n), \quad k = 0,1,...,k_n - 1;$$

$$\tilde{u}_{n+1}^{(0)} = \Phi_{n+1}\Phi_n^{-1}\tilde{u}_n^{(k_n)}, \quad n \geq N, \quad \tilde{u}_N^{(0)} = \Phi_N u_N^{(0)} \in \tilde{\Omega}_N.$$

Similarly, along with the projection-iteration method (25), a process based on a modified Newton-like method can be applied:

$$\tilde{u}_n^{(k+1)} = \tilde{u}_n^{(k)} - \tilde{D}_n(\tilde{u}_n^{(0)})(\tilde{A}_n\tilde{u}_n^{(k)} - \tilde{f}_n), \quad k = 0,1,...,k_n - 1; \quad (25)$$

$$\tilde{u}_{n+1}^{(0)} = \Phi_{n+1}\Phi_n^{-1}\tilde{u}_n^{(k_n)}, \quad n \geq N, \quad \tilde{u}_N^{(0)} = \Phi_N u_N^{(0)} \in \tilde{\Omega}_N .$$

Although such modified projection-iteration processes converge more slowly than process (24) based on Newton's method, they are less laborious, since for each $n \geq N$ they use operators $[\tilde{A}_n'(\tilde{u}_n^{(0)})]^{-1}$ or $\tilde{D}_n(\tilde{u}_n^{(0)})$ corresponding only to the initial point $\tilde{u}_n^{(0)} \in \tilde{\Omega}_n$.

We note, finally, that, as follows from the proofs of theorems on the convergence of projection-iteration methods based on Newton's method and its modification for solving nonlinear operator equations of the form (1), the convergence of approximations sequences $\{\tilde{u}_n^{(k_n)}\}_{n=N}^{\infty}$, $\{\Phi_n^{-1}\tilde{u}_n^{(k_n)}\}_{n=N}^{\infty}$ to a solution u^* in X, as well as the convergence of elements $u_n^{(k_n)}$ and $\bar{\Phi}_n u^*$ in $\tilde{X}_n$ when $n \to \infty$ occurs with an arbitrary choice of numbers k_n. In particular, some numbers k_n can be equal to 1. However, as n grows, the amount of computational work required to find the next approximation increases. Therefore, it is necessary to strive to approximate a sought solution as best as possible for a given n due to a suitable choice of k_n, and only then proceed to the solution of the next approximate equation. On the other hand, one should not choose a number k_n for a given n too large, since, starting from a certain moment, an increase in the number of iterations does not lead to a significant improvement in the next approximations with respect to a solution of the original equation.

Thus, the question arises about the appropriate choice of numbers k_n ($n \geq N$). Some recommendations on this matter are given in [1, 2].

Let us consider a method of choosing numbers k_n in such a way that the element $\tilde{u}_{n+1}^{(0)} = \Phi_{n+1}\Phi_n^{-1}\tilde{u}_n^{(k_n)}$ is a good initial approximation for the $(n+1)$-th approximate equation of the form (19), that is, so that the discrepancy $\tilde{r}_{n+1}^{(0)} = \tilde{A}_{n+1}\tilde{u}_{n+1}^{(0)} - \tilde{f}_{n+1}$ takes on as small a quantity as possible. Let us estimate this discrepancy for any $n \geq N$:

$$\| \tilde{r}_{n+1}^{(0)} \|_{\tilde{X}_{n+1}} = \| \tilde{A}_{n+1}\tilde{u}_{n+1}^{(0)} - \tilde{f}_{n+1} \|_{\tilde{X}_{n+1}} =$$

$$= \| \tilde{A}_{n+1}\tilde{u}_{n+1}^{(0)} - \tilde{f}_{n+1} + \Phi_{n+1}\Phi_n^{-1}(\tilde{r}_n^{(k_n)} - \tilde{A}_n\tilde{u}_n^{(k_n)} + \tilde{f}_n) \|_{\tilde{X}_{n+1}} \leq \| \tilde{r}_n^{(k_n)} \|_{\tilde{X}_n} +$$

$$+ \| \tilde{A}_{n+1}\tilde{u}_{n+1}^{(0)} - \Phi_{n+1}\Phi_n^{-1}\tilde{A}_n\tilde{u}_n^{(k_n)} \|_{\tilde{X}_{n+1}} + \| \Phi_{n+1}\Phi_n^{-1}\tilde{f}_n - \tilde{f}_{n+1} \|_{\tilde{X}_{n+1}} =$$

$$= \| \tilde{r}_n^{(k_n)} \|_{\tilde{X}_n} + \tilde{\theta}_n,$$

where

$$\tilde{\theta}_n = \| \tilde{A}_{n+1}\tilde{u}_{n+1}^{(0)} - \Phi_{n+1}\Phi_n^{-1}\tilde{A}_n\tilde{u}_n^{(k_n)} \|_{\tilde{X}_{n+1}} + \| \Phi_{n+1}\Phi_n^{-1}\tilde{f}_n - \tilde{f}_{n+1} \|_{\tilde{X}_{n+1}}, \; n \geq N.$$

Since $\| \tilde{r}_n^{(k_n)} \|_{\tilde{X}_n} \to 0$, $k_n \to \infty$ under the conditions of Theorem 3, then the order of smallness of $\| \tilde{r}_{n+1}^{(0)} \|_{\tilde{X}_{n+1}}$ for a given n is determined by the

quantity $\tilde{\theta}_n$. Therefore, it is sufficient to choose a number k_n so that the quantities $\| \tilde{r}_n^{(k_n)} \|_{\tilde{X}_n}$ and $\tilde{\theta}_n$ have the same order of smallness; in particular, the role of k_n can be played by the smallest of numbers k $(k = 0,1,...)$ satisfying the inequality

$$\| \tilde{r}_n^{(k)} \|_{\tilde{X}_n} \le C \cdot \tilde{\theta}_n, \quad n \ge N, \tag{30}$$

where $C > 0$ is a constant.

When solving equations (19), there is no need to take all numbers $n = N, N+1,...$ sequentially, that is, from the n-th approximate equation, one can pass to the equation with index $n+\ell$, where $\ell \ge 1$. The idea underlying the above method of choosing numbers k_n allows us to find the most acceptable number $n+\ell$ $(\ell \ge 1)$ of the approximate equation (19) following the n-th one [2]. Namely, if the number k_n of iterations for the n-th approximate equation has already been determined, then, using inequality (30), we can write that

$$\| \tilde{r}_{n+1}^{(0)} \|_{\tilde{X}_{n+1}} \le (C+1) \cdot \tilde{\theta}_n, \quad n \ge N.$$

And since a similar condition can also be satisfied for the quantities $\| \tilde{r}_{n+j}^{(0)} \|_{\tilde{X}_{n+j}}$, where $\tilde{r}_{n+j}^{(0)} = \tilde{A}_{n+j} \tilde{u}_{n+j}^{(0)} - \tilde{f}_{n+j}$, $\tilde{u}_{n+j}^{(0)} = \Phi_{n+j} \Phi_n^{-1} \tilde{u}_n^{(k_n)}$, $j > 1$, then the role of ℓ can be played by the largest of numbers j $(j = 1,2,...)$ satisfying the inequality

$$\| \tilde{r}_{n+j}^{(0)} \|_{\tilde{X}_{n+j}} \le (C+1) \cdot \tilde{\theta}_n, \quad n \ge N .$$

Some other ways to choose numbers k_n in the projection-iteration methods of solving nonlinear equations, as well as their application in solving specific problems, are contained in [1, 3, 17–21].

REFERENCES

[1] Гарт, Л.Л. *Проекційно-ітераційні методи розв'язання операторних рівнянь та задач нескінченновимірної оптимізації*, Дис… д-ра фіз.-мат. наук, 01.05.01, МОН України, Дніпро: ДНУ, 2016, 293 с. [Hart, L.L. *Projection-iteration methods for solving operator equations and infinite-dimensional optimization problems*, Thesis … Doctor's degree in phys.-math. sciences, 01.05.01, Ministry of education and science of Ukraine, Dnipro: DNU, 2016, 293 p.]

[2] Балашова, С.Д. *Приближенные методы решения операторных уравнений*, Днепропетровск: ДГУ, 1980, 112 с. [Balashova, S.D. *Approximate methods for solving operator equations*, Dnepropetrovsk: DSU, 1980, 112 p.]

[3] Балашова, С.Д., Гарт, Л.Л. *Об одном подходе к решению эллиптических нелинейных задач*, Математические модели и вычислительные методы в прикладных задачах, Днепропетровск: ДГУ, 1996, 24–29. [Balashova, S.D., Hart, L.L. *On one approach to solving elliptic nonlinear problems*, Mathematical models and computational methods in applied problems, Dnepropetrovsk: DSU, 1996, 24–29.]

[4] Канторович, Л.В. *Функциональный анализ и прикладная математика*, Успехи математических наук, 1948, 3(6), 89–185. [Kantorovich, L.V. *Functional analysis and applied mathematics*, Advances in Mathematical Sciences, 1948, 3(6), 89–185.]

[5] Канторович, Л.В. *О методе Ньютона для функциональных уравнений*, Доклады АН СССР, 1948, 59(7), 1237–1240. [Kantorovich, L.V. *On Newton's method for functional equations*, Reports of the USSR Academy of Sciences, 1948, 59(7), 1237–1240.]

[6] Канторович, Л.В., Акилов, Г.П. *Функциональный анализ*, СПб.: Невский Диалект, 2004, 816 с. [Kantorovich, L.V., Akilov, G.P. *Functional analysis*, St.Petersburg: Nevsky Dialect, 2004, 816 p.]

[7] Мысовских, И.П. *О сходимости метода Л.В. Канторовича для решения нелинейных функциональных уравнений и его применениях,* Вестник ЛГУ, 1953, 11, 25–48. [Mysovskikh, I.P. *On the convergence of the L.V. Kantorovich method for the solution of nonlinear functional equations and its applications*, Vestnik of Leningrad State University, 1953, 11, 25–48.]

[8] Вертгейм, Б.А. *Об условиях применимости метода Ньютона*, Доклады АН СССР, 1956, 110(5), 719–722. [Vertgeim B.A., *On conditions for the applicability of Newton's method,* Reports of the USSR Academy of Sciences, 1956, 110(5), 719–722.]

[9] Yamamoto, T. *Historical developments in convergence analysis for Newton's and Newton-like methods*, Journal of Computational and *Applied Mathematics*, 2000, 124(1–2), 1–23.

[10] Deuflhard, P. *Newton methods for nonlinear problems: affine invariance and adaptive algorithms*, Springer Series in Computational Mathematics, Vol. 35, Springer-Verlag, Berlin, 2004, 424 p.

[11] Polyak, B.T. *Newton-Kantorovich method and its global convergence*, Journal of Mathematical Sciences, 2006, 133(4), 1513–1523.

[12] Argyros, I.K. *On Newton's method for solving nonlinear equations and function splitting*, Numerical Mathematics: Theory, Methods and Applications, 2011, 4(1), 53–67.

[13] Ezquerro Fernández, J.A., Hernández Verón, M.Á. *The classic theory of Kantorovich.* In: Newton's method: an updated approach of Kantorovich's theory. Frontiers in Mathematics, Birkhäuser, Cham, Switzerland, 2017, 1–38.

[14] Гарт, Л.Л. *К вопросу о сходимости метода Ньютона при условиях типа Коши*, Вопросы прикладной математики и математического моделирования, Днепропетровск: ДГУ, 1997, 152–155. [Hart, L.L. *On the question of the Newton's method convergence under the conditions of Cauchy type*, Problems of applied mathematics and mathematical modeling, Dnepropetrovsk: DSU, 1997, 152–155.]

[15] Гарт, Л.Л. *Ітераційні процеси розв'язання нелінійних операторних рівнянь, подібні до методу Ньютона, та їх модифікації*, Питання прикладної математики і математичного моделювання, Дніпро: Ліра, 2017, 17, 32–41. [Hart, L.L. *Iterative Newton-like processes for solving nonlinear operator equations and their modifications*, Problems of applied mathematics and mathematical modeling, Dnipro: Lira, 2017, 17, 32–41.]

[16] Hart, L.L. *Projection-iteration realization of a Newton-like method for solving nonlinear operator equations*, Journal of Optimization, Differential Equations and their Applications, 2019, 27(1), 56–66.

[17] Hart, L.L., Polyakov, N.V. *Projection-iteration realization on the Newton-Kantorovich method for solving nonlinear integral equations*, Journal of Automation and Information Sciences, 2012, 44(1), 40–49.

[18] Hart, L.L. *The application of projection-iteration methods to solving optimal control problems for systems of ordinary differential equations*, Hamburger Beiträge zur Angewandten Mathematik, Institut für Angewandten Mathematik der Universität Hamburg, Deutschland, Reihe A, 2000, 152, 1–17.

[19] Гарт, Л.Л., Поляков, М.В. *Застосування проекційно-ітераційного підходу, основаного на методі прямих, до розв'язування нелінійної еліптичної крайової задачі*, Питання прикладної математики і математичного моделювання, Дніпропетровськ: ДНУ, 2005, 68–77. [Hart, L.L., Polyakov, N.V. *Application of a projection-iterative approach based on the method of lines to solving a nonlinear elliptic boundary value problem*, Problems of applied mathematics and mathematical modeling, Dnipropetrovsk: DNU, 2005, 68–77.]

[20] Гарт, Л.Л. *О численном моделировании решения нелинейного параметрического уравнения проекционно-итерационным методом*, Питання прикладної математики і математичного моделювання, Дніпропетровськ: ДНУ, 2011, 66–75. [Hart, L.L. *On numerical modeling a solution of a nonlinear parametric equation by the projection-iteration*

method, Problems of applied mathematics and mathematical modeling, Dnipropetrovsk: DNU, 2011, 66–75.]

[21] Гарт, Л.Л. *Проекционно-итерационный метод численного анализа нелинейного уравнения с параметром*, Питання прикладної математики і математичного моделювання, Дніпропетровськ: ДНУ, 2012, 72–82. [Hart, L.L. *Projection-iteration method for the numerical analysis of a nonlinear equation with a parameter*, Problems of applied mathematics and mathematical modeling, Dnipropetrovsk: DNU, 2012, 72–82.]

CHAPTER 5

HEAT AND MASS TRANSFER FLOW FILLED WITH HYBRID NANOFLUID BY NON-ISOTHERMAL MOVING SURFACE: A TRANSPIRATION AND THERMAL RADIATION APPROACH

Sultana JAHAN [1] & Mohammad FERDOWS [1,*]

[1] Prof. Research Group of Fluid Flow Modelling and Simulation, Department of Applied Mathematics, University of Dhaka, Dhaka-1000, Bangladesh.
[*] Prof. Corresponding author: ferdows@du.ac.bd ,ORCİD: 0000-0002-0949-3898

INTRODUCTION

For getting excellent thermal efficiency, researchers and scientists introduce a colloidal solvent namely nanofluid [1]. As it has more heat transfer properties than regular fluid (such as water, ethylene glycol, engine oil) [2], it is considered as a favorable working fluid in the industrial and engineering field. Having the particles of nanometer size with regular fluid is beneficial for the heat transfer to augment in any application area. The effects of the chemical reaction of nanofluid were investigated through a stretching sheet [3]. The reason behind the thermal efficiency regarding the dispersion of the suspended nanoparticle has been investigated [4].

Hybrid nanofluid is the upgraded version of nanofluid, which has even more thermal efficiency than both nanofluid and regular fluid. Representing the whole new idea of hybrid nanofluid in the area of nanotechnology, material science, and engineering has been experienced remarkable growth with the potential influence of this fluid. Hybrid nanofluid (is composed by the combining mixture of two or more different nanoparticles in regular nanofluid disperses in the base fluid which has upgraded thermal conductivity along with rheological behavior and thermophysical properties [5]. As it has hybrid nanoparticles which have more capability of increasing the heat transfer rate with effects named synergistic [6]. Adding a small number of nanoparticles, it is found that the thermal conductivity is increased up to twice [7]. Due to the higher thermal conductivity, it has a vast applications area in the branches of the heat exchanger,

nuclear system cooling, coolant in machining, transformer cooling, solar collector, micropower generation, heat sink, boiling, electronic cooling, refrigeration, drug reduction, biomedical [8].

Boundary layer flow is a very thin region where viscous force plays a significant role in the surface over which fluid is flowing over, the viscosity can be neglected without significant effects on the solution outside of the boundary layer. All the changes of flow pattern are occurred by the boundary layer effect at the flow region. With the phenomenal vicious force, it has been used in some exceptional interesting areas in the branches of engineering including chemical, nuclear, aeronautical, marine, environmental, mechanical engineering. The boundary layer is the part of the airflow close to the wing on the aircraft wing [9]. Multiple types of boundary layers can coexist near a surface simultaneously like velocity boundary layer, mass boundary layer, and temperature boundary layer [10]. It has been used in some exceptional interesting areas in the branches of engineering including chemical, nuclear, aeronautical, marine, environmental, mechanical engineering. By using boundary layer flow [11-14] theory, many types of research have been examined to predict the flow behavior of hybrid nanofluid.

To get the proper prediction about hybrid nanofluid several effects and physical properties are used over the different surfaces with different hybrid nanoparticles. With the suction and hydrodynamic [15] effects on moving surface, it is examined that the Magnetic parameter increased the rate of heat transfer. Increasing distribution of

temperature has been found with the influence of viscous dissipation [16]. Boundary layer separation with decelerated velocity has been noticed [17] for the effect of melting parameter. The range of moving parameter rises for the suction in fluid flow [18] so that delays in boundary layer separation has been identified. The dual solution has been found for the unsteadiness parameter also the stability analysis has checked [19]. It is also noticed that the delay of the boundary layer separation is occurred by an increasing amount of volume fraction of mixed convective [20] hybrid nanofluid. The existence of a dual solution has been found for the opposing flow [21-23]. The effects like thermal radiation [24] and chemical reaction in a dissipative hybrid nanofluid have been investigated [25]. A mixed convective 3D nanofluid has been investigated [26], hence found a great augment in thermal distribution with Brownian motion parameter. On velocity, temperature, and concentration profile shows significant impact [27] which is satisfied thermally. To find out the flow behavior even better, researchers are examined natural [28], mixed [29-31], and forced convection [32].

Engine oil is the basic lubricant used in machineries due to its thermophysical properties to enhance the heat transfer in the system. Some research has been done to find out the impact [33] of engine oil-based micro and nanosized particles. Discussing the rotating phenomena, a study has been reported with tribological effect [34], hence, to enhance the thermal distribution with the wall temperature [35]. Adding more nanoparticles in the solution velocity recedes down

but an augment in temperature has been found [36]. Also, the heat transfer rate gets 23.17% higher [37] by Maxwell hybrid nanofluid.

Through the above survey, our present study is highly motivated to investigate theoretically and numerically the flow behavior of hybrid nanofluids toward flow and heat transfer through non-isothermal moving surfaces [38]. The problem of moving solid surfaces with the boundary layer behavior plays a vital role in many branches of engineering sector. Especially, in the feed rolling, which is constructed by the travel between the heat generated materials, manufacturing of materials by extrusion, wind up rolling, cooling of electronic chips or metallic sheets, production of glass fiber and paper, crystal growing, and many more. As engine oil is the basic lubricant for the engines of the machineries, our study is focused to prevent energy wastage regarding high temperature. Here, a special hybridization of $TiO_2 - CuO$ as a homogeneous combination with engine oil, is considered to predict the thermal distribution in the system. Furthermore, the investigation is also influenced by the effects of thermal radiation [39], transpiration [40], and Brownian motion [41]. To our best knowledge, no study has been investigated or reported to obtain this special solution of engine oil-based hybridized nanoparticles. This special solution finds excellent agreement through the validation with previous well known research.

Table 1: Thermophysical properties of base fluid and nanoparticles:

Thermophysical properties	Engine Oil	Titania (TiO_2)	Copper Oxide (CuO)
Heat capacity, C_p(J/kgK)	1910	686.2	533
Density, ρ(kg/m^3)	884	4250	6500
Thermal conductivity, κ(W/mK)	0.144	8.9538	17.65
Thermal expansion β×10^{-5}(1/K)	70	0.9	1.80

Here, the thermophysical properties of hybrid nanofluid including dynamic viscosity, effective density, effective heat capacity, effective thermal conductivity and effective thermal expansion.

$$c_1 = \frac{\mu_{hnf}}{\mu_f} = \frac{1}{(1-\varphi_1)^{2.5}(1-\varphi_2)^{2.5}}$$

$$c_2 = \frac{\rho_f}{\rho_{hnf}} = \frac{\rho_f}{(1-\varphi_2)\left[(1-\varphi_1)\rho_f+\varphi_1\rho_{n1}\right]+\varphi_2\rho_{n2}},$$

$$c_3 = \frac{(\rho C_p)_f}{(\rho C_p)_{hnf}} = \frac{(\rho C_p)_f}{(1-\varphi_2)\left[(1-\varphi_1)(\rho C_p)_f+\varphi_1(\rho C_p)_{n1}\right]+\varphi_2(\rho C_p)_{n2}}$$

$$c_4 = \frac{k_{hnf}}{k_{nf}}, \frac{k_{hnf}}{k_f} = \frac{k_{n2}+2\varphi_2 k_{n2}+k_{nf}(2-2\varphi_2)}{k_{n2}-\varphi_2 k_{n2}+k_{nf}(2+\varphi_2)}$$

$$where, \frac{k_{nf}}{k_f}\left(\frac{k_{n1}+2k_f-2\varphi_1(k_f-k_{n1})}{k_{n1}+2k_f+\varphi_1(k_f-k_{n1})}\right)$$

$$c_5 = \frac{(\rho\beta)_{hnf}}{(\rho\beta)_f} = \frac{(1-\varphi_2)\left[(1-\varphi_1)(\rho\beta)_f+\varphi_1(\rho\beta)_{n1}\right]+\varphi_2(\rho\beta)_{n2}}{(\rho\beta)_f};$$

FLOW ANALYSIS

Considering, a steady laminar mixed convective two-dimensional flow over non isothermal moving surface. Here, X and Y represent the Cartesian coordinates, y-axis is perpendicular to x-axis which is measured along with the moving plate. By assuming that the uniform free steam velocity U of surface moves toward and away from the origin. The velocity U is parallel to the plate located $y = 0$ as drawn in **Fig-A**. velocity components of x and y axes are represented by u, v respectively, the temperature T and the concentration C, are constant and the surface temperature and ambient temperature are T_w and T_∞ such that $T_w > T_\infty$. C_∞, C_w represent the ambient and surface nanoparticle concentration, where $C_w > C_\infty$. With this boundary layer flow assumption, the governing equations [38,39,41] of hybrid nanofluid flow are expressed as following:

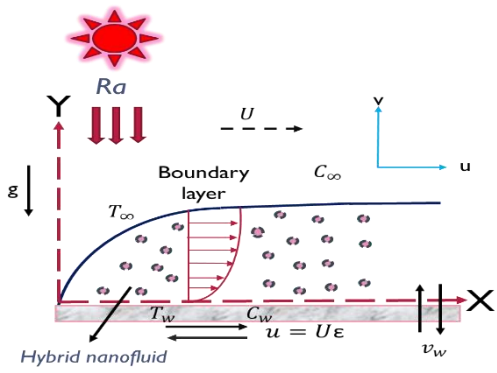

Fig A: Physical Model

$$\frac{\partial u}{\partial x} + \frac{\partial v}{\partial y} = 0 \tag{1}$$

$$u\frac{\partial u}{\partial x}+v\frac{\partial v}{\partial y}=\ \nu_{hnf}\frac{\partial^2 u}{\partial y^2}+\frac{g(\rho\beta_T)_{hnf}}{\rho_{hnf}}(T-T_\infty)+\frac{g(\rho\beta_C)_{hnf}}{\rho_{hnf}}(C-C_\infty) \quad (2)$$

$$\left(\rho C_p\right)_{hnf}\left(u\frac{\partial T}{\partial x}+v\frac{\partial T}{\partial y}\right)=\kappa_{hnf}\frac{\partial^2 T}{\partial y^2}+\left(\rho C_p\right)_s\left[D_B\frac{\partial C}{\partial y}\frac{\partial T}{\partial y}+\left(\frac{D_T}{T_\infty}\right)\left(\frac{\partial T}{\partial y}\right)^2\right]+\frac{16\sigma}{3k^*}\frac{\partial}{\partial y}(T^3\frac{\partial T}{\partial y}) \quad (3)$$

$$u\frac{\partial C}{\partial x}+v\frac{\partial C}{\partial y}=D_B\frac{\partial^2 C}{\partial y^2}+\frac{D_T}{T_\infty}\frac{\partial^2 T}{\partial y^2} \quad (4)$$

The boundary conditions are as following:

$$u=U_\infty\varepsilon, v=v_w(x)\ ,\ \ T=T_w=T_\infty+Ax^\lambda, C=C_w=C_\infty+Bx^\lambda$$
at $y=0$

$$u\to U_\infty, C\to C_w, T\to T_w \text{ as } y\to\infty \quad (5)$$

In this, A and B are constant λ is the power law exponent. Here, ε is constant moving parameter, U_∞ is the free stream velocity. the surface temperature, Further, D_B and D_T indicates the Brownian diffusion and thermophoretic diffusion coefficients, the ratio of effective heat capacity is $\tau=(\rho C_p)_s/\left(\rho C_p\right)_f$, here, ν_{hnf}, $\sigma_{hnf}, g, (\beta_T)_{hnf}, (\beta_C)_{hnf}$ $(\rho C_p)_{hnf}$ are denoted as kinematic viscosity, electrical coductivity, gravity acceleration, thermal

expansion coefficient, concentration expansion coefficient and heat capacity of hybrid nanofluid.

The following similarity transformation are using here [38,39,41]

$$\eta = y\sqrt{\frac{U}{2xv_f}}\,,\ \psi = \sqrt{2Uxv_f}\,f'(\eta)\,,\ u = Uf'(\eta),$$

$$v = \sqrt{\frac{Uv_f}{2x}}\,(\eta f'(\eta) - f(\eta)),\ \theta(\eta) = \frac{T-T_\infty}{T_w-T_\infty}\,,\ \phi(\eta) = \frac{C-C_\infty}{C_w-C_\infty},$$

$$\frac{T}{T_\infty} = (1 + (\theta_w - 1)\theta(\eta))$$

So that,

$$v_w(x) = -\sqrt{\frac{Uv_f}{2x}}\ f(0) \tag{6}$$

We consider $S = f(0)$, which indicates the muss flux constant, if $S > 0$ that means the suction of fluid and $S < 0$ means the injection of the fluid.

Assuming the similarity variable from equation (6), (2), (3) & (4) are transformed into the following non-linear ODE's;

$$c_1c_2f''' + ff'' + 2c_5c_2\lambda_t\theta + 2c_5c_2\lambda_c\phi = 0 \tag{8}$$

$$c_3 \frac{1}{Pr}\Big((c_4 + Ra[1 + (\theta_w - 1)\theta]^3)\theta'' + 3Ra[1 + (\theta_w - 1)\theta]^2(\theta_w - 1)\theta'^2\Big)$$

$$+f\theta' - 2\lambda f'\theta + Nbc_3\theta'\phi' + Ntc_3\theta'^2 = 0$$

$$\phi'' + Lef\phi' - 2\lambda Lef'\phi + \frac{Nt}{Nb}\theta'' = 0 \qquad (9)$$

Subject to:

$$f(0) = S, \qquad f'(0) = \varepsilon, \qquad \theta(0) = 1, \qquad \phi(0) = 1 \qquad (10)$$

$$f'(\eta) \to 1, \theta(\eta) \to 0, \phi(\eta) \to 0 \; as \; \eta \to \infty$$

There is indication of primes which denotes the differentiation with respect to η. Also, λ_t, λ_c Pr, Nt, Nb, Le, Ra, θ_w represents Mixed convection due to temperature, mixed convection due to concentration, Prandtl number, thermophoresis parameter, Brownian motion parameter, Lewis number, Thermal radiation and temperature parameter.

$$Pr = \frac{\nu_f(\rho c_p)_f}{k_f}, \text{Le} = \frac{\nu_f}{D_B}, Nt = \frac{\tau D_T(T_w - T_\infty)}{\nu_f T_\infty}, \; Nb = \frac{\tau D_B(C_w - C_\infty)}{\nu_f}, Ra = \frac{16\sigma T_\infty^3}{3k_f k^*}, \theta_w = \frac{T_w}{T_\infty}, \lambda_c = \frac{Gr_t}{Re_x^2}, \; \lambda_t = \frac{Gr_c}{Re_x^2}$$

$$Gr_t = \frac{g(\beta_T)_f(T_w - T_\infty)x^3}{\nu^2}, Re_x = \frac{Ux}{\nu}, Gr_c = \frac{g(\beta_c)_f(C_w - C_\infty)x^3}{\nu^2}$$

Here, ε > 0 and ε < 0 represents the downstream movement and the upstream movement of the plate. from

The quantities of physical interest are the skin friction coefficient C_f and the local Nusselt number Nu_x and Sherwood number Sh_x which are defined as

$$C_f = \frac{\tau_w}{\rho_f U^2} \ , Nu_x = \frac{x q_w}{\kappa_f (T_w - T_\infty)} \ , \qquad (11)$$

$$Sh_x = \frac{x q_m}{D_B (C_w - C_\infty)}$$

where the shear stress along the surface is τ_w, the heat flux q_w and the mass flux is q_m of the moving surface are given by

$$\tau_w = \mu_{hnf} \left(\frac{\partial u}{\partial y}\right)_{y=0} \ , q_w = -\kappa_{hnf} \left(\frac{\partial T}{\partial y}\right)_{y=0} \ ,$$

$$q_m = -D_B \left(\frac{\partial C}{\partial y}\right)_{y=0} \qquad (12)$$

Using (6), (11) and (12), we get

$$Re_x^{1/2} C_f = \frac{1}{\sqrt{2}} \frac{\mu_{hnf}}{\mu_f} f''(0), \quad Re_x^{-1/2} Nu_x$$
$$= -\frac{1}{\sqrt{2}} \frac{\kappa_{hnf}}{\kappa_f} \theta'(0), \quad Re_x^{\frac{1}{2}} Sh_x = -\frac{1}{\sqrt{2}} \frac{\mu_{hnf}}{\mu_f} \phi'(0)$$

ANALYSIS OF OUTCOMES & BRIEF DISCUSSION

To elucidate the thermophysical properties of the hybrid nanofluid, the present result is conducted with the 1% volume fraction of TiO_2, i.e. φ_1=0.01 and 1% volume fraction of the CuO i.e. φ_2=0.01. To further investigation dissimilar volume fractions of CuO are added into the mixture to finalize the TiO_2-$Cuo/engine\ oil$ throughout the study. We consider the Prandtl number Pr=30 for the base fluid (engine oil) to get better accuracy [36]. The initial suitable assumption and the thickness of the boundary layer η_∞ is chosen for the values of the pertinent parameter used here. MAPLE computational software scheme [42,43] are accommodated the complex boundary condition (10) and the nonlinear couple boundary layer equations (7)-(9) are reported and all the outcomes are demonstrated in Fig 1-31. With the moving parameter $\varepsilon > 1$, the velocity profile shows diminish effect and with $\varepsilon < 1$ an increment in velocity profile has been found. Also, we are interested for the case where Lewis number Le> 1.

Table 2: Values for $\boldsymbol{f''(0)}$ for regular fluid $\boldsymbol{(\varphi_1 = \varphi_2 = 0)}$ when **S=0** and **ε=0**

Cortell [16]	Ishak et al [44]	Waini et al [38]	Present result
0.469602	0.469601	0.469600	0.469600

Table 3: Values for $f''(0)$ for regular fluid $(\varphi_1 = \varphi_2 = 0)$ when **S=0** and **ε=0.1**

Pr	Olanrewaju [25]	Haile & Shankar [24]	Aladdin, Bachok, Pop [15]	Present result
0.71	0.462512	0.462512	0.462512	0.462512
1	0.462512	0.462512	0.462512	0.462512

Table 4: Values for $f''(0)$ for regular fluid $(\varphi_1 = \varphi_2 = 0)$ when **S=0, Pr=6.2** with various values of ε

ε	Merkin [21]	Ahmad & Pop [22]	Waini et al [20]	Present result
-0.1	0.46105	0.46105	0.46105	0.46105
-0.15	0.44907	0.44907	0.44907	0.44907
-0.2	0.43015	0.43015	0.43015	0.43015
-0.25	0.40152	0.40152	0.40152	0.40154
-0.30.	0.35664	0.35664	0.35664	0.35671

The numerical processes are compared with the previous study to validate the result of this present study through the table 2-4. For the regular fluid $\varphi_1 = \varphi_2 = 0$ when S=0and ε=0 and the other parameters are absent, we find the excellent agreement in Table 2 by [16,44]. In Table 3 with different value of Prandtl number (Pr =0.71,1) when regular fluid $\varphi_1 = \varphi_2 = 0$, S=0 and ε=0.1, is also compared to clarify the higher accuracy [25,24,15] of the present research. We also compare the result for the downstream movement of the plate, i.e., $\varepsilon < 0$ with the previous well known study [21,22,20] in Table 4.

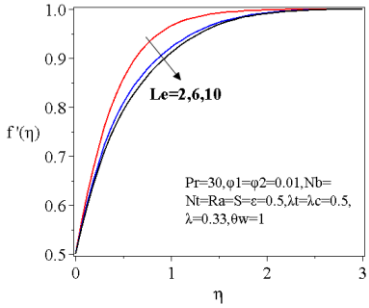

Fig 1: Impact of Le on f'(η)

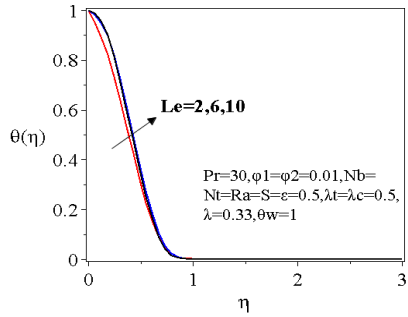

Fig 2: Impact of Le on θ(η)

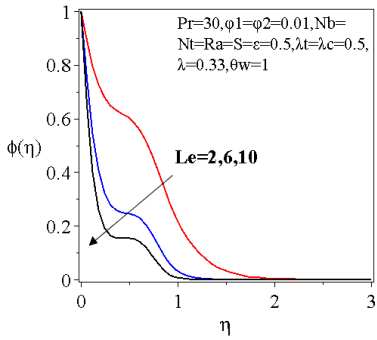

Fig 3: Impact of Le on ϕ(η)

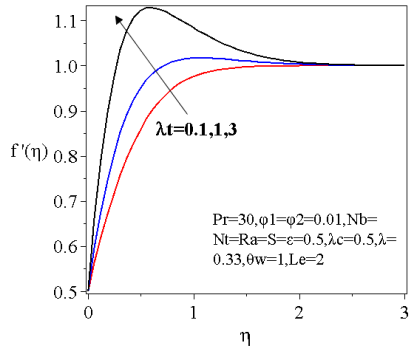

Fig 4: Impact of λt on f'(η)

Fig 1-3 disclose the distribution of Lewis number Le on velocity, temperature and concentration constituents. The resulting outcomes are examined for the greater value of Le (Le> 1). Which implies that the concentration boundary layer thickness is smaller than thermal boundary layer thickness. As Lewis number represent the ratio of thermal diffusivity to Brownian diffusion which also state that the volume fraction $\phi(\eta)$ will increase for the small value of Brownian diffusivity. For this reason, the higher value of Le reports a lessen performance on the concentration of fluid. Further, the fluid motion shows a declination in the velocity region with the greater value of

Lewis number. Whereas, the temperature of the fluid enhances by the rise in Lewis number.

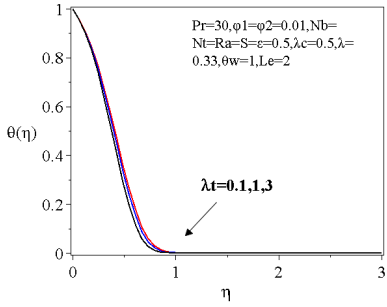

Fig 5: Impact of on λt θ(η)

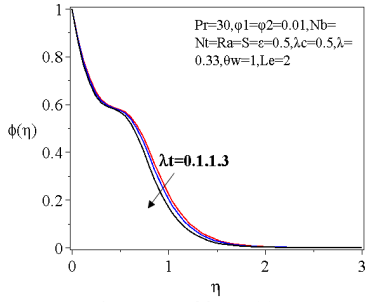

Fig 6: Impact of λt on φ(η)

Fig 4-6 illustrated the evalution in the velocity $f'(\eta)$, temperature $\theta(\eta)$**,** concentration $\phi(\eta)$ profile for the different quantities of mixed convection due to temperature, λ_t. Here we consider the values of λ_t=0.1,1,3, these values are stands for free, mixed and forced convection respectively. The velocity profile reveals a significant growth which accelerated the motion of fluid by λ_t for higher value. Momentum boundary layer thickness also rises for this reason. The temperature of the fluid recedes down through the increasing value of mixed convection which has been observed in temperature profile. Further, a reduction in λ_t also reduce the concentration of nanoparticle

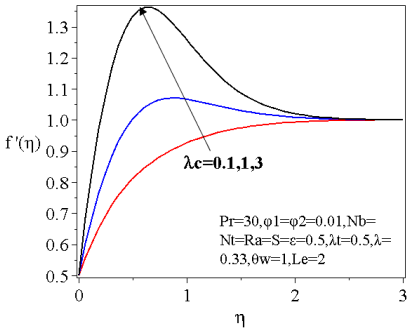

Fig 7: Impact of λc on f'(η)

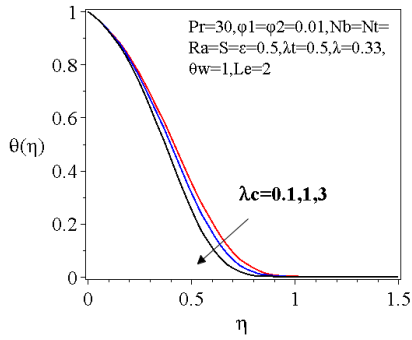

Fig 8: Impact of λc on θ(η)

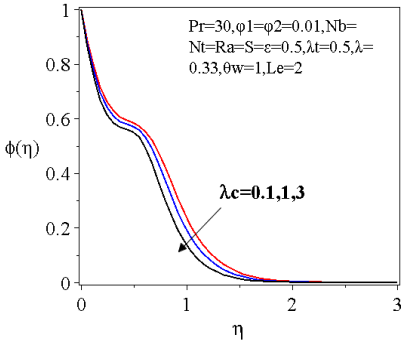

Fig 9: Impact of λc on φ(η)

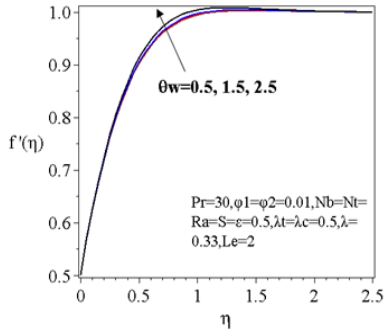

Fig 10: Impact of θw on f'(η)

Fig 7-9 shows the consequence of the mixed convection due to concentration parameter λ_c, on the fluid velocity, temperature and concentration profile. A strong increment on the velocity region has been found with the enlarge values of λ_c, As this particular parameter is occurred in the momentum equation. λ_c is proportional to the Grashof quantity due to concentration Gr_c, which is the ratio of the buoyancy strength to the glutinous hydrodynamic energy. Thermal conductivity of the fluid reduces due to the deceleration in temperature profile through higher values of λ_c. However, a depletion has reported in nanoparticle concentration with the rising value of mixed convection due to concentration.

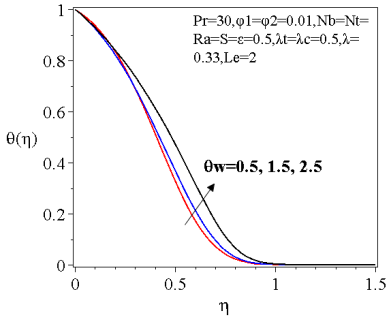

Fig 11: Impact of θw on θ(η)

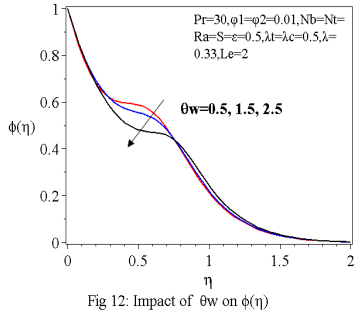

Fig 12: Impact of θw on ϕ(η)

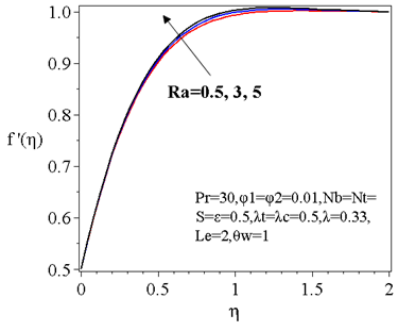

Fig 13: Impact of Ra on f'(η)

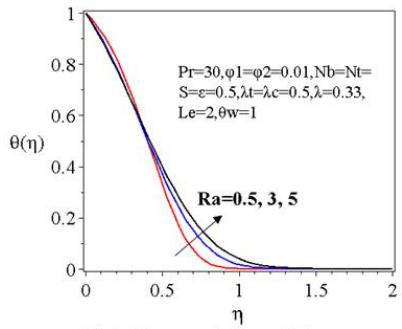

Fig 14: Impact of Ra on θ(η)

Fig 10-12 portrays to implies the impact of temperature ratio θ_w in velocity, temperature and concentration profile. The outcomes state an augment in the energy boundary layer thickness and also in thermal distribution with the increasing quantity of temperature ratio. Physically temperature ratio is proportional to the surface temperature, T_w and reciprocal to the ambient temperature or free stream temperature, T_∞, which indicates that with the enlarge quantity of θ_w surface temperature increases but the fluid temperature decrease. Due to the declination in the heat transfer rate the fluid remains cool. An improvement in velocity profile has been noticed which rises the motion of the liquid. With the escalating value of temperature ratio θ_w, the concentration profile shows a lessen report.

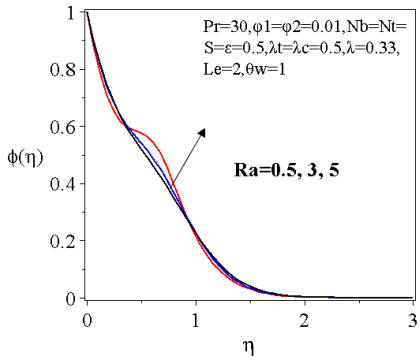

Fig 15: Impact of Ra on ϕ(η)

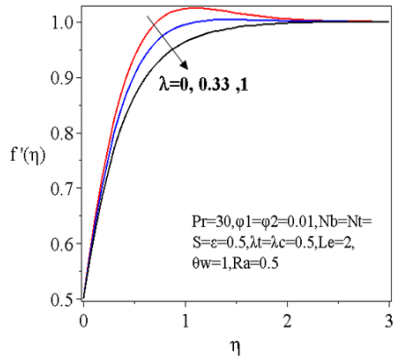

Fig 16: Impact of λ on f'(η)

Fig 13-15 exhibit the dissimilarity of velocity, temperature and concentration represent through diversified quantities of thermal radiation Ra, where Pr=30, $\varphi_1 = \varphi_2 = 0.01, \theta_w = 1, Nb = Nt = 0.5, S = \varepsilon = 0.5, \lambda = 0.33, \lambda_t = \lambda_c = 0.5$. Impact of thermal radiation for increasing value on velocity profile shows increment which enhance the fluid motion. Whereas, the temperature profile reports a significant improvement, as resultant the thermal boundary layer thickness growth is noticed. The thermal radiation parameter R is inversely proportional to the Stephan number (also known as stark number) which elucidate the significance of thermal radiation transport on the basis of heat transfer conduction. Thus, the enlargement of R shows a supremacy over the conduction of the fluid. Consequently, greater values of R indicate a strong increment on the fluid flow through radiative heat transfer energy, which has been poured in fluid by causing growth in temperature. Further, a depletion on the concentration magnitudes of nanoparticles is found with the increasing amount of thermal radiation and satisfy the solution asymptotically.

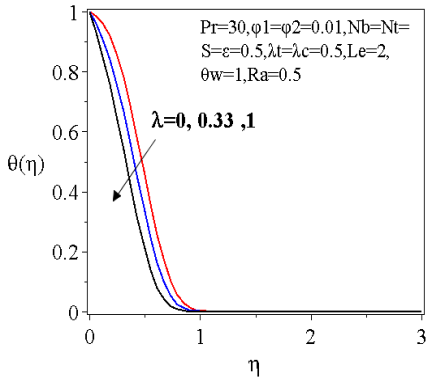

Fig 17: Impact of λ on θ(η)

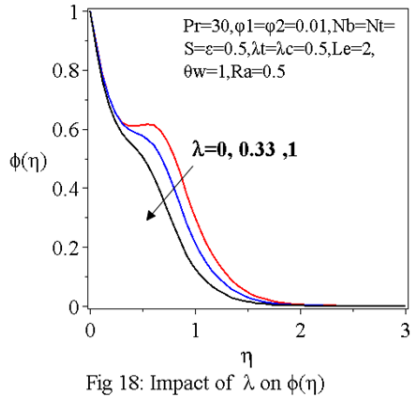

Fig 18: Impact of λ on ϕ(η)

Fig 16-18 visualize this disparity of power law exponent λ on velocity $f'(\eta)$, temperature $\theta(\eta)$, concentration $\phi(\eta)$ region. Here, we scrutinize the solution with the value of Pr=30, $\varphi_1 = \varphi_2 = 0.01, \theta_w = 1, Nb = Nt = Ra = 0.5, S = \varepsilon = 0.5, \lambda = 0.33, \quad \lambda_t = \lambda_c = 0.5.$ we also consider the the values of λ=0, 0.33, 1, these values stand for the isothermal surface to uniform temperature, uniform heat flux surface and non-isothermal surface respectively. Consequence revels a reduction in the fluid motion, therefore, with the larger quantity of power law exponent causes a diminish in flow rate. The power law exponent appears in the equation (5) of boundary condition, which reduce the viscous force due to slower flow rate. On the other hand, the heat distribution responses with a strong existence of heat generation due to the depletion in temperature profile. As a result, the large value of λ help the fluid to stay cool. In the concentration region, a declination in concentration magnitudes of nanoparticle is observed with the growth in power law exponent.

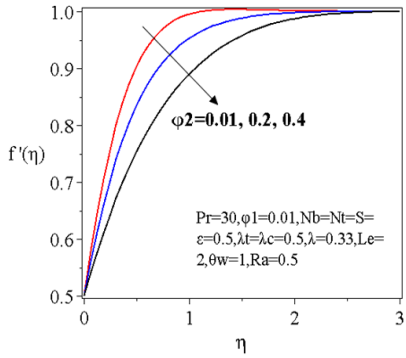

Fig 19: Impact of φ2 on f'(η)

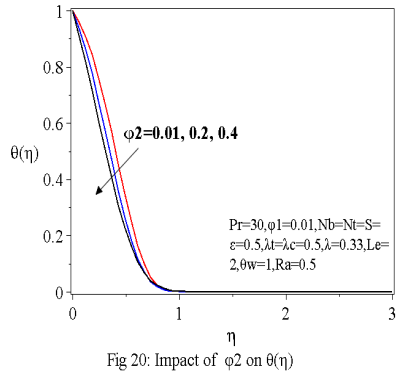

Fig 20: Impact of φ2 on θ(η)

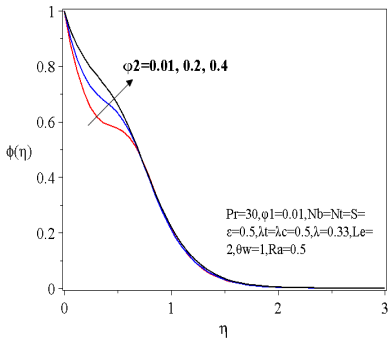

Fig 21: Impact of φ2 on ϕ(η)

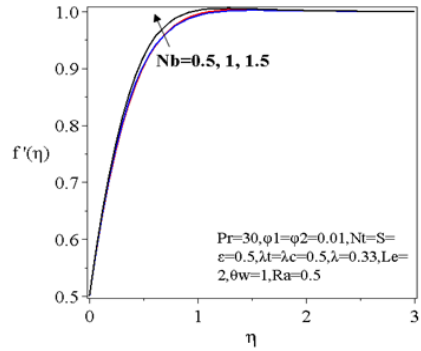

Fig 22: Impact of Nb on f'(η)

Fig 19-21 illustrate the evolution of dissimilar volume fraction φ_2 in velocity $f'(\eta)$, temperature $\theta(\eta)$**,** concentration $\phi(\eta)$ profile. The velocity profile reports a lessen fluid speed through the larger volume fraction φ_2.i.e the hydrodynamic boundary layer thickness decreases. The distribution of flow confirms a significant mechanism for escalating convection coefficients. However, temperature of the fluid recedes down as the viscosity of the fluid improve with the increment of φ_2 and hence the flow decelerated with the viscous force. Thus, thermal conductivity of the fluid revels a declination in heat transfer system. In conclusion, by adding nanoparticle of CuO to $TiO_2 - engine\ oil$ cool the resultant hybrid nanofluid. Further, an increment

in volume fraction enhances the concentration profile and satisfy the solution asymptotically for the free stream condition (Eq 10).

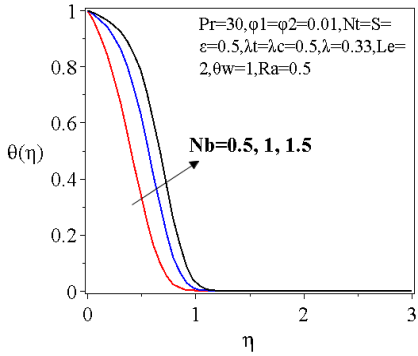

Fig 23: Impact of Nb on θ(η)

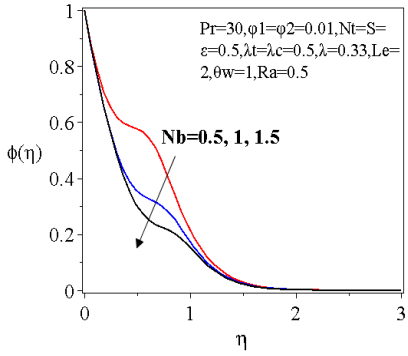

Fig 24: Impact of Nb on ϕ(η)

Fig 22-24 depicted to analyze the impact of Brownian motion parameter Nb in the velocity, temperature and concentration profile. As the parameter increases the fluid motion is also accelerated. The temperature of the liquid upsurges rapidly which enhance the thermal boundary layer thickness. A reverse phenomenon has been found in concentration profile as the growth in Brownian motion parameter. This elucidate that the higher rate of Nb Brownian motion parameter declines the performance of mass transfer in between the surface and free stream flow. Due to the random fluid motion of the nanoparticles suspended which caused by the continuous collision between the base fluid particle and nanoparticles.

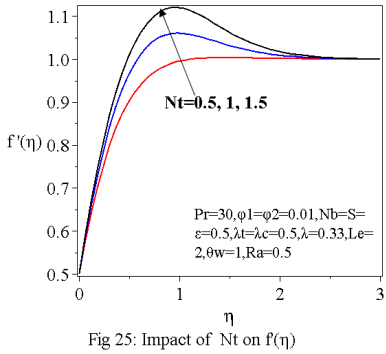

Fig 25: Impact of Nt on f'(η)

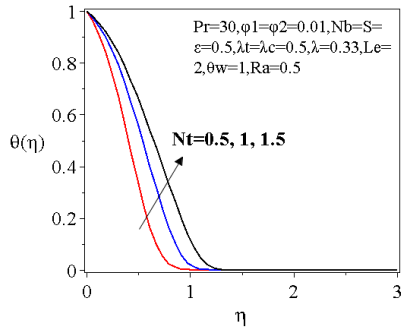

Fig 26: Impact of Nt on θ(η)

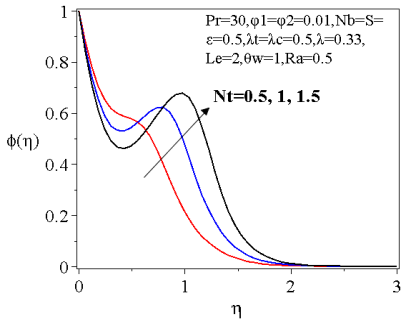

Fig 27: Impact of Nt on ϕ(η)

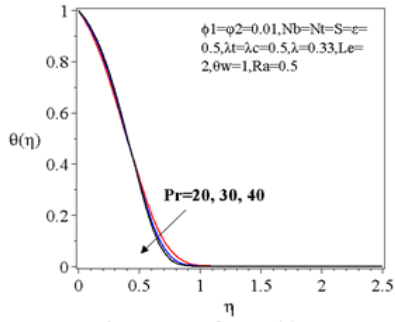

Fig 28: Impact of Pr on θ(η)

Fig 25-27 display the variation of the velocity, temperature and concentration region of the fluid for the impact of the thermophoresis parameter. Nt accelerate the fluid motion as the velocity profile shows a growth, which implies that for the greater Nt the boundary layer thickness of momentum get higher. As the thermal performance of the liquid rises, the heat transfer rate is also enhanced by the increment on thermophoresis parameter Nt. A major slip mechanism is observed which surplus the thermal boundary layer thickness rapidly. The reason behind this behavior, the heat transfer rate is directly proportional to the thermophoresis diffusion. In the concentration profile, we notice a powerful increment throughout the liquid region.

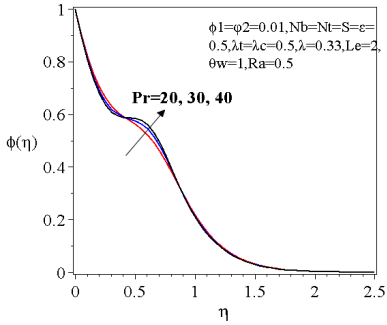

Fig 29: Impact of Pr on φ(η)

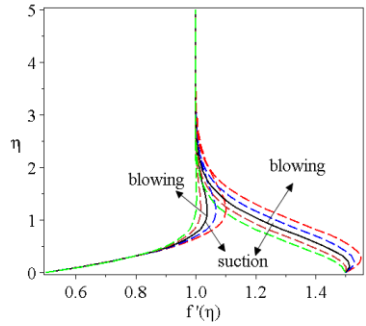

Fig 30: The impact of S on f'(η)

Fig 28-29 demostrate the consequence of the Prndtl Number Pr, on the temperature $\theta(\eta)$ and concentration $\phi(\eta)$ profile. The temperature of the liquid diminishes with the rising Pr (Pr$\gg$ 1). This represents the thermal boundary layer thickness became smaller. Physically this situation implies that the Prandtl number Pr reciprocal to the thermal diffusivity, as the result for higher increment in Pr causes a reduction in thermal conductivity, which recedes down the process of conduction. A dissimilarity has been found in concentration region; Pr enhance the concentration of fluid flow with the escalating quantities.

The demonastration in **Fig 30**, is showing the effect of blowing and suction on velocity profile with the solid line for the positive range of ε, which is ε=0.5 and 1.5. here, the plate is moving away from the origin with the half speed of the free stream velocity for the value of ε=0.5 and the speed gets two time faster than free streem which measuered for the value of ε=1.5. In both cases, blowing decreses the skin friction coeffecient denoted by $f''(0)$ and increses the boundary layer thickness, the opposite factor is observed for suction.

Table 5: Result computed for the dissimilar quantities of fluid flow parameters when $Pr = 30,\ \varphi_1 = \varphi_2 = 0.01, \theta_w = 1, Nb = Nt = 0.5, S = \varepsilon = 0.5, \lambda = 0.33,$ $\lambda_t = \lambda_c = 0.5, Ra = 0.5, Le = 2.$

λ_t	λ_c	Ra	θ_w	λ	Nb	Nt	Le	φ_2	S	Pr	$f''(0)$	$-\theta'(0$	$-\phi'(0$
0.1											1.06423	0.57653	2.08867
1											1.64302	0.56344	2.16961
3											2.83356	0.55754	2.31556
	0.1										0.96659	0.57731	2.04318
	1										0.14456	0.55461	2.21332
	3										3.22284	0.52931	2.46489
		0.5									1.32563	0.56561	2.12620
		3									1.33621	0.81645	1.86815
		5									1.34660	0.90578	1.76899
			0.5								1.32437	0.51456	2.17828
			1.5								1.32972	0.63925	2.04729
			2.5								1.35003	0.66071	1.99700
				0							1.42039	0.16293	2.03487
				0.33							1.32563	0.55561	2.12620
				1							1.21297	0.99595	2.43119
					0.5						1.32563	0.56561	2.12620
					1						1.34072	0.21509	2.19063
					1.5						1.38181	0.13189	2.14346
						0.5					1.32563	0.56561	2.12620
						1					1.47684	0.37799	2.49118

						1.5					1.57613	0.30073	2.79608
							2				1.11522	0.66123	2.00909
							6				0.96407	0.23898	4.77154
							10				0.90812	0.14894	7.00817
								0.01			1.32563	0.56561	2.12620
								0.2			0.99613	0.89737	1.77829
								0.4			0.65600	1.32862	1.30061
									-0.50		1.17288	0.30482	1.09384
									-0.25		1.21343	0.34337	1.34313
									0		1.25123	0.39079	1.61411
									0.25		1.28800	0.45777	1.88536
									0.50		1.32563	0.56561	2.12620
										20	1.32826	0.66283	2.02808
										30	1.32563	0.56561	2.12620
										40	1.32473	0.51545	2.17599

The numerical assumption of skin friction coefficient $f''(0)$, heat transfer rate $-\theta'(0)$ and mass transfer rate $-\phi'(0)$ has been observed through **Table 5**. Here, we notice the mixed convection due to temperature λ_t, mixed convection due to temperature λ_c, Brownian motion parameter Nb and thermophoresis parameters are elevated the skin friction coefficient and mass transfer rate but reduced the heat transfer rate. With the imposed higher amount of thermal radiation Ra and temperature ratio θ_w, heat transfer rate and skin friction

coefficient are increased, whereas the mass transfer rate is decreased. Larger values of Lewis number Le and Prandtl number Pr are escalated mass transfer rate but receded down the skin friction coefficient and heat transfer rate. Power law exponent λ shows increment in both heat and mass transfer rate but decline in skin friction coefficient. With the larger volume fraction φ_2 , the heat transfer rate strongly shows an improvement but reverse tendency is noticed for skin friction coefficient and mass transfer rate. For the large quantity of suction/injection parameter S, the skin friction coefficient, heat transfer rate and the mass transfer rates get higher.

From the **Fig 31**, we get a clear observation of the volume fraction φ_2 on $f''(0), -\theta(0)$ and $-\phi(0)$ against the moving parameter ε. For the increasing amount of volume fraction φ_2 , skin friction coefficient decreased. Physically, the reason behind this performance indicates that, by adding more nanoparticle the viscosity of the fluid gets higher and slow down the fluid motion. The positive quantities for $f''(0)$ is stands for persevere a drag force on the surface where the negative value indicate otherwise. When $f''(0) = 0\ and\ \varepsilon = 1$, this situation stands when the free stream velocity and surface velocity are same. On the other hand, the heat transfer rate has a strong resistance, as the increment of the φ_2 elevates the heat transfer rate. Hence, the thermal boundary layer thickness increased. A reduction in mass transfer coefficient is also noticed due to the larger quantity of φ_2. For the downstream movement $\varepsilon = -1$, the mass transfer rate is same for the different range of volume fraction.

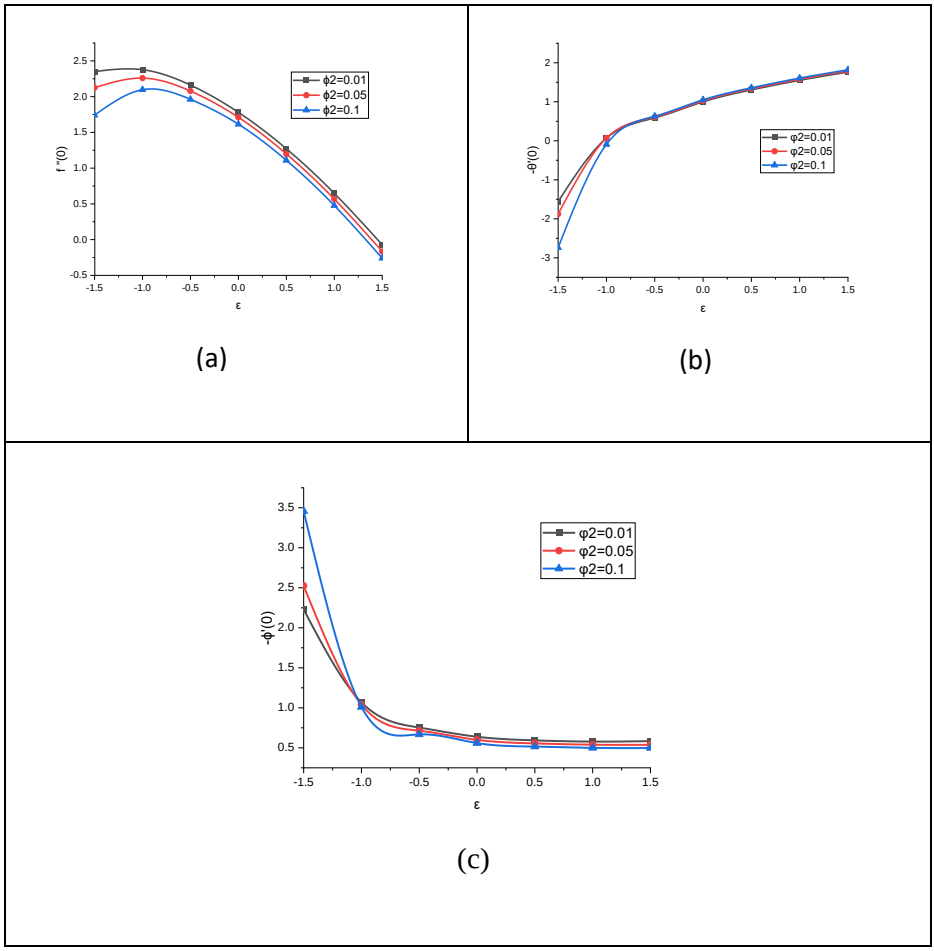

CONCLUSION

With the scheme of MAPLE software, the simulation and numerical solutions are examined for the incompressible laminar steady hybrid nano coating fluid flow through the moving surface. This study has a significant impact with the thermal radiation and transpiration effects, which are simultaneously considered with Brownian motion. With the mathematical model and graphical presentation, the flow energy and

mass transport are equally observed for diversified parameters. Further, the skin friction coefficient, mass and heat transfer rates are also numerically and graphically demonstrated for the volume fraction of CuO, φ_2. The final outcomes are given below:

- The concentration boundary layer is thinner than thermal boundary layer (as we consider $Le > 1$) and the thermal boundary layer is thinner than momentum boundary layer ($Pr \gg 1$).
- Mixed convection due to temperature and mixed convection due to concentration both parameters upsurge the fluid motion (wider boundary layer of momentum) with the larger inputs.
- With the greater values of volume fraction φ_2, leads to the higher heat transfer rate as the temperature $\theta(\eta)$ get uplifted. Declination is found for the velocity and concentration region.
- Rise in the thermal radiation Ra, which is elevated the velocity and the temperature of the fluid and reduced the concentration.
- Temperature ratio parameter θ_w, upsurge the temperature of the fluid with the greater value.
- Velocity, temperature and concentration profile recede down for the uplifting values of power law exponent λ.
- The skin friction coefficient, heat transfer rate and mass transfer rate elevate with the increasing value of transpiration parameter.
- Thermal distribution shows a great performance which is influenced by both Brownian motion parameter, Nb and thermophoresis parameter, Nt.

Acknowledgement: This study was funded by the Bose Center for Advance Study and Research in Natural Science, University of Dhaka, Dhaka-1000. We, therefore, acknowledge with thanks Bose Center for Advance study and Research in Natural Science for financial support**.**

REFERENCES

[1] S.U.S Choi, Eastman, J A. “Enhancing thermal conductivity of fluids with nanoparticles” ASME International engineering congress and exhibition FED 231MD, pp 99-105, 1995.

[2] H. Masuda, A. Ebata, K. Teramae, N. Hishinuma, “Alteration of thermal conductivity and viscosity of liquid by dispersing ultra-fine particles”, Netsu Bussei, 7, 227-233, 1993. https://www.sid.ir/en/journal/ViewPaper.aspx?ID=312989

[3] J. Buongiorno, W. Hu, Nanofluid coolants for advanced nuclear power plants, 5705, Proceedings of ICAPP '05, Seoul, 15-19, 2005.

[4] S.A. Khan, Y. Nie, B. Ali, “Multiple slip effects on magnetohydrodynamic axisymmetric buoyant nanofluid flow above a stretching sheet with radiation and chemical reaction”, Symmetry 11 (9), 1171, 2019. https://doi.org/10.3390/sym11091171

[5] L. Syam Sundara, K.V. Sharmab, Manoj K. Singha, A.C.M. Sousa, “Hybrid nanofluids preparation, thermal properties, heat transfer and friction factor – A review”, Renewable and Sustainable Energy Reviews, Vol 68, Pages 185-198, 2017. https://doi.org/10.1016/j.rser.2016.09.108

[6] J Sarkar, P Ghosh, A Adil, “A review on hybrid nanofluids: Recent research, development and applications”, Renewable and Sustainable Energy Reviews, Vol 43, pp 164-177, 2015.

[7] S.U.S. Choi, Z.G. Zhang, W. Yu, F.E. Lockwood, E.E. Grulke,“Anomalously thermal conductivity enhancement in nanotube suspension”, Appl. Phys. Lett. 79,2252–2254, 2001. https://doi.org/10.1016/j.rser.2014.11.023

[8] Iskandar Waini, Anuar Ishak, Ioan Pop, “Hybrid nanofluid flow and heat transfer over a nonlinear permeable stretching/shrinking surface”, International Journal of Numerical Methods for Heat & Fluid Flow, Vol 29, Page 3110-3127, 2019. https://doi.org/10.1108/HFF-01-2019-0057

[9] L. Prandtl, U¨ ber Flu¨ ssigkeitsbewegungen bei sehr kleiner Reibung, Verhandlg. III Intern. Math. Kongr. Heidelberg, pp. 484– 491, 1904.

[10] Asterios Pantokratoras, “A common error made in investigation of boundary layer flows”, Applied Mathematical Modelling, vol 33, pp 413–422, 2009. https://doi.org/10.1016/j.apm.2007.11.009

[11] Waini, I., Ishak, A. and Pop, I., "Hybrid nanofluid flow and heat transfer over a permeable biaxial stretching/shrinking sheet", International Journal of Numerical Methods for Heat & Fluid Flow, Vol. 30 No. 7, page 3497-3513, 2019. https://doi.org/10.1108/HFF-07-2019-0557

[12] Khashi’ie, N.S., Arifin, N.M., Pop, I., Nazar, R., Hafidzuddin, E.H. and Wahi, N., "Non-axisymmetric Homann stagnation point flow and heat transfer past a stretching/shrinking sheet using hybrid nanofluid", International Journal of Numerical Methods for Heat & Fluid Flow, Vol. 30, page 4583-4606, 2020. https://doi.org/10.1108/HFF-11-2019-0824

[13] Waini, I., Ishak, A. and Pop, I., "Hybrid nanofluid flow towards a stagnation point on an exponentially stretching/shrinking vertical sheet with buoyancy effects", International Journal of Numerical Methods for Heat & Fluid Flow, vol 30, 2020. https://doi.org/10.1108/HFF-02-2020-0086 , 2020

[14] I. Waini, A. Ishak & I. Pop, “Hybrid nanofluid flow towards a stagnation point on a stretching/shrinking cylinder”, Scientific Reports, Vol 10, 2020. https://doi.org/10.1038/s41598-020-66126-2 , 2020.

[15] Aladdin; N Bachok; Pop, I., “Cu-Al2O3/water hybrid nanofluid flow over a permeable moving surface in presence of hydromagnetic and suction effects”, Alexandria Engineering Journal, 59, 657-666, 2020. https://doi.org/10.1016/j.aej.2020.01.028 .

[16] R. Cortell, “Flow and heat transfer in a moving fluid over a moving flat surface”, Theor. Comput. Fluid Dyn. 21, 435–446, 2007. https://link.springer.com/article/10.1007/s00162-007-0056-z

[17] Ishak, A., N Bachok , Pop, I.,“Melting heat transfer in steady laminar flow over a moving surface”, Heat and Mass Transfer, 46, 463–468, 2010. https://link.springer.com/article/10.1007/s00231-010-0592-8 .

[18] N Bachok , Ishak, A., Pop, “Boundary layer flow over a moving surface in a nanofluid with suction or injection”, Acta Mechanica Sinica volume 28, 34–40, 2012. https://link.springer.com/article/10.1007/s10409-012-0014-x

[19] I. Waini, A. Ishak & I. Pop, “Unsteady flow and heat transfer past a stretching/shrinking sheet in a hybrid nanofluid”, International Journal of Heat and Mass Transfer 136, 288-297, 2009. https://doi.org/10.1016/j.ijheatmasstransfer.2019.02.101.

[20] Waini, I.; Ishak, A.; Gorsan ,T; Pop, I. , ”Mixed convection of a hybrid nanofluid flow along a vertical surface embedded in a porous medium”, International Communications in Heat and Mass Transfer, 114, 104565, 2020. https://doi.org/10.1016/j.icheatmasstransfer.2020.104565

[21] J.H. Merkin, “Mixed convection boundary layer flow on a vertical surface in a saturated porous medium”, J. Eng. Math. 14 (1980) 301–313. https://link.springer.com/article/10.1007/BF00052913

[22] S. Ahmad, I. Pop, “Mixed convection boundary layer flow from a vertical flat plate embedded in a porous medium filled with nanofluids”, Int. Commun. Heat Mass Transf. 37, 987–991, 2010 https://doi.org/10.1016/j.icheatmasstransfer.2010.06.004

[23] N.C. Roşca, A.V. Roşca, T. Groşan, I. Pop, “Mixed convection boundary layer flow past a vertical flat plate embedded in a non-Darcy porous medium saturated by a nanofluid”, Int. J. Number. Methods Heat Fluid Flow. 24, 970–987, 2014. https://doi.org/10.1108/HFF-09-2012-0199

[24] E. Haile, B. Shankar, “Boundary layer flow of nanofluids over a moving surface in the presence of thermal radiation, viscous dissipation and chemical reaction”, Appl. Appl. Math. Int. J. (AAM) 10 (2), 952–969, 2015.

[25] P.O. Olanrewaju, M.A. Olanrewaju, A.O. Adesanya, “Boundary layer flow of nanofluids over a moving surface in a flowing fluid in the presence of radiation”, Int. J. of App. Sci. and Tech. 2 (1) (2012).

[26] Samaira Aziz, Iftikhar Ahmad, Nasir Ali & Sami Ullah Khan, “Magnetohydrodynamic mixed convection 3‐D simulations for chemically

reactive couple stress nanofluid over periodically moving surface with thermal radiation". Journal of Thermal Analysis and Calorimetry volume 146,435–448, 2021. https://link.springer.com/article/10.1007/s10973-020-09962-8

[27] Prabhakar Besthapua, Rizwan Ul Haq, Shankar Bandaria Qasem M.Al-Mdallalc, "Mixed convection flow of thermally stratified MHD nanofluid over an exponentially stretching surface with viscous dissipation effect", Journal of the Taiwan Institute of Chemical Engineers, 71, 307-314, 2017. https://doi.org/10.1016/j.jtice.2016.12.034

[28] A. Alsabery, H. Kadhim, M. Ismael, I. Hashim, A. Chamkha, "Impacts of Amplitude and Heat Source on Natural Convection of Hybrid Nanofluids into a Wavy Enclosure via Heatline Approach", Waves in Random and Complex Media, pp. 1–25, 2021. https://doi.org/10.1080/17455030.2021.1896819

[29] Sohail Nadeem, Shafiq Ahmad, Muhammad Naveed Khan, "Mixed convection flow of hybrid nanoparticle along a Riga surface with Thomson and Troian slip condition", Journal of Thermal Analysis and Calorimetry, Vol.:(0112 33456789), 143:2099–2109, 2021. https://doi.org/10.1007/s10973-020-09747-z

[30] Ali Arefmanesh, Alireza Aghaei, Hamidreza Ehteram, "Mixed convection heat transfer in a CuO–water filled trapezoidal enclosure, effects of various constant and variable properties of the nanofluid", Applied Mathematical Modelling, 40, 815–831, 2016. https://doi.org/10.1016/j.apm.2015.10.043

[31] Dulal Pala, Gopinath Mandal, "Influence of thermal radiation on mixed convection heat and mass transfer stagnation-point flow in nanofluids over stretching/shrinking sheet in a porous medium with chemical reaction", International Communications in Heat and Mass Transfer 114 104565, 2020. https://doi.org/10.1016/j.nucengdes.2014.01.032

[32] S. Saleem, Hina Firdous, S. Nadeem, A. U. Khan, "Convective Heat and Mass Transfer in Magneto Walter's B Nanofluid Flow Induced by a Rotating

Cone", Arabian Journal for Science and Engineering, 44:1515–1523, 2010. https://doi.org/10.1007/s13369-018-3598-z

[33] E. Omrani, P.L. Menezes, P.K. Rohatgi, Effect of micro-and nano-sized carbonous solid lubricants as oil additives in nanofluid on tribological properties, Lubricants 7 (3) (2019) 25, https://doi.org/10.3390/ lubricants7030025.

[34] J. Huang, J. Tan, H. Fang, F. Gong, Wang, J. Tribological and wear performances of graphene-oil nanofluid under industrial high-speed rotation, Tribol. Int. 135, 112–120, 2019. https://doi.org/10.1016/ j.triboint.2019.02.041

[35] M. Arif, F. Ali, N.A. Sheikh, I. Khan, Enhanced heat transfer in working fluids using nanoparticles with ramped wall temperature: applications in engine oil, Adv. Mech. Eng. 11 (11), 2019. https://doi.org/10.1177 /1687814019880987 , 1687814019880987.

[36] Asmat Ullah Yahya, Nadeem Salamat, Wen-Hua Huang, Imran Siddique, Sohaib Abdal, Sajjad Hussain "Thermal characteristics for the flow of Williamson hybrid nanofluid (MoS2 + ZnO) based with engine oil over a stretched sheet", Case Studies in Thermal Engineering 26, 101196, 2021. https://doi.org/10.1016/j.csite.2021.101196

[37] Muhammad Arif, Poom Kumam, Dolat Khan, Wiboonsak Watthayu, "Thermal performance of GO-MoS2/ engine oil as Maxwell hybrid nanofluid flow with heat transfer in oscillating vertical cylinder", Case Studies in Thermal Engineering, 27, 101290, 2021. https://doi.org/10.1016/j.csite.2021.101290

[38] Waini, I.; Ishak, A.; Pop, I., "Flow and heat transfer of a hybrid nanafluid past a permeable moving surface", Chinese Journal of Physics, 66, 606-619, 2020. https://doi.org/10.1016/j.cjph.2020.04.024

[39] F. Mabood , G.P. Ashwinkumar & N Sandeep, "Effect of nonlinear radiation on 3D unsteady MHD stagnancy flow of Fe3O4/Graphene-water hybrid nanofluid", International Journal of Ambient Energy, 2020 https://doi.org/10.1080/01430750.2020.1831593

[40] P.D. Weidman, D.G. Kubitschek, A.M.J. Davis, “The effect of transpiration on self-similar boundary layer flow over moving surfaces”, International Journal of Engineering Science, 44, 11–12, 730-737, 2006. https://doi.org/10.1016/j.ijengsci.2006.04.005

[41] N Bachok; Ishak, A.; Pop, I., “Boundary-layer flow of nanofluids over a moving surface in a flowing fluid”, International Journal of Thermal Sciences, 49,1663-1668,2010, https://doi.org/10.1016/j.ijthermalsci.2010.01.026

[42] W.A. Khan & A. Aziz, “Natural convection flow of a nanofluid over a vertical plate with uniform surface heat flux”, International Journal of Thermal Sciences, 50, 1207-1214, 2011. https://doi.org/10.1016/j.ijthermalsci. 2011.02.015

[43] O.D. Makinde & A. Aziz, “Boundary layer flow of a nanofluid past a stretching sheet with a convective boundary condition”, International Journal of Thermal Sciences, 50, 1326-1332, 2011. https://doi.org/ 10.1016/j.ijthermalsci.2011.02.019

[44] A. Ishak, R. Nazar, I. Pop, “The effects of transpiration on the flow and heat transfer over a moving permeable surface in a parallel stream”, Chem. Eng. J. 148, 63–67, 2009. https://doi.org/10.1016/j.cej.2008.07.040

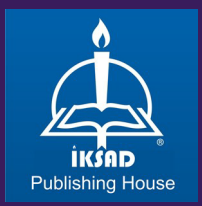

ISBN: 978-625-7562-89-8